EUVE Guest Observer Program Handbook

UCB/EUVE Call for Observing Proposals
97-EUVE-06
Appendix C

Extreme Ultraviolet Explorer

Guest Observer Center Documentation

The EUVE Guest Observer Center

September 12, 1997

TABLE OF CONTENTS

LIST OF FIGURES

LIST OF TABLES

Acknowledgements

The author, Anne Miller, wishes to thank everyone who assisted in preparing this edition of the *Handbook*. Special thanks for help with this edition go to Drs. Mark Abbott, Jean Dupuis, Pat Jelinsky, Antonella Fruscione, Mihalis Mathioudakis, and Damian Christian of the EUVE Guest Observer Center. Thanks also to Dr. Carol Christian, EGO Center scientist, Eric Olson, EGO Center manager, and and to Bill Boyd, and Martin Sirk, who continue to improve the instrument calibration. The author wishes to thank the principal investigator, Stuart Bowyer, and Roger Malina for advice and support. This work has been supported by NASA contract NAS530180, which is administered by the Center for Extreme Ultraviolet Astrophysics of the University of California, Berkeley.

PREFACE

This *Handbook* will acquaint potential Guest Observers with the Extreme Ultraviolet Explorer (EUVE) Spectrometer, Scanning Telescopes, and Deep Survey Scanner. It should be used as a guide to preparation of proposals, and as a basic source of information about the EUVE mission and scientific payload. It does not contain statements of NASA policies concerning proposal evaluation, target selection or Peer Review processes. Anyone wishing detailed information about the rules and deadlines governing this program should consult the current UCB/EUVE Call for Observing Proposals for the EUVE Guest Observer Program, issued 15 October 1997, and available from the Center for EUV Astrophysics (CEA) at the University of California, Berkeley (UCB), at the address given in Chapter 1.

Fourth edition: July, 1995

This is the fourth edition of the *EUVE Guest Observer Handbook*, released to accompany the fourth EUVE NASA Research Announcement (NRA) in July, 1995, and only updated slightly for the sixth announcement, released in October 1997. At this writing, the EUVE Guest Observer (EGO) Program is in its fourth year-long cycle of observations. The instrument characteristics and performance have remained stable throughout the last year. The material in this *Handbook* is therefore largely unchanged from that released for Cycle III in 1994. The most significant changes are:

a) References to names and locations of online resources.
b) Information on changes to EUVE's default operations configuration.
c) Deep Survey data are now routinely delivered to all GOs.
d) Spacecraft operation and GO program now run by the CEA.

All proposers should have both the *Handbook* and *Addendum* for preparing their 1997 proposals.

The instrument calibration data available via the CEA *ftp* site and the WWW have not changed since Cycle IV, but their location has changed to a new directory. Please read about the potential for significantly lower backgrounds in future observations, as described in the *Addendum*.

The information in the *Handbook* reflects the EGO Center's current understanding of the instruments and is provided on a best-effort basis. The characteristics of the EUVE science instruments may change in the future. Questions concerning the contents of this document should be directed to the EUVE Guest Observer Center at the University of California, Berkeley.

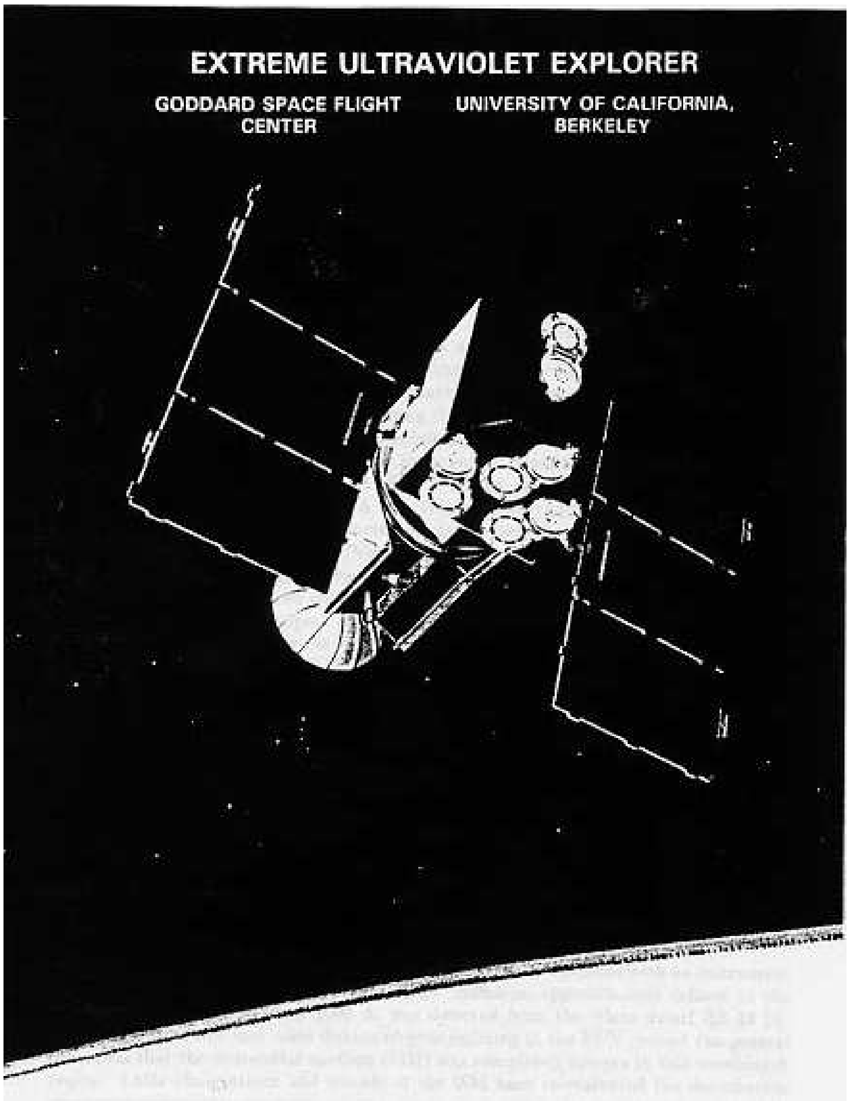

The Extreme Ultraviolet Explorer

Chapter 1

THE EXTREME ULTRAVIOLET EXPLORER

1.1 Introduction

The Extreme Ultraviolet Explorer (EUVE) is a NASA explorer-class satellite mission devoted entirely to observations in the wavelength range from 70 to 760 Å. The science payload incorporates five separate instruments: four photometric imaging systems and a three-channel EUV spectrometer. During the first phase of the mission, the imaging instruments were used to conduct a complete sky survey in four different bands in the EUV. The survey results are available to the scientific community in the first EUVE sky survey bright source list and the first EUVE all-sky catalog. The second part of the mission has been conducted by NASA as a Guest Observer program, for which pointed spectroscopic observations are conducted for guest scientists under proposals submitted to NASA and supported by the EUVE Guest Observer Center at Berkeley. The mission lifetime will extend through at least a fifth year of observations. Further extensions of the EUVE mission will be partially contingent upon review processes. To support an extended mission, please contact the chair of the EUVE Science Advisory Board (ESAB)[1] or the EUVE Guest Observer Center (address below).

The EUVE Guest Observer (EGO) Program is supported by the EUVE Guest Observer Center (EGO Center) at the Center for Extreme Ultraviolet Astrophysics (CEA), at the University of California, Berkeley. The policies of the EGO Program are specified in the recent UCB/EUVE Call for Observing Proposals. This *Handbook* is produced by the EGO Center as a guide to choosing appropriate targets for observation and preparing proposals. The rest of this chapter gives a broad overview of the EUVE mission and the EGO Center.

1.2 The EUVE Mission

1.2.1 Scientific Background

The first non-solar observations in the extreme ultraviolet were made with an instrument on the Apollo-Soyuz spacecraft in 1975. EUV radiation, approximately defined as the wavelengths between 100 and 1000 Å, was detected from the white dwarf HZ-43 [3]. The discovery of this and other distant objects emitting in the EUV revised the general consensus that the interstellar medium (ISM) was completely opaque in this wavelength region. Later observations and models of the ISM have re-evaluated the distribution and EUV

[1] Dr. Steve Howell, University of Wyoming, Laramie, WY 82071; 307/766-5402; (showell@mothra.uwyo.edu).

photoabsorption of interstellar hydrogen and helium [15], [6]. They suggested that a sky survey might detect sources as far as 1000 parsecs from the sun, or farther in some directions, depending on the distribution of neutral interstellar material. The Voyager and EXOSAT missions and the ROSAT EUV all-sky survey and EUVE sky survey have since discovered other sources, making a list of more than 1000 objects that emit measurable radiation in the EUV. Types of objects that have been observed in the EUV are planetary atmospheres, hot stellar coronae, late type and cataclysmic variable (CV) stars, hot stellar remnants, and active galactic nuclei (AGN). The local ISM also emits measurable amounts of EUV radiation.

The EUVE instruments were built under contract from NASA Goddard Space Flight Center by the Space Astrophysics Group (SAG), which is part of the CEA. The science payload is integrated with the Multimission Modular Spacecraft (MMS), NASA's Explorer Platform,. It was launched on June 7, 1992, into a 550 km circular orbit with an inclination of 28°. After initial testing and calibration, the satellite started surveying the sky in great circles with the three co-aligned "Scanner" instruments at 3 revolutions per orbit (RPO). The survey observations were completed in January, 1993. At the same time, a parallel "deep survey" was conducted along a two-degree strip covering about half the ecliptic. The first year of pointed observations with the EUV spectrometer were begun immediately after completion of the all-sky survey.

EUVE Mission Timeline

- 1983: Fabrication of the instruments begins at Berkeley.
- 1989: Instruments and their electronics completed.
- 1990: Science payload calibrated and delivered to NASA-GSFC for integration.
- June 7, 1992 EUVE launched from Cape Canaveral Air Station aboard a Delta II launch vehicle.
- July 11, 1992 EUVE all-sky survey observations begin.
- January 22, 1993 Guest Observation Cycle I begins.
- August 17, 1993 First Target of Opportunity (TOO) observed: SS Cygni.
- August, 1993 Mini IOC and Thermal testing to determine effect of wider pointing range on the spacecraft and power systems.
- October, 1993 Pointing range increased to 90 degrees from antisun
- January 23, 1994 Beginning of GO Cycle II observations.
- February 20, 1995 Beginning of GO Cycle III observations.
- March 1, 1996 Beginning of GO Cycle IV observations.
- March 1, 1997 Beginning of GO Cycle V observations.
- March 1, 1998 Beginning of GO Cycle VI observations (planned).

1.2.2 Science Goals and Instrument Overview

The first scientific goal of the mission was to make a complete sky survey in four bandpasses between 70 and 800 Å that located sources to better than 1 arc minute and obtained absolute flux measurements. The three scanning survey instruments each comprise a grazing incidence telescope, a two-dimensional imaging microchannel plate (MCP) detector, and logic and event-processing electronics (see figure A-1 and A-4 in *Appendix A* of this *Handbook*). Two of the scanners, Scanners A and B, are identical short-wavelength imaging systems, each employing two filters between 70 and 290 Å. The third instrument, Scanner C, is similar, but operates in two longer-wavelength regions from 400 to 700 Å. Their principles of operation and design parameters are described further in chapter 2 and *Appendix A* of this *Handbook*. The resolution of the resulting sky map for fully scanned sources is approximately 2 arc minutes.

The sky survey observations were completed in January, 1993, and the list of optically identified bright sources [16] from the survey is available from the CEA/EUVE *ftp* site, or from the Astrophysics Data System (ADS). See also the First EUVE Source Catalog [2]. Average exposure times for the objects on the bright source list is 800 seconds, with the longest exposures at higher celestial latitudes.

In addition to the all-sky survey, a long-exposure "deep survey" was carried out during the scanning phase. The Deep Survey instrument uses half the light from the fourth of the telescopes, called the Deep Survey/Spectrometer (DS/S) telescope, which is mounted perpendicular to the scanner telescopes on the science payload (see figure 1-1). It is similar to the other scanners in design, and has two broad band spectroscopic filters similar to those of the short wavelength scanners, which cover two bandpasses between 60 and 285 Å (see figure 2-1).

The DS instrument was pointed in the anti-sun direction along the satellite's axis of rotation during the survey. As a result of this more restricted scanning pattern, long exposures on the order of 20,000 seconds/$0.1°$ pixel over a $2° \times 180°$ swath of sky along the ecliptic plane were obtained. This produced a survey section with sensitivity greater than that of the other Scanners alone, by about a factor of about 10.

The second scientific goal of the mission is to make pointed spectroscopic observations in the EUV. The DS/S telescope also feeds light to the EUV spectrometer, which has three overlapping bandpasses covering the entire 70–760 Å window, with a resolution ($\lambda/\Delta\lambda$) of 100–400. Targets include sources discovered in the recent sky surveys, as well as previously known sources and other likely candidates. Individual spectral lines from point sources can be detected with a 3-σ threshold of approximately 7×10^{-4} photons/cm^2/second in 40,000 seconds. A more detailed description of the DS/S instrument and its calibration follows in chapters 2 and 3 of this *Handbook*.

1.2.3 Explorer Platform and Mission Operations

The Explorer Platform used by EUVE consists of the Multimission Modular Spacecraft (MMS) and accompanying Platform Equipment Deck (PED). The MMS is a 3-axis stabilized, zero-momentum satellite with a stellar reference attitude control system, manufactured by the Fairchild Space Company [7]. The PED forms the interface between the spacecraft and scientific payload. It incorporates solar panel modules, antennae, and other mission-specific equipment. In this section the MMS/PED combination will be referred to as "the spacecraft." Figure 1-1 shows the configuration of the science payload and its relation to the spacecraft in the integrated EUVE satellite.

The satellite attitude, or "aspect" is continually reported and is periodically adjusted by the modular attitude control system (MACS). The MACS can point the spacecraft using guide stars in its two fixed-head star trackers (FHST's) or one guide star and a digital fine sun sensor (DFSS) as reference points. To maintain pointing, the system updates attitude estimates obtained from the satellite inertial reference unit (IRU) gyros with information from the guide star positions in the star trackers, according to the stars' recorded positions. The satellite can be pointed and maintained with an accuracy of at 10–60 arc seconds (3σ), depending on the number of reference stars available for a given pointing. It refers to an onboard catalog of over 1000 guide stars. Aspect reports is updated in the telemetry every 1.024 seconds.

Pointing and other instrument commands are relayed from the EUVE Science Operations Center (ESOC) at CEA to the satellite via GSFC and TDRSS satellite links. Command uplink capability and real time data transmission occur in contacts of 16 minute duration as often as twice per orbit. Transmissions are received by the spacecraft command and data handler (C&DH), which directs spacecraft commands to the on board computer (OBC) and payload commands to the payload's command and data processor (CDP). At the same time, data from the spacecraft are received on the ground for use in verifying source intensities and spacecraft health and aspect information.

All satellite telemetry is transmitted via TDRSS satellite and NASCOM link to the satellite communications station at Goddard Space Flight Center (GSFC). The spacecraft C&DH module creates the telemetry (TM) stream by interleaving the scientific data with science payload engineering analog voltages with spacecraft housekeeping information in a standard digital transmission format. The spacecraft has two tape recorders for telemetry storage between data transmissions. Each has a capacity of 1×10^9 bits. The TM transmission rate is 32 KBPS, of which one half is allocated to the science instruments. After the telemetry is received by Goddard via TDRSS, the scientific and instrument health data are separated and relayed to the ESOC at CEA in batch mode every three hours. The total time elapsed from satellite recording to receipt of data at Berkeley is roughly eight hours.

1.3 EUVE Guest Observer Center

The EUVE Guest Observer Center was formed under a contract between NASA and UCB to support all activities of the mission's pointed phase which involve the Guest Observer directly. The EGO Center provides this *Handbook* and other informative material to proposers, facilitates proposal processing, and conducts technical reviews of proposals before they are submitted to the Peer Review Panel. After the proposal selection process, the EGO Center is responsible for data acquisition and preliminary processing, and provides the data, software tools, and support to GOs throughout their analysis [17]. The EGO Center provides direct assistance to proposers and GOs at all times.

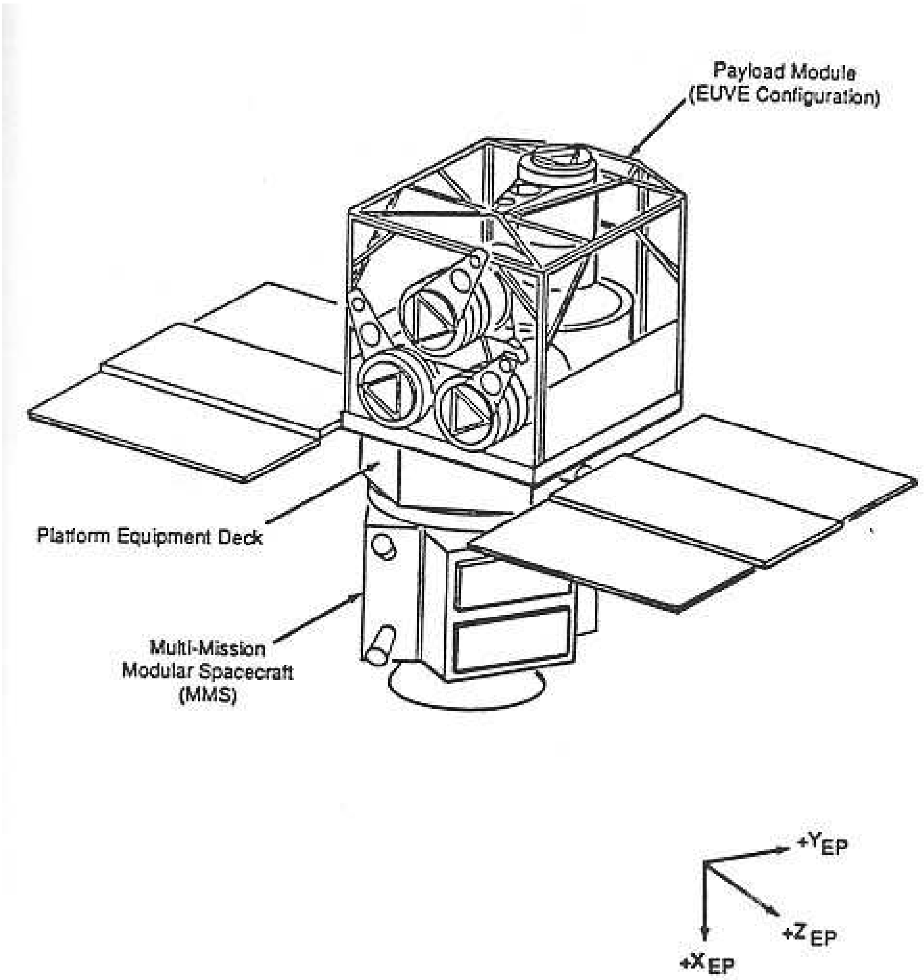

Figure 1-1: EUVE-Explorer Platform configuration

The Technical Justification section of each proposal is reviewed by EGO Center scientists to verify projected throughputs, and analysis goals in terms of the most current knowledge of instrument and to flag special pointing and timing requirements. The Peer Review Panel, assembled by NASA from various related fields, judges the proposals on general scientific merit, and selects those technically approved proposals thought to promise the best scientific returns. After both reviews are complete, a Peer Review Panel meeting is held to combine the information and make final decisions on awards of time. The Review Panel also determines target priorities: high scientific priority (type 1) and other approved targets (type 2), as described in Appendix A of the UCB/EUVE Call for Observing Proposals. The EGO Center provides the Peer Review Panel with technical support and information about the scheduling process.

Proposals for Targets of Opportunity (TOO), which are not part of the regular proposal cycle, may be honored under the rules given in the Call for Observing Proposals. The projected response time is now on a best-bet effort after TOO request approval. See sections 3.9 and 4.2 for more details on TOO's and scheduling.

After telemetry is received in the Berkeley ESOC, it is immediately stored on tape and later transferred to optical disks. The appropriate telemetry for each observation is then selected from storage by the EGO Center and restructured to separate photon data and collate relevant engineering quantities. Photon event data are processed to remove the primary instrument effects, and first-cut spectra are extracted for the GO. All photon data taken from the three spectrometer channels during pointed observations are proprietary to the Guest Observers named in the applicable proposal for a standard interval, given in the Call for Proposals.

After the Guest Observer proprietary period, data enter the public domain and are accessible through the EUVE public data archive [23]. The archive is most easily accessed via the CEA *WWW* site. See section 1.4.1 below, for URL information.

1.4 Using This Manual

The previous sections have given only a brief description of the EUVE mission and the EGO Program. The balance of this *Handbook* describes the EUVE spectroscopic and photometric instruments in more detail, and provides information on resources and services to be provided for Guest Observers. Chapter 2 begins with a brief overview of the basic components and operating principles of the instruments for those unfamiliar with the methods of EUV instrumentation, and describes the design of the EUVE Spectrometer and its calibration. The Deep Survey imaging system is also described. More detailed descriptions of the survey instruments are deferred to *Appendix A*.

Chapter 3 contains more precise information characterizing the Spectrometer's performance, and presents formulas for use with source models in planning observations. The functions and formulas provided should be sufficient for assessing the scientific viability of various types of observations, estimating count rates from prospective targets, calculating exposure times, and completing part 2 of the Target Summary Form. Chapter 3 ends with a look-up guide to the symbols and formulas used in the text.

Chapter 4 is an introduction to observing with EUVE and doing data reduction at the Center for EUV Astrophysics. The processes of technical review, schedule planning, data acquisition, and interaction of Guest Observers with the EGO Center are briefly described. Data analysis facilities and programming support are outlined.

The appendices include descriptions of the survey instruments, a partial list of project acronyms, and a detailed bibliography on the interstellar medium (ISM).

This *Handbook* is Appendix C to the UCB/EUVE Call for Observing Proposals for the EUVE Guest Observer Program. Copies of the Call for Proposals may be obtained from the CEA-EUVE *WWW* or *ftp* site, listed in section 1.4.1 below, or from the EGO Center:

EUVE Guest Observer Center
University of California at Berkeley
The Center for EUV Astrophysics
2150 Kittredge Street
Berkeley, CA 94720
(510) 642-3032
FAX: (510) 643-5660
email: egoinfo@cea.berkeley.edu

The reader should refer to the current EUVE Call for Proposals for schedules, proposal due dates, forms, submission instructions, and policies specific to proposal preparation. The UCB/EUVE Call for Observing Proposals, also provides contact information for other questions in these areas. If in any instance the language of this *Handbook* conflicts with that of the Call for Proposals, statements in the current UCB/EUVE Call for Observing Proposals take precedence. Questions on the instrumentation that are not answered by this *Handbook* should be directed to:

EUVE Guest Observer Center
c/o Dr. Damian Christian
University of California at Berkeley
Center for EUV Astrophysics
2150 Kittredge Street
Berkeley, CA 94720-5030
email: egoinfo@cea.berkeley.edu

All *egoinfo* mail is answered promptly by the appropriate EGO Center scientist or staff person.

1.4.1 Electronic Access to NRA Materials

Both the EUVE *ftp* and *WWW* sites contain copies of all appendices and forms for this Call for Proposals, and tabulated calibration data in this *Handbook*, as well as other information relevant to the EUVE mission.

The easiest way to list and view the available materials is to use the World Wide Web (abbreviated *WWW*). The *WWW* Uniform Resource Locator (URL) of the CEA Home Page is:

http://www.cea.berkeley.edu/

Materials specifically regarding this Call for Proposals are available via CEA's *WWW* site at URL:

http://www.cea.berkeley.edu/nra97

For FTP access to this Call for Proposals, on the CEA Home Page select the highlighted item labeled **"FTP Access"**. This will list the top level directory of the CEA *ftp* site. Select the directory *nra97* to view the Call for Proposals materials. Be sure to view the file *README* in this directory to get the most up-to-date instructions and information on the these materials. Note that any World Wide Web client can be used.

If you wish to use standard *ftp*, the **Internet** address for the CEA/EUVE *ftp* site is:

> **EUVE NRA materials on** ***ftp*:**
>
> **ftp.cea.berkeley.edu**
> or
> **128.32.154.12**

In the following command examples, a percent sign (%) is used to indicate a prompt in the user's operating system. Start the *ftp* program by typing:

```
% ftp ftp.cea.berkeley.edu
```

to open the CEA/EUVE *ftp* site. Use the login name "anonymous" and give your full **Internet** address as the password. The Call for Proposals materials are in the subdirectory *pub/nra97*. You can always go to this directory with the *cd* command:

```
ftp> cd /pub/nra97
```

The command *ls* will list the directory's contents. The file *README.txt* contains information about each of the files in the directory. All users should read *README* to get the most up-to-date instructions on the Call for Proposals materials.

The way to read a file in *ftp* is to transfer it to your system using the command *get*, and view it in your local operating system. Make sure to select "binary mode" before transferring any files by typing the command *bin*. For example, to obtain a copy of *README.txt*, set *ftp* to binary transfer mode, and use the *ftp* command *get*:

```
ftp> bin

ftp> get README
```

Use the information in *README* to decide which files you want. You can obtain any of the other files with a similar command. Always make sure that *ftp* is set to binary transfer mode before using *get*. To obtain all the Call for Proposals materials in a single compressed tar file, *get* the file *nra.tar.Z* (this file is rather large):

ftp> `get nra.tar.Z`

The EUVE public archive site is also accessible at the same *ftp* address, or via the *WWW* at CEA's HomePage. The public archive contains software, EUVE news, sample extracted spectra, bright source lists, and numerous publications.

EUVE SCIENCE PAYLOAD AND INSTRUMENTATION

2.1 Science Payload Configuration

The physical configuration of the science payload is illustrated in figure 1-1, along with the coordinate system frequently used to refer to the science payload and spacecraft. The three scanning instruments are stacked to point along the spacecraft -Y axis, which is the DS/S X axis. The DS/S points away from the PED along the spacecraft -X axis. This is also the DS/S Z axis and the spacecraft spin axis in sky-survey mode.

2.2 The EUVE Spectrometer

The instruments designed for the EUVE mission are the product of over two decades of development by the Space Astrophysics Group in Berkeley. This section will describe the EUVE Spectrometer by first describing its components and then the complete system and its calibration. The Deep Survey instrument will also be described, as some data from the Deep Survey are routinely provided to Guest Observers.

The Spectrometer is a three-fold symmetric slitless objective design based on variable line space grazing incidence reflection gratings. Photon images are accumulated simultaneously in three bandpasses with effective spectral resolutions of $\lambda/\Delta\lambda \sim 200$–400 in 3 bandpasses from 70–760 Å. The instrument is pictured in cross section in figure 2-1, and its physical characteristics are summarized in table 2-2. The Spectrometer and Deep Survey instruments share the DS/S mirror. The regions of the mirror devoted to the Spectrometer and Deep Survey are defined at the front aperture, which is an annulus divided into six segments. Each of the Spectrometer channels receives a beam of light from one of three alternating segments. This division gives each channel a geometric area of ~ 75 cm^2. After the mirror, each converging beam then strikes one of three gratings which focus the spectra onto three detectors, arranged in a circle around the central Deep Survey detector.

The throughput of the EUVE Spectrometer is determined by the combined effects of the mirrors' and gratings' coating reflectivities, which are functions of both wavelength and grazing angle, the filter transmissions, and the quantum efficiency functions of the detector photocathode materials.

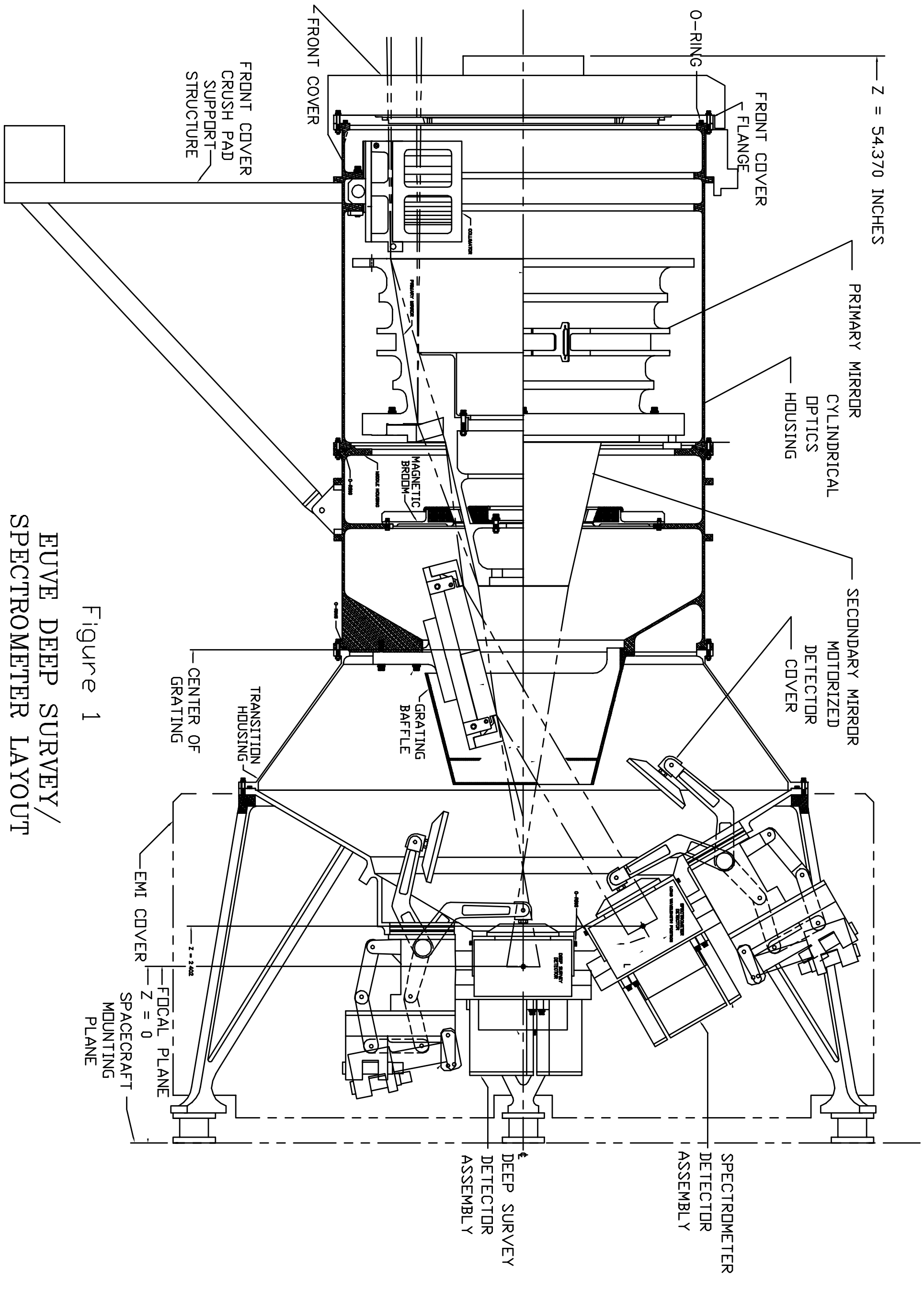

Figure 2-1: The EUVE Spectrometer in cross-section

2.2.0.1 The DS/S Telescope

Mirror reflectivities in the EUV are generally maximized by the use of grazing incidence optics. All the EUVE instruments employ polished metal grazing incidence mirrors, which provide very compact imaging systems with relatively large fields of view, and adapt well to the stringent requirements of space platforms.

The DS/S telescope is a Wolter-Schwarzschild Type II design, with a concave primary and a convex secondary. The mirror has a focal length of 136 cm and is f/3.3, with a total geometric area of over 450 cm^2. The primary and secondary mirrors are both gold-coated. Characteristics of the optic are summarized in table 2-1. Reflectivity tests were performed on the finished mirror, using light between 44 Å and 1216 Å. The results are shown in figure 2-2.

Table 2-1: The DS/S Mirror

Focal Length	136.242 cm
f/ratio	3.3
Geometric Area	452.97 cm^2
Field of View	2° diameter
Average Graze Angles (primary, secondary)	9°, 5.5°
Surface coating	sputtered Au, $\sim$ 350 Å
FWHM (Optical)	1.6 $''$
HEW (Optical)	12 $''$

The point spread function and the half energy width and scattering of the mirrors have been measured at Berkeley's EUV calibration facilities [4] to assure acceptable standards of imaging.

Measurements of the point spread function in the EUV give the angular resolution at the center of the field of view as approximately 18 arc seconds. When coupled to a 50 mm EUVE MCP detector, this produces and instrument plate scale of 6.60 μ per arc second. The focused image size at optical wavelengths is about 12 arc seconds' half-energy width (HEW) after polishing.

The mirror collects light through an annular aperture divided into six segments. Three segments feed the Deep Survey imaging system, which is described further in section 2.3. Baffles before the telescope, near the midpoints of the primary and secondary mirrors, and side baffles on the grating assemblies help exclude diffuse geocoronal radiation from the telescope and scattered light from all the detectors. To exclude charged particles, the telescope is equipped with a magnetic broom, between the secondary baffle and secondary mirror. It is designed to divert electrons with energies up to 15 kV, and thermal ions with energies up to .3 eV. Each detector is also protected by a 10 Newton repellor grid, biased to 28 V.

2.2.1 Collimators and Sky Background

In order to achieve good spectral resolution, any EUV spectrometer must be designed to limit the effect of diffuse sky radiation. The medium and long wavelength channels of the EUVE Spectrometer have wire-grid collimators placed directly after the aperture before the mirror, which limit the grazing angles of the incident light to exclude some of the sky background. They consist of 15 etched molybdenum grids, spaced exponentially and held in a thermally stable claw structure, also of molybdenum. The transmission profile of the stack is triangular in the dispersion direction, and limits the beam to 20 arc minutes FWHM.

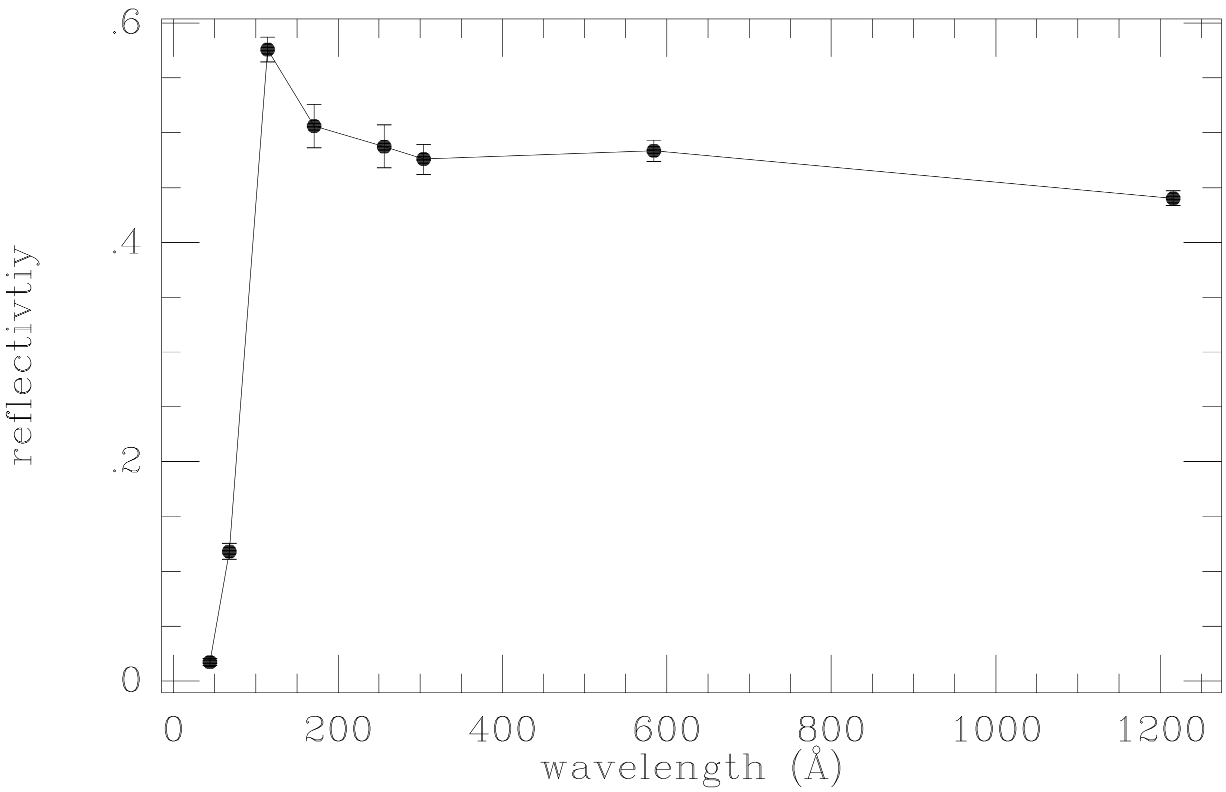

Figure 2-2: DS/S mirror reflectivity in the EUV

The transmission of of each collimator assembly was tested in visible light. The collimator relative transmissions were measured in the EUV by comparing the Spectrometer throughputs, measured as a function of off-axis angle, before and after installation of the collimators in the medium and long wavelength channels. Alignment to the boresight of the instrument was also determined. Both collimators function as designed, with peak transmissions of 64.2% and 65.4% in the medium and long wavelength channels, respectively. Figure 2-3 illustrates the collimator relative transmission measured in the long wavelength channel. Relative transmission is the ratio of Spectrometer channel throughput with the collimator installed to that measured without the collimator.

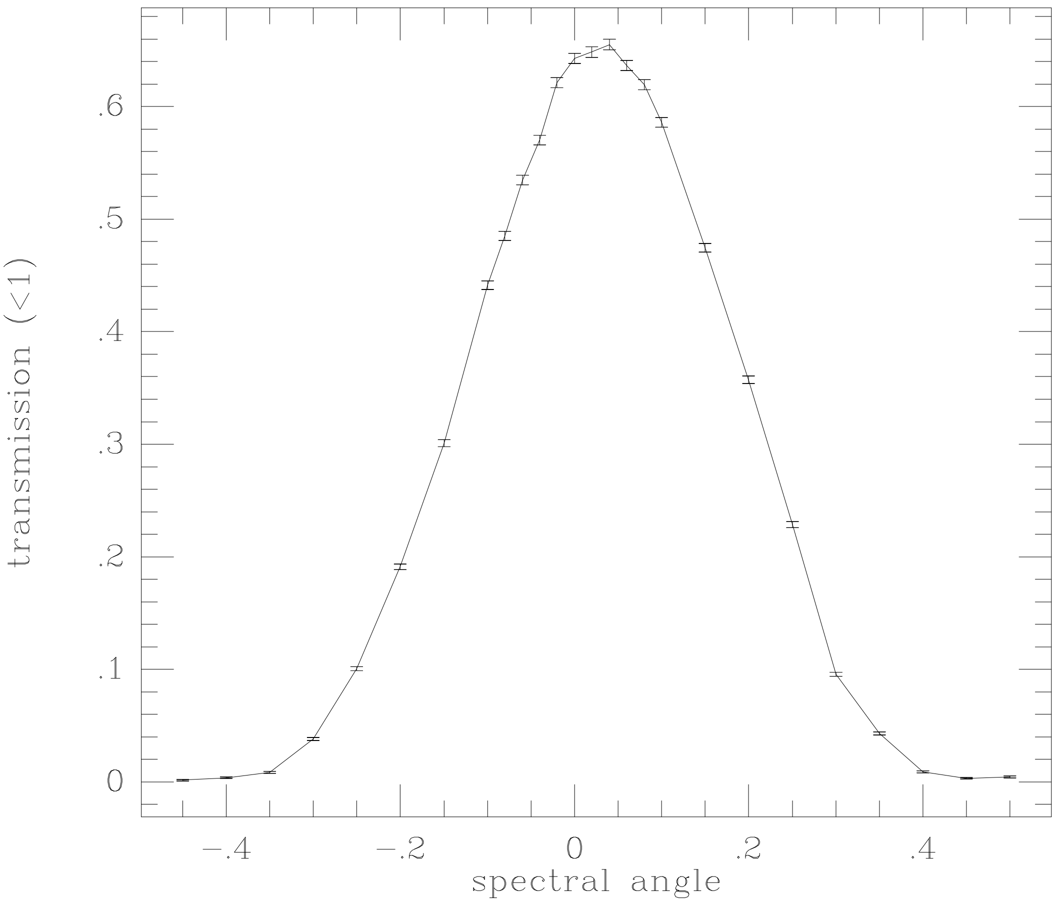

Figure 2-3: Long Wavelength collimator transmission

2.2.2 Variable Line Space Gratings

The EUVE Spectrometer incorporates plane diffraction gratings with continuously varying line spacing, placed in the converging beam of the telescope to diffract the light as it approaches the focus. Like concave gratings, they obviate the use of other focusing optics after dispersion. Unlike uniformly spaced rulings, variable line space gratings can produce nearly stigmatic spectra using straight, conventionally ruled grooves [13],[12].

The gratings are blazed for use in the first inside order. "Inside" will be used to mean diffracted orders at angles between the surface normal and the specular direction, and will be referred to with a minus sign when represented numerically, e.g. -1st order. The gratings cover three overlapping bandpasses; short wavelengths from 70 to 190 Å, medium wavelengths from 140 to 380 Å, and long wavelengths from 280 to 760 Å. The groove densities range from 415 to 3550 grooves/mm. The gratings were ruled by Hitachi, Inc. at the Naka optical works in Japan. The short wavelength grating is coated with rhodium to optimize the reflectivity between 70 and 190 Å. The medium and long wavelength gratings have platinum surface coatings.

2.2.3 Spectrometer Filters

Thin film filters, a few thousand Å thick, completely cover each detector. They define broad bandpasses while screening out bright geocoronal and interplanetary lines such as Lyman alpha radiation and some higher orders of diffraction. The Spectrometer filter configuration is shown in figure 2-4. The materials are Lexan and boron in the short wavelength, aluminum and carbon in the medium, and aluminum in the long wavelength channel. The measured transmissions for the Spectrometer Lexan and aluminum filter materials are plotted in figures 2-5 and 2-6 in both log and linear coordinates. Material thicknesses are included in table 2-2.

The two longer wavelength filters have an off-axis quadrant[1] of material which covers the same bandpass as one of the shorter channels. At these positions, which correspond to off-axis angles of approximately 0.5°, some wavelengths that would normally lie in the shorter channel's range appear in the longer wavelength channel in second order ($n = -2$), and are passed by the alternate filter. Wavelengths from parts of the shorter bandpass that overlap the longer channel also appear in first order. These off-axis locations are configured to be used as backups to duplicate the short and medium channels, should either of these detectors fail.

2.2.4 Microchannel Plate Detectors

All the EUVE detectors are Microchannel plate (MCP) detectors. MCP detectors are electron-amplification devices that provide two-dimensional imaging and time-tagging of individual EUV photon events [25, 28].

[1] The sections of a filter are numbered from 0 and referred to as quadrants, regardless of the number of sections in any one filter.

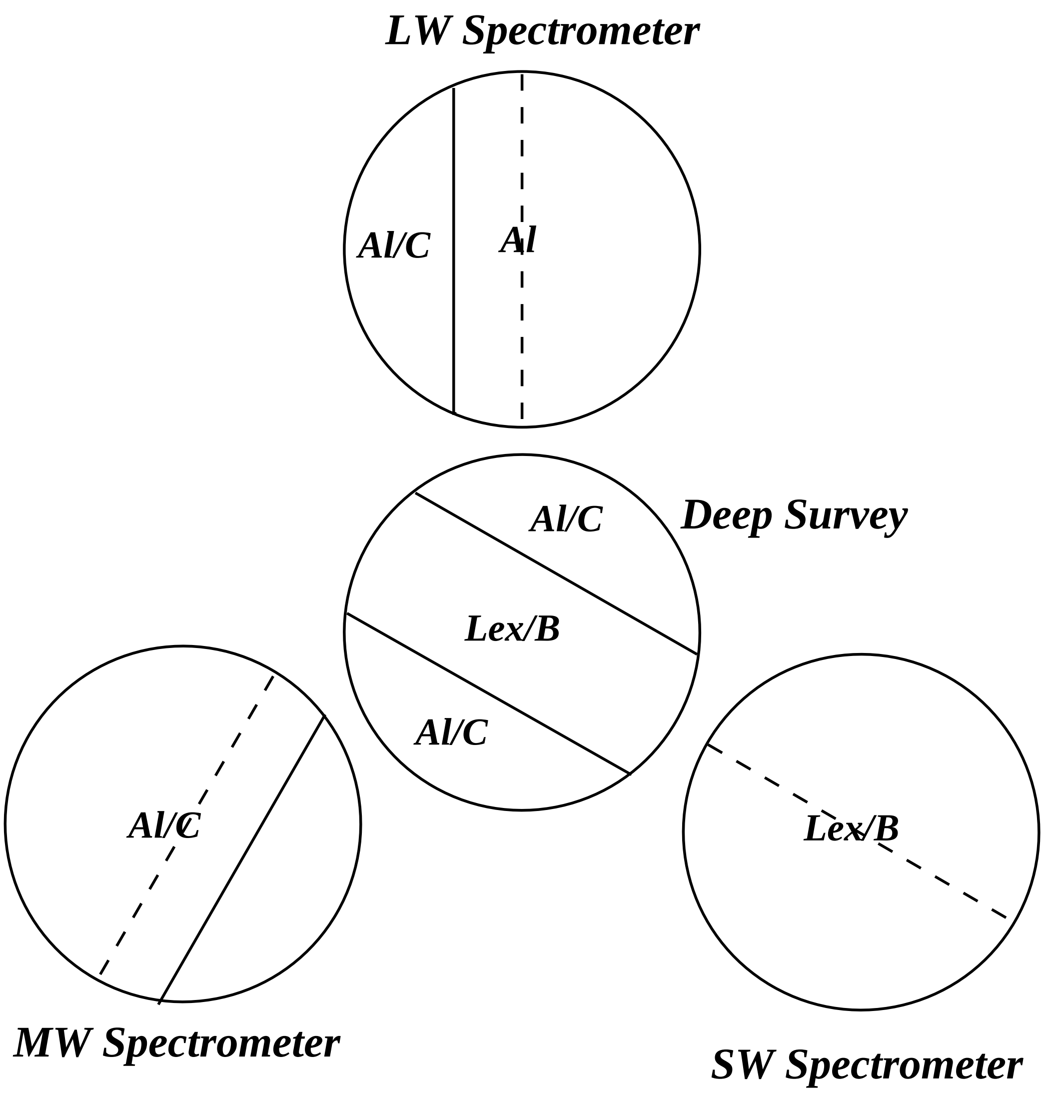

Figure 2-4: Spectrometer filter configuration. Dashed lines show orientation of spectra.

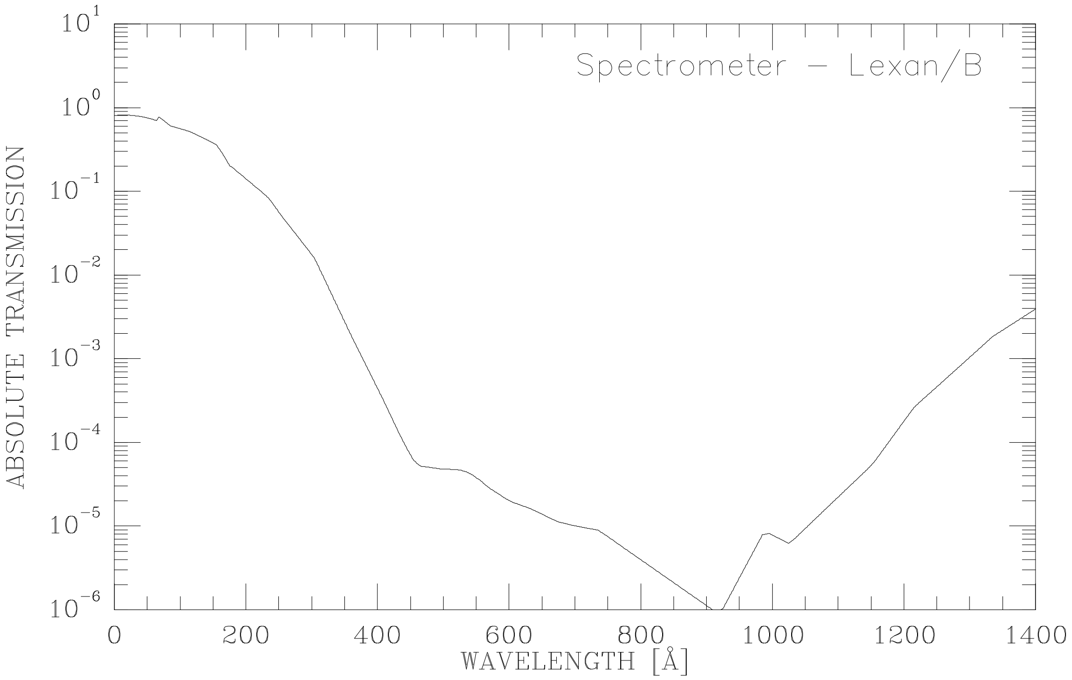

Figure 2-5: a) Spectrometer Lexan filter transmissions. Log scale.

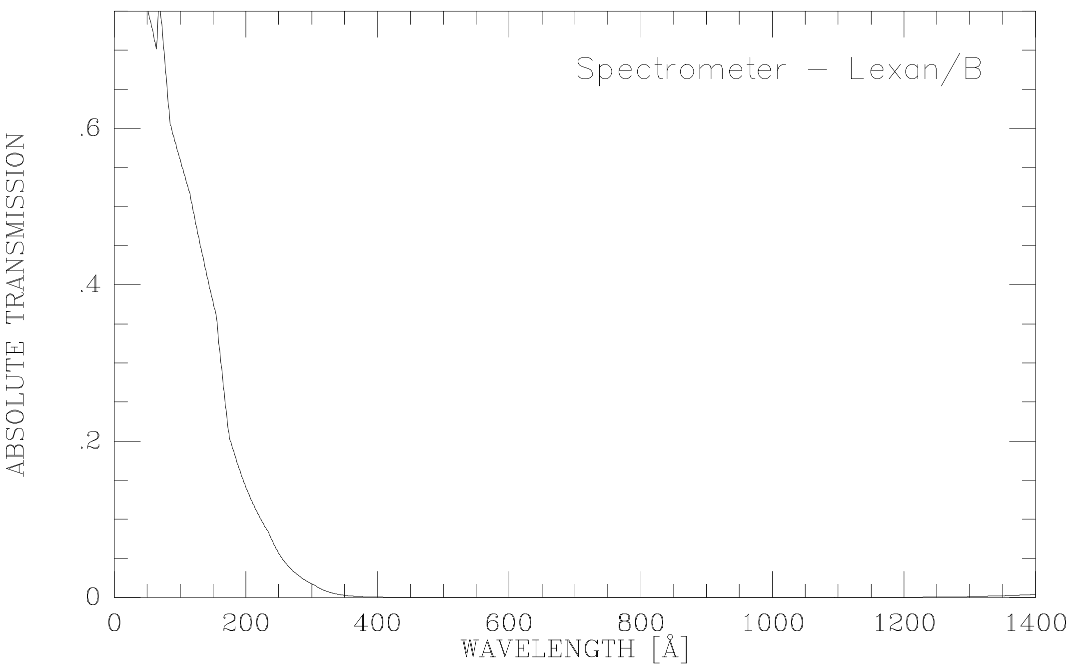

Figure 2-5: b) Spectrometer Lexan transmission. Linear scale.

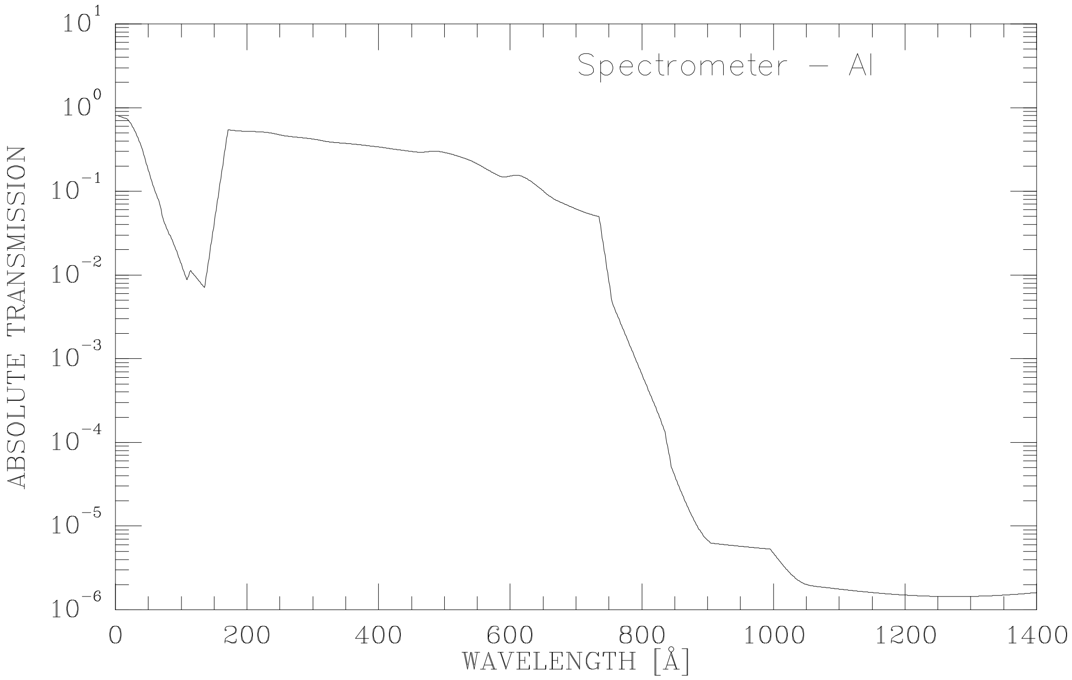

Figure 2-6: a) Spectrometer aluminum filter transmissions. Log scale.

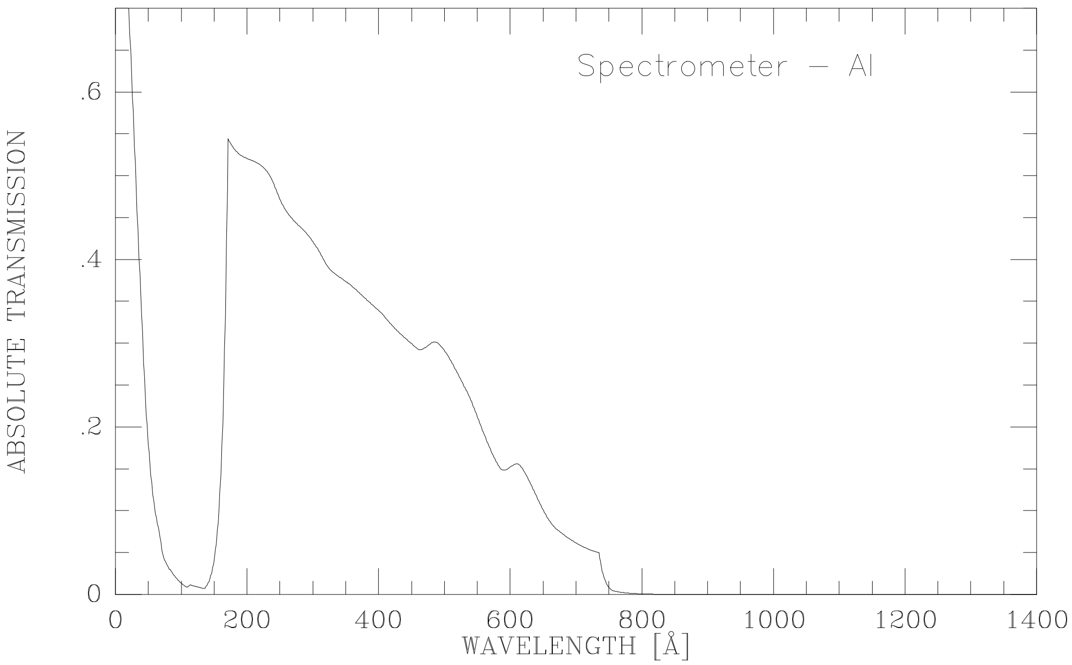

Figure 2-6: b) Spectrometer aluminum transmission. Linear scale.

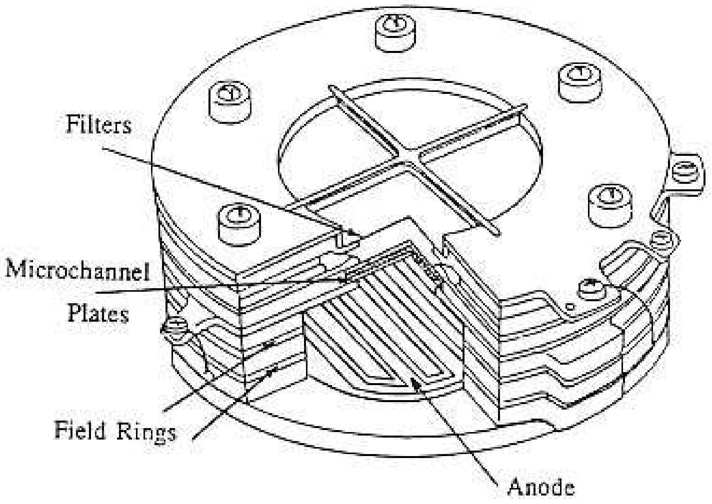

Figure 2-7: Cut away view of EUVE detector.

Figure 2-7 shows a cut-away view of a typical EUVE scanner detector. The Spectrometer has three MCP detectors, arranged at 120° intervals around the central Deep Survey detector. Recall that the Spectrometer filter design is shown in figure 2-4.

Each detector employs a biased stack of three porous quartz MCP's with a channel-length-to-diameter ratio of approximately 80:1. The stack acts as an electron multiplier, and is backed by a conducting anode, partitioned into a graduated "wedge, strip, and zigzag" pattern (see Figure 2-8). The top plate has an applied photocathode of potassium bromide (KBr) [21], to enhance the photoelectric response at EUV wavelengths. When a photon excites the front surface, a bias of 4-5 kV causes cascading electrons to form a cloud of 2-3$\times 10^7$ e^- which then strikes the divided anode.

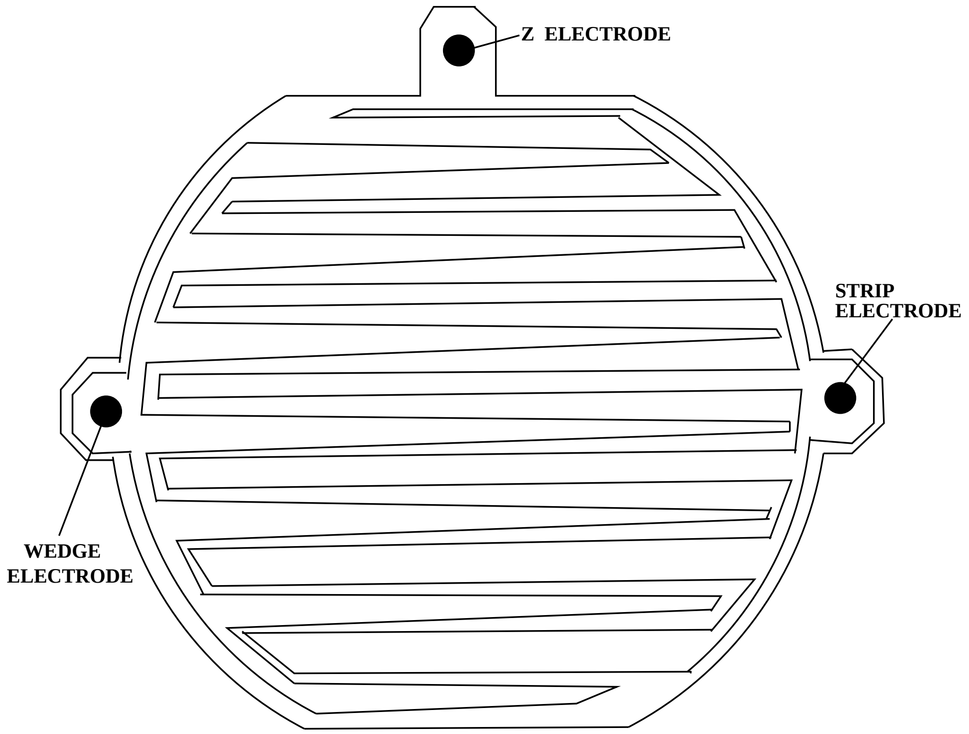

Figure 2-8: Wedge and strip anode pattern for MCP detector.

Event positions (X,Y) are calculated by on-board instrument software (ISW) from the division of the charge cloud among the wedge, strip, and zigzag areas of the anode. The detectors record positions $0 - 2047$ in each dimension, and a single pixel is about $29 \times 29\mu$. This results in a pixel size of roughly $4.\widehat{25''}$ when remapped to the sky.

All the detectors are equipped with four stimpulser, or "stim" pins, which periodically excite the anode at standard positions, and are used to monitor position stability. The detectors have been placed at the sagittal intersection to produce good imaging over the whole detector, rather than optimized spectral focus at one point.

MCP Fixed Pattern Noise

It has been known for some time that the EUVE spectrometer detectors exhibit a characteristic fixed pattern noise that produces quasi-periodic modulations in continuum spectra. This effect is caused by event locations being shifted near the boundaries of the "bundles" of quartz tubes which make up the MCP's.
A microchannel plate is a cross-section of many bundles of thin quartz tubes. The the bundles are packed together in a hexagonal pattern to make the microchannel boule. In the process, the areas at the edges of the bundles tend to get a few flattened tubes. In the finished microchannel plate, the deformed bundle borders form a regular hexagonal pattern where the surface has more "wall" than "hole".
When a photon event creates an electron cascade in the channel plates, the center of the electron cloud may be displaced if it falls on distorted channels, especially if this happens in the last plate, just before the cloud strikes the anode. Flux is conserved, but events are shifted away from the (regularly spaced) bundle borders. Shifts can occur in either the spectral or the imaging direction. A net modulation of 10 - 20% can be observed in continuum spectra on a scale of 16–20 pixels if enough events are accumulated.
This effect can cause spurious absorption or emission features to appear, and can displace existing line centers. The effect is most noticeable and troubling in observations of bright continuum sources, such as white dwarf stars. The observing strategy used to minimize this effect is usually referred to as "dithering", and is described in sections 3.3 and 4.2.

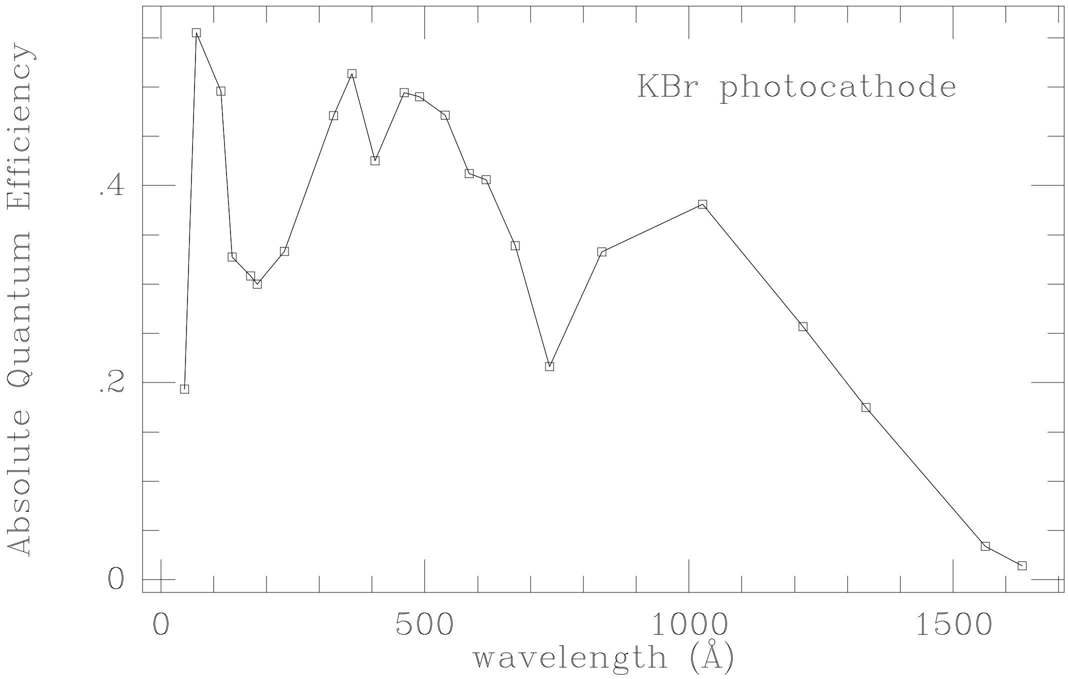

Figure 2-9: KBr photocathode QE for Spectrometer detector.

The quantum efficiency of each photocathode was measured at various EUV wavelengths. An example set of measurements is shown in figure 2-9. Spectral and angular resolution are both addressed quantitatively in chapter 3.

Table 2-2: The EUVE Spectrometer

	Short λ	**Medium λ**	**Long λ**
bandpass	70–190 Å	140–380 Å	280–760 Å
geometric area	72.44 cm^2	72.44 cm^2	72.44 cm^2
resolution element ($\Delta\lambda$)	0.367 – 0.636Å	0.731 – 1.27Å	1.46 – 2.54Å
collimator FWHM (spectral direction)	none	$20'$	$20'$
grating optical coating	rhodium	platinum	platinum
filter material	Lexan/boron 1588Å/1172Å	Al/carbon 1566Å/431Å	aluminum 1553Å
detector diameter	50 mm $5^\circ \times 2^\circ$	50 mm $5^\circ \times 2^\circ$	50 mm $5^\circ \times 2^\circ$
photocathode material	KBr	KBr	KBr

2.2.4.1 Instrument Electronics

Each detector in the science payload is supported by a separate set of amplifiers and analog-to-digital converters (ADCs), which convert the charge cloud partitions into pulses and calculate the X-Y coordinates of each photon event.

A separate telescope interface (TIF) unit handles logical switching and photon event data for each detector, and a relay interface (RIF) unit, controls power switching for the detector and mechanical door.

Data from all the detectors is processed by a central command, data, and power unit (CDP), which transmits photon data, commands and engineering information between the science payload and the spacecraft. The CDP also controls the spacecraft power interface via a redundant Remote Interface Unit (RIU). The simplified block diagram of the EUVE science payload in figure 2-10 shows the parallelism of the TIF's, and the redundant CDP modules.

Photon events in the several quadrants on each detector are input to telemetry (TM) by means of an algorithm called "primbsching", executed in the CDP, that allocates equal weight to events from each quadrant of the operating detectors. The algorithm guarantees an equal number of event "slots" to each quadrant; this prevents a single bandpass with high backgrounds from saturating the tes. The telemetry can transmit up to 437 events per second from any combination of the satellite detectors.

2.2.5 Spectrometer Calibration

This section gives a qualitative account of the the Spectrometer calibration, to acquaint users with the current level of knowledge about the instrument. Quantitative results of measurements and useful characteristic functions are given in chapter 3. New results are made available periodically through the CEA/EUVE *ftp* site and the NASA ADS, and referenced in the literature as they are produced.

The performance of each individual component for the EUVE science payload was tested in the vacuum ultraviolet calibration facility at Berkeley. Tests of the fully assembled Spectrometer measured effective area and order efficiency as a function of wavelength, imaging under various temperature conditions, and spectral resolution. The tests employed both monochromatic light and full spectra from several sources of EUV light. All calibration measurements used NIST calibrated EUV and FUV photodiodes as primary standards and were cross-checked with instrument simulations. More specific information about ground-based calibration of the EUVE Spectrometer may be found in [31] and [14].

In-orbit calibration observations with the Spectrometer were made each month during the first two years after launch, and continue as needed. The Spectrometer wavelength scale, and the imaging and effective areas of all EUVE instruments are monitored on an ongoing basis. Measurements of the DS/S boresight position are made using the positions of images in the Deep Survey instrument. Early results of in-orbit calibrations are summarized in [5]. The instrument characteristics given in Chapter 3 and available in tabular form from the CEA *ftp* site represent the most recent results of instrument monitoring in the areas discussed below.

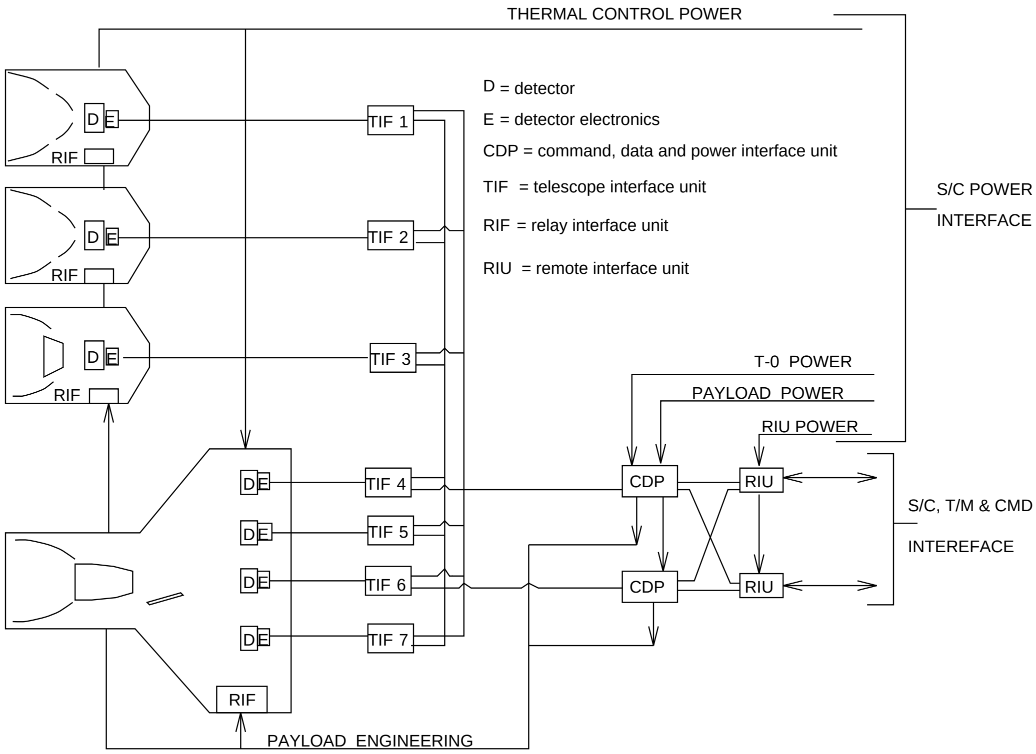

Figure 2-10: EUVE science payload electronics block diagram

2.2.5.1 Effective Area Calibration

Because of the lack of "standard stars" in the EUV, effective areas for the Spectrometer are determined from model spectra for continuum sources. Observations of white dwarf stars provide the baseline measurements. Calibration targets are selected to minimize order confusion. After spectra are extracted, white dwarf model spectra for the object are input to a Spectrometer simulation program, and the model parameters adjusted to produce simulated data that match the observed spectra as nearly as possible. In most cases, the effective temperature and gravity are well constrained by other optical and ultraviolet spectra. The resulting models are then compared whenever possible to photometric and spectroscopic EUV/soft X-ray observations of the same target made with the ROSAT Wide Field Camera, EXOSAT, HUT, IUE, and various rocket experiments. The effective area function is then adjusted to bring the measurements into better agreement. This process is repeated until the effective area function is stable and consistent with accepted error levels in the other measurements.

2.2.5.2 Wavelength Calibration and Spectral Resolution

The above method of arriving at the effective area by comparing spectra relies on an accurate wavelength solution. Spectrometer channel wavelength scales have been calibrated in-orbit by making observations of several well-known line-emission sources before and during the sky survey. Wavelength solutions are determined from line identifications in spectra obtained with both boresight and off-axis pointings during pre-launch and in-orbit calibrations. Polynomial functions of the detector coordinates and the off-axis angles are fit to the observed line positions to produce a wavelength vs. position function. This approach allows the assignment of both a wavelength and a position angle to each photon event, and is independent of aspect correction to a first approximation. An example of an emission spectrum used in the wavelength calibration is plotted in figure 2-11.

2.2.5.3 Spectral Resolution Measurements

The full width at half maximum (FWHM) for a number of unblended lines has been measured in spectra from EUVE calibration observations of late type stars and other emission sources. The results are consistent with pre-launch measurements. These tests check both the spectral resolution of the Spectrometer and the pointing stability of the spacecraft.

2.2.5.4 Polarization

Since grazing incidence reflections tend to be strongly polarizing, polarization in the Spectrometer was measured in pre-launch calibration. As a result of these measurements, some correction for polarization effects in the EUV may be possible[2] for some observations. The Spectrometer throughput for linearly polarized light varies sinusoidally as the instrument is rotated, and the amplitude of the resulting curve characterizes the Spectrometer's response at that wavelength. The modulation is also more pronounced when the polarization vector is oriented radially to the aperture plane (see figure 3-20 for aperture and detector orientations). The throughput amplitude was measured with monochromatic beams of polarized light at a number of wavelengths, and roll angles up to 135 degrees. A simulation of this function, based on Spectrometer raytraces and scaled to bring it into agreement with the calibration measurements, is plotted in figure 2-12. The amplitudes have been normalized by dividing by the average throughput.

[2] Removal of polarization effects is not directly supported by the EGO Center

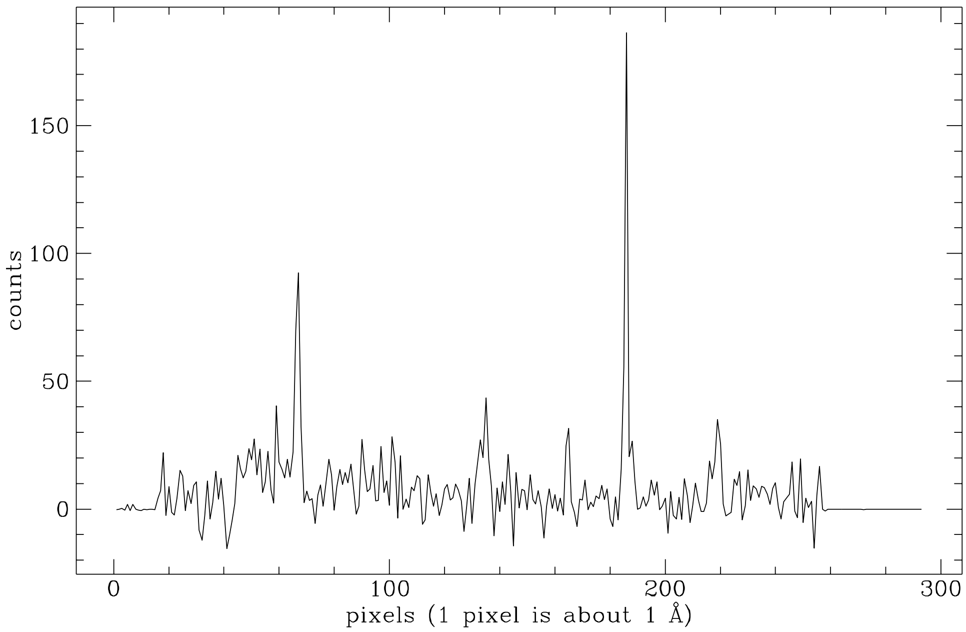

Figure 2-11: SW spectrum of the calibration target AU Mic.

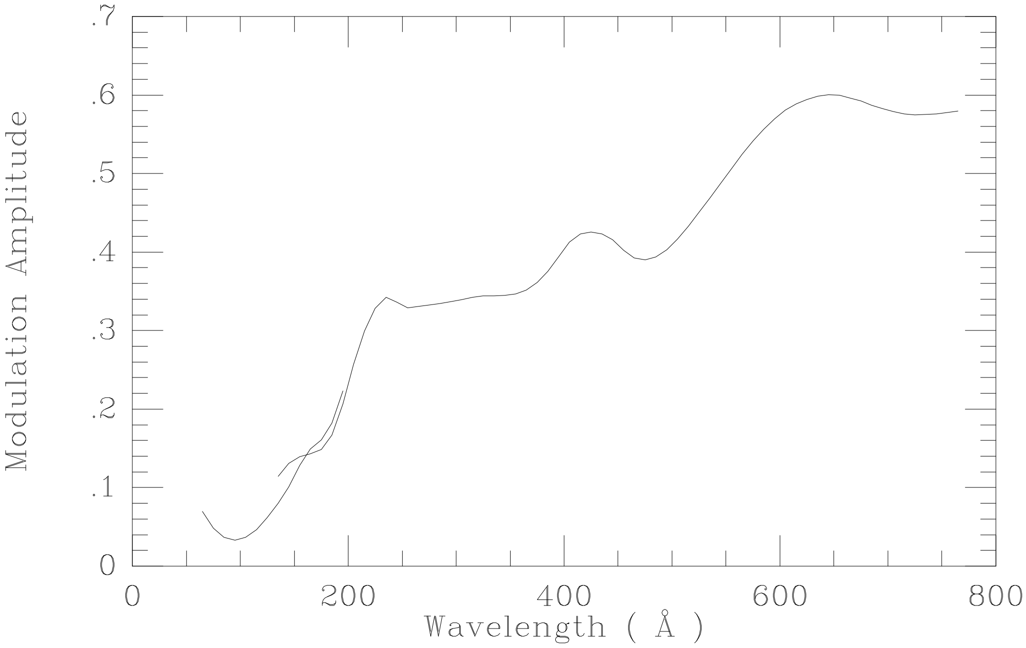

Figure 2-12: Throughput modulation amplitude of a fully polarized source normalized by average throughput. Results of instrument simulation.

2.3 The Deep Survey: an EUV Imaging System

Each of the EUVE survey instruments, is composed of a two-stage grazing incidence mirror, and an MCP detector, with thin film filters. The sky survey instruments (Scanners A, B, and C) are described further in Appendix A. The Deep Survey instrument is a short-wavelength imaging system which takes advantage of the larger geometric area of the DS/S telescope. It is coaxial with the Spectrometer and shares the same mirror assembly.

2.3.0.5 Wavelength Coverage in the Deep Survey Instrument

The Deep Survey instrument operates in a short-wavelength region similar to the bandpasses of Scanners A and B. Its detector is located at the central focus of the DS/S telescope. The detector has a MgF_2 photocathode which enhances quantum efficiency between 50 and 800 Å. The filter is divided into three sections (see figure 2-4). The center section is boron-coated Lexan. Two panels of aluminum and carbon on either side define a second bandpass. Parameters of the detector and filters are listed in table 2-3. Transmissions of the Deep Survey filter materials are shown in figure 2-14. A plot of the effective area, as modeled from pre-launch and in-orbit calibrations, is shown in figure 2-13.

The Deep Survey operates continuously during the pointed phase of the mission. DS Lexan band count rates and image centroids may be used in some data analysis options to help define spacecraft pointing or produce broad band light curves. Obtaining images and count rates in the aluminum/carbon filter during pointed observations will require pointing the DS/S off-axis. However, the instrument PSF degrades considerably for points near the edge of the field of view. Therefore, DS images from the Al/C filters will require longer exposures in proportion to the FWHM, than images from the Lexan filter, to achieve the same photometric signal-to-noise.

2.3.1 Deep Survey Detector Gain

The Deep Survey detector, is known to have developed an area of decreased gain, or "dead spot". This is probably because of extended exposure to very high count rates, during observations of the white dwarf HZ43 in February, 1993. The spot is an area of approximate diameter $\overset{\frown}{4'}$ in X by $\overset{\frown}{3'}$ in Y, centered at $X = 1033, Y = 1035 \pm 1$, where the quantum efficiency has been degraded by up to 80% at the center. The outer dimensions roughly limit the area with less than 85% of the normal QE. Current strategy to minimize the dead spot's impact on DSS science is to point the instrument off-axis, at an angle which places the DS image outside the areas with the worst gain, while not significantly defocussing either the DS image or the spectrum.

Table 2-3: Deep Survey filters and detector

Deep Survey

Filter Quadrant	**Material**	**Bandpass**	**Broadband MDF**
0 (center)	1498 Å Lexan/1172 Å boron	40–190 Å	2.3 μJy
1,2 (sides)	2039 Å Al/399 Å carbon	160–385 Å	110.0 μJy

Detector Photocathode	MgF_2

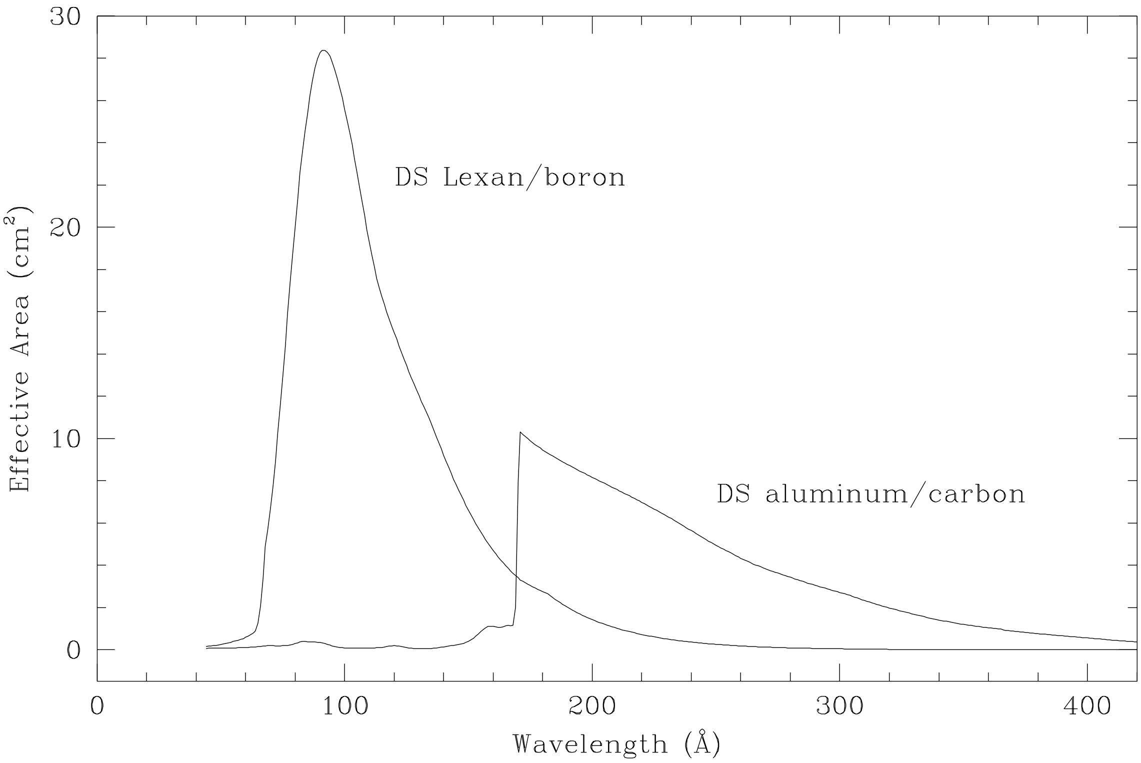

Figure 2-13: Effective areas for the Deep Survey instrument. The shorter wavelength curve is a fit to measurements of the central Lexan/B filter[3]. The longer wavelength curve is derived from measurements of both the Al/C quadrants.

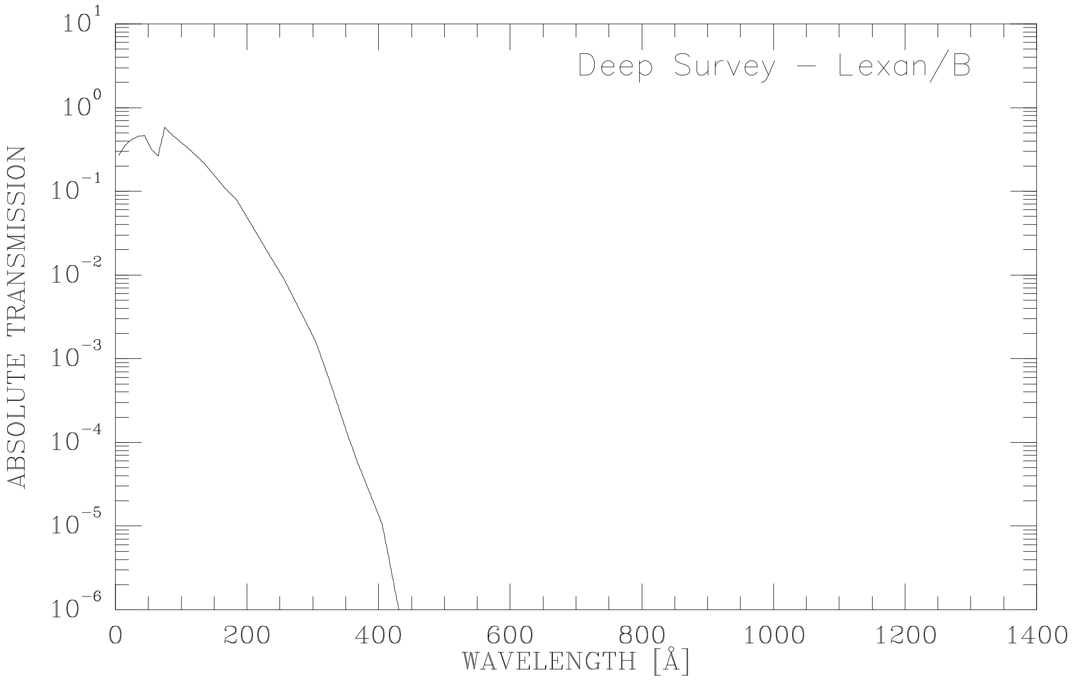

Figure 2-14: a) Deep Survey Lexan filter transmission. Log scale.

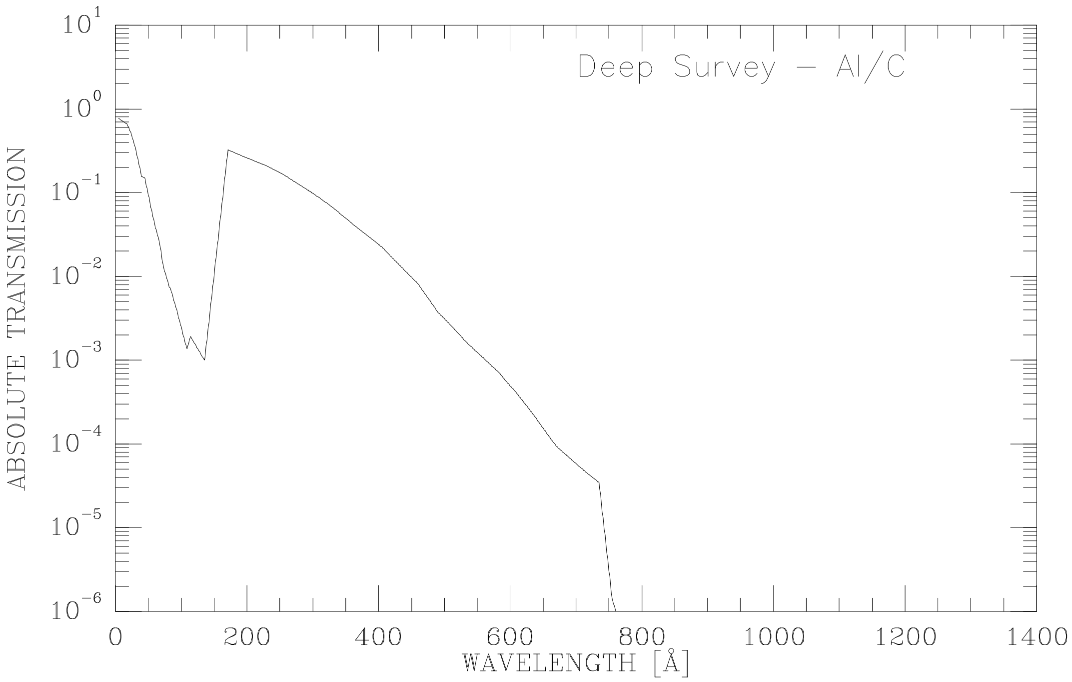

Figure 2-14: b) Deep Survey aluminum/carbon filter transmission. Log scale.

PLANNING OBSERVATIONS

3.1 Introduction

In completing their proposal forms, proposers must confirm as nearly as possible the technical feasibility of their observations by submitting a separate Technical Justification for each one. This chapter provides calibration information about the EUVE Spectrometer, and guidelines for calculating observation parameters. Section 3.2 contains information on various software and data resources that are made available electronically by the EGO Center to help with Techinical Justification. Section 3.3 is provided to help determine quickly whether a prospective target is observable and merits further calculation to determine the required exposure time. In Sections 3.4, 3.5, and 3.6, the instrument's performance is described in terms of the effective area, spectral resolution, and average background, each a characteristic function of wavelength. These functions represent the most current knowledge of the instrument's performance and operating environment, based on both pre-launch measurements and in-orbit calibration observations.

The functions can be used with model source spectra to calculate instrument count rates and exposure times, generate simulated raw count spectra for proposed targets, and simulate the resolution of instrument spectra. The application of all the instrument characteristics to Technical Justification is discussed and illustrated with example calculations using simulated source spectra and the properties of the Spectrometer.

Section 3.7 provides two variations on a basic formula for calculating signal-to-noise levels for proposed observations once the source and background count rates have been estimated. Integration times for a required signal-to-noise level. can also be calculated from instrument count rates. In addition to the Technical Justification, these quantities are also required to fill out part 2 of the Target Summary Form which must be submitted with each proposal for Spectrometer observations. Technical Justifications for observations with the Scanners or Deep Survey instrument should follow similar lines, using the broadband instrument characteristics in sections 2.3 and A.3.

Sections 3.10, 3.8 and 3.11 present suggestions for planning spectroscopy of diffuse and extended sources, time-critical observations, and multiple sources. Section 3.9 outlines the treatment of proposals for targets of opportunity (TOO). The chapter ends with summary tables of reference constants and useful equations.

It is understood that estimates and simulations are somewhat uncertain. The guidelines of this chapter are intended to encourage well-prepared proposals, which can be considered comparable for the purposes of technical review. Proposers should consult the current UCB/EUVE Call for Observing Proposals, for the specific content requirements. Any necessary clarification of the *Handbook* contents may be obtained by sending mail to:

egoinfo@cea.berkeley.edu

3.2 Electronic Resources for Proposers

As stated in chapter 1, documentation and forms for the UCB/EUVE Call for Observing Proposals, including the forms and instructions for electronic submission, are available from the EGO Center via the CEA/EUVE anonymous *ftp* site, and the *WWW* site. In addition to the text and forms, a number of useful files and software tools are also available to aid applicants in preparing their proposals. You can access the *ftp* site by typing:

% `ftp ftp.cea.berkeley.edu`

or

% `ftp 128.32.154.12`

or by using the World Wide Web (*WWW*) URL:

http://www.cea.berkeley.edu/

Some of the following information is redundant with section 1.4.1, but different parts of the *ftp* site will be referenced, and some resources are available only through the *WWW*.

3.2.1 Access to *ftp* and *WWW* Online Software

The easiest way to access all electronic resources for proposal preparation is via the *WWW*. All materials specifically regarding this Call for Proposals are available via CEA's *WWW* site at URL:

http://www.cea.berkeley.edu/nra97

The Uniform Resource Locator (URL) for the CEA HomePage is:

http://www.cea.berkeley.edu/

After opening the Home Page, proposers can use mouse selections to access the *ftp* site, print the required materials, save them to disk, or obtain copies of the EGO Center software and instrument reference data. To access the CEA *ftp* site via the CEA *WWW* HomePage, select the item labeled **"FTP Access"**. This will list the top level directory of the CEA/EUVE *ftp* site. Select the directory *nra97* to view the recent Call for Proposals material. Be sure to view the file *README.txt* in this directory to get the most up-to-date instructions on accessing Call for Proposals material.

If necessary, one may obtain Call for Proposals information by sending mail to the *egoinfo* mail address given in section 3.1 above, but this will require additional turn-around time.

3.2.2 Instrument data files

Tabular listings of the Spectrometer effective area, spectral resolution, and background count rates used throughout this chapter are available from the CEA/EUVE *ftp* site. These functions are presented graphically in this chapter, and interpolated values are used in many of the example calculations.

Instrument function files are in the directory */pub/nra97/data*. To obtain data files using *ftp*, log onto the CEA/EUVE *ftp* site as in section 1.4.1, and go to the directory */pub/nra97/data*:

ftp> `cd /pub/nra97/data`

Be sure to view the *README_dat.txt* in this directory. Use the *ftp* command *get* to obtain the information file *README_dat.txt*:

ftp> `bin`

ftp> `get README_dat.txt`

This file contains a directory to the data files. The file names are:

README_dat.txt	Information on data file formats
(sw/mw/lw)_mdf.txt	Minimum detectable flux functions
(sw/mw/lw)_ea1.txt	Effective area in -1st order, for short, medium, and long wavelength channels
(sw/mw/lw)_res.txt	Channel spectral resolutions
(sw/mw/lw)_bgspec.txt	Channel background spectra
(sw/mw)_ea2.txt	Channel effective areas in -2nd order
lw_ea234.txt	-2nd, -3rd, and -4th order effective areas for long wavelength channel
data.tar	A single tar file containing all the above data files.

Then use the *get* command to obtain selected data files, or the entire set of files in tar file format.

3.2.3 IRAF/EUV Software Packages

Some tasks in the IRAF/EUV data reduction software will be helpful to experienced IRAF users for proposal preparation. The simulated instrument spectra used to illustrate the example calculations were produced in IRAF with version 1.4 of the IRAF/EUV software packages, and version 1.8.1 of the reference data. The tasks **mkeuvspec**, for rebinning continuum spectra, and the Spectrometer simulation task **specmod**, were used. The software packages are available in complete form from the CEA/EUVE *ftp* site, in the directory

/pub/software/euv1.7 [1]. It is strongly recommended that users obtain the *README* file and read that first. The */pub/software/euv1.7* directory site includes instructions for installing the packages in your local IRAF environment. The calibration data necessary for running some of the tasks reside in the *ftp* directory */pub/reference/egodata1.14*. A Software User's Guide may be obtained from the */pub/documents* directory.

The IRAF/EUV task **specmod** was used to produce the simulated observation spectra shown in this chapter. **Specmod** takes a list of line fluxes or a one-dimensional spectrum image in photons/cm^2/sec as input, and multiplies each value by the user-supplied integration time, and the instrument effective area. The resulting spectrum is convolved with an instrument point spread function, and rebinned with a bin width (w) chosen by the user.

Note that the input to **specmod** must be in units of photons/cm^2/sec. Model spectra for continuum sources generally have units of photons/cm^2/sec/Å, and must be converted into an IRAF spectral image in photons/cm^2/sec before being input to **specmod**, using the IRAF/EUV task **euvtools.mkeuvspec**. **Mkeuvspec** takes a two-column ASCII file of wavelength and photons/cm^2/sec/Å as input, interpolates and partitions the spectrum according to the output resolution specified by the user, and multiplies each value by the desired output bin width to produce a spectrum in photon flux units for input to **specmod**. It is generally advisable when rebinning input spectra for **specmod** to choose a resolution greater than that required for the simulated spectrum to be produced, by a factor of 2–4.

3.2.4 WWW Utilities

The CEA *WWW* HomePage also contains an Guest Observer HomePage, which provides a number of services, including two routines that may be helpful in writing GO proposals. Select the **"Science"** link, followed by **"The Guest Observer Program"** links, to view the GO HomePage. Following the **"Resources for Proposers and Observers"** and **"Science Tools and Software"** links, followed by link item titled **"Target Visibility"** will lead to a service that creates a plot showing the approximate suitability of a target for viewing over a period of one year, based on target coordinates and instrument/spacecraft pointing constraints. The selection titled **"ISM Server"**[2] calculates the attenuation of a number of sample wavelengths, given the column densities of HI, HeI, and HeII. These services are only provided via the *WWW*.

3.3 Observability

For an object to be observable with EUVE, its position must be accessible to the chosen instruments for a sufficient period, and its flux must be bright enough after attenuation by the intervening HeI/HIcolumn to be detected by the instruments in the requested exposure time. For technical reviews, it is assumed that proposed targets have been tested for suitability of position and minimal observability by the proposer.

[1] This directory is separate from the Call for Proposals directory, *nra97*

[2] based on the description of the ISM absorption in "Interstellar Medium Continuum, Autoionization, and Line Absorption in the Extreme Ultraviolet" by T. Rumph, C.S. Bowyer, and S. Vennes, 1994 AJ (in press)

The Technical Justification of observations does require specific demonstration that each proposed target will produce spectra with the expected count rates and signal-to-noise ratio. Demonstrations may be based on either source and ISM models, or previous observations in the EUV. In cases where the object has already been observed in the EUVE all-sky survey, ROSAT WFC sky survey or with a comparable spectroscopic instrument, proposers can apply these results directly to the Technical Justification.

Any special pointing requests, including requests for dithered observations, should be justified in terms of required S/N. Dithering refers to a strategy of making many pointings near a target, to wash out pseudo-periodic fixed pattern noise in the detectors. At this time, dithering is only applied to sources with a continuum spectrum whose S/N is 10 or more in a single resolution element($\Delta\lambda$). The size of a resolution element is defined in section 3.5. Proposers should request dithering for targets with unknown EUV brightness or spectral distribution, but the EGO Program cannot guarantee this treatment for any proposed source. See section 4.2 for operational details of dithered observations.

In addition, it has been determined that the Deep Survey detector has been damaged near the center. For this reason, observations of EUV objects with instrument count rates greater than 1-3 counts per second in the Deep Survey instrument will be disallowed within .3 degrees of boresight. Higher count rates may be acceptable near the outside of the field of view, but images will be poorly focussed.

3.3.1 Source Position

Observations with EUVE are conducted under some constraints on certain target positions at some times. Pointing directions are limited to no more than 90 degrees from the anti-sun direction. There are also some restrictions on roll angles to prevent excessive heating of the spacecraft in some attitudes. Proposers should be aware that these constraints will impose an upper limit on the total amount of time that any particular target can be observed during the pointed period covered by the current Call for Proposals.

The suitability of a target may be tested for a limited range of roll angles using the **Target Visibility** routine available through the GO Homepage on the *WWW* (see sections 3.2 and 3.2.1). This program plots and lists suitability of a target, on a scale of $0-1$ for each day over in a year. A suitability of 0 means the target is not observable, and a value of 1 means that conditions for beginning a continuous observation of the required length are optimal on that day. Suitability is based on anti-sun angle, a range of ± 10 degrees in roll angle, earth occultation of the target, availability of guide stars, and interference from bright objects, like the moon, in the star trackers. Each calendar day corresponds to approximately 25 ksec of nighttime observing.

An example of the output of **Target Visibility** for the white dwarf HZ43 is shown in figure 3-1.

Suitability of HZ43

- Right Ascension: 13:16:21.9 (199.0913)
- Declination: +29:05:57.0 (29.0992)
- Exposure: 40000

Suitability 04/01/94 – 04/01/95

The following image is a plot of the suitability values listed below. The suitability is plotted for one year starting with this month. Suitability curves vary from 0 (not suitable) to 1 (best suitability). These results are very coarse with a resolution of 1 day and only sampling roll angles at 10 degree.

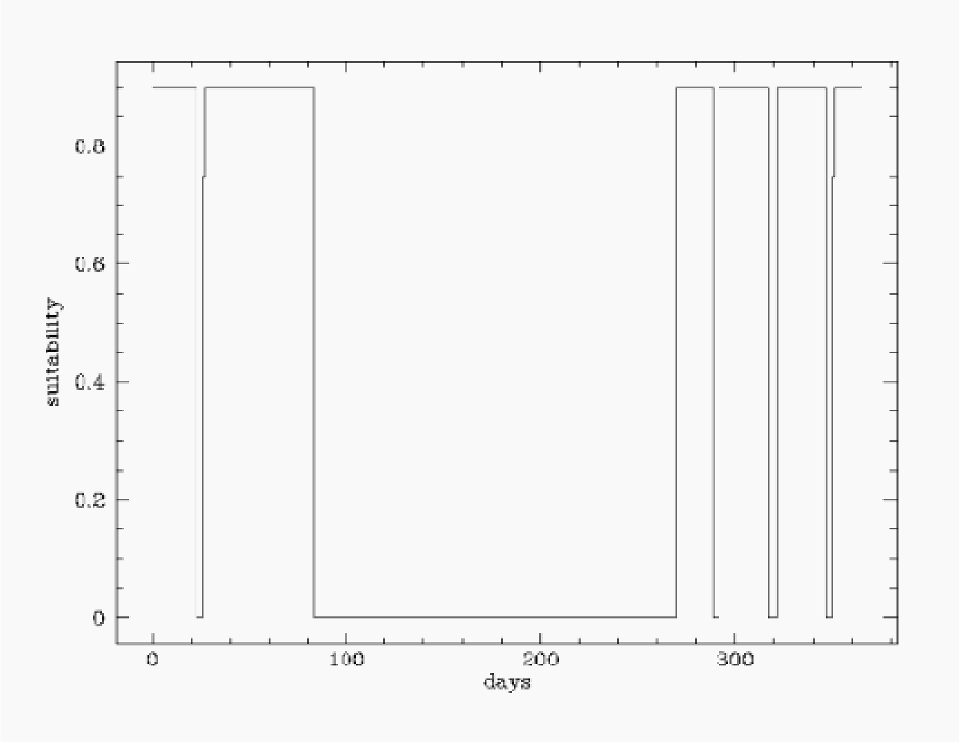

Days From 04/01/94 Through 04/01/95

Figure 3-1: Target visibility for example object HZ43 during one year, for roll angles in the range $(-10 - +10)$.

The suitability is about .9 for just under half the days in the year starting on April 6, 1994. For many targets, this program will report a large number of days when the target suitability is above .5, but this does not take into account any requirements for the scheduling of other targets, which may be more constrained. Proposers requesting repeated observations may want to run the visibility routine to confirm that their target(s) will be available for several times the required period. Proposers whose observations are in any way time-critical (e.g. TOO's, periodic events, or coordinated observations) can use the visibility routine to check which parts of the year their target is available.

Note that the existence of days with high suitability does not guarantee that the target will be scheduled on the first, or even any, of these days. The main utility of the program is to identify targets which are mostly unsuitable, or which would be difficult to schedule if other requirements were added, as in programs of coordinated observations. Other physical limitations on pointing and scheduling than those mentioned may further limit target availability. Refer to section 4.3 in chapter 4 for more detail on policies concerning satellite pointing and the handling of anomalies in the observation schedule.

3.3.2 Model Spectra and Predicted Fluxes

In cases where the target flux to the telescope is not available from existing observational data, proposers should use a model spectrum for the target which accounts for both the source flux and interstellar absorption. The Scientific Justification section of such proposals must explain briefly how input fluxes rates for each proposed target were derived, including the type of source flux model and the simulation of absorption by the interstellar HeI/HI column. The assumed hydrogen column density to each source must also be noted on the Target Summary Form. Simulated spectra are not required in the proposals, but proposers are encouraged to present a spectral model for continuum sources if possible, as this can be very helpful for both the Technical Justification, and the technical review process.

Any model spectrum used for Technical Justification must represent the source flux *at the telescope.* This means that both the source physics AND the effect of interstellar medium (ISM) absorption must be accounted for. All instrument characteristics and equations given in this chapter are intended for use with estimates of source flux *after* ISM absorption.

Proposers may wish to use the "ISM server" routine in the GO *WWW* HomePage to calculate the effects of ISM attenuation on their model spectra. Proposers should keep in mind that this routine is based on a particular model of the ISM [18]. It provides estimates of attenuation, but accuracy cannot be guaranteed, and results are highly dependent on the choice of column densities input. The same routine is also available as the IRAF task **euvspec.ism** in the IRAF/EUV software package, version 1.4.

Absorption models and hydrogen column densities can be found in a number of references, such as [18], [15], and [10]. A more complete list of references for column densities to specific targets is included in Appendix C of this *Handbook.* A table of attenuation factors produced by the ISM server for a HeI/HIration of .1 is included in in the directory *nra97/data* of the CEA/EUVE *ftp* site. If a particularly low column density (e.g. $\leq 10^{18}$) is assumed, the proposer must justify the figure on the basis of a previous observation of the same source or one nearby.

Throughout the rest of this chapter, line emission sources and continuum objects are often treated separately. Model spectra for emission sources may consist of a list of fluxes in photons/cm^2/sec. Each line will be treated as a δ-function, and fluxes should represent an integration over the width of the line. Model spectra for continuum sources must be expressed in units of photons/cm^2/sec/Å as a function of wavelength in all Technical Justification materials. Bin sizes must be clearly stated, and the wavelength of each bin will be assumed to be at the center. Sources with lines as wide or wider than a resolution element, or those with both continuum and emission features, should be treated as continuum sources. Spectra representing diffuse or extended sources, such as the moon, clouds, or filaments, may be expressed in photons/cm^2/sec/Å/sr. Note that these units are proportional to, but not equivalent to Rayleighs.

3.3.3 Minimum Detectable Flux

Observability of potential targets in the EUV can be tested at a go/no-go level by comparing model spectra to calculated minimum detectable flux functions. Curves representing the minimum detectable flux (MDF) as a function of wavelength have been made by folding the Spectrometer effective area function together with the expected background rates from diffuse airglow, scattered light, and detector noise at each wavelength. This produces a "bottom line" spectrum which the source flux ($\mathcal{F}$) at the telescope must exceed to be detected at the $3-\sigma$ level within a nominal exposure ($\mathcal{T}$) of 40K seconds.

The MDF function thus represents the calibrated sensitivity of the instrument, in units of photon flux from the source, and can be compared directly to flux measurements or model source spectra in the appropriate units. Model source spectra to be compared to the MDF must include interstellar absorption between the source and the instrument.

Separate MDF functions are included for sources characterized by emission lines and by continuum spectra. Both functions exhibit the wavelength cutoffs of the filter materials in each channel, and the effect of diffuse geocoronal light, which causes the peaks at 304 Å and from 584 to 608 Å, where 304 appears in second order.

At its lowest points, the MDF is determined mostly by the Spectrometer effective areas, intrinsic channel plate noise, and the rate of particle detections. See section 3.6 for a discussion of the count rates associated with these sources of background.

NOTE: SHOWING THAT EXPECTED SOURCE FLUX EXCEEDS THE MDF IS NOT ADEQUATE TECHNICAL JUSTIFICATION for any observation. The MDF functions are provided to help observers quickly assess the viability of targets before embarking on these more complex calculations. Ability to obtain acceptable signal-to-noise levels within a specified integration time must also be demonstrated.

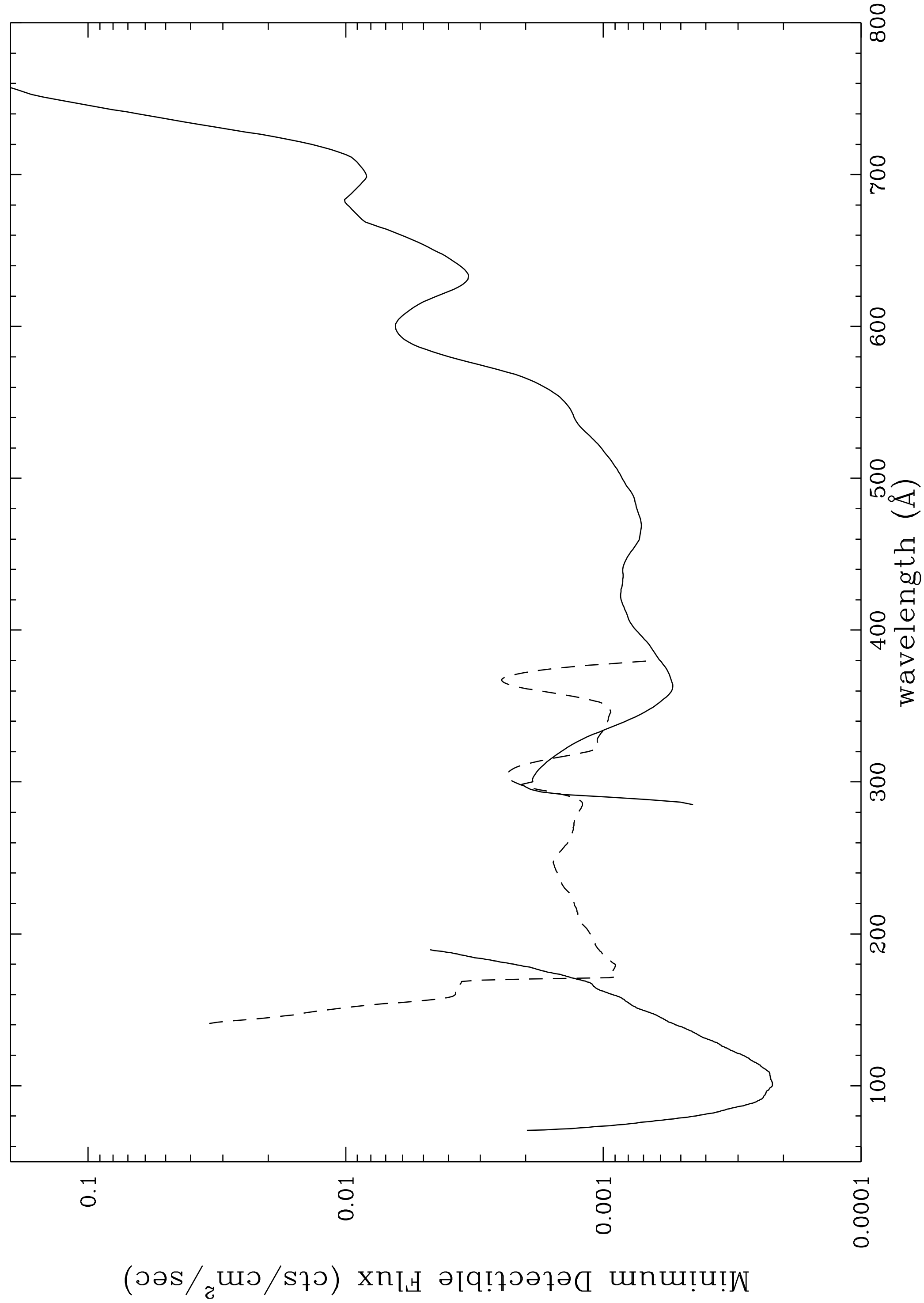

Figure 3–2: Minimum detectable flux for line sources; dashed line is medium wavelength channel.

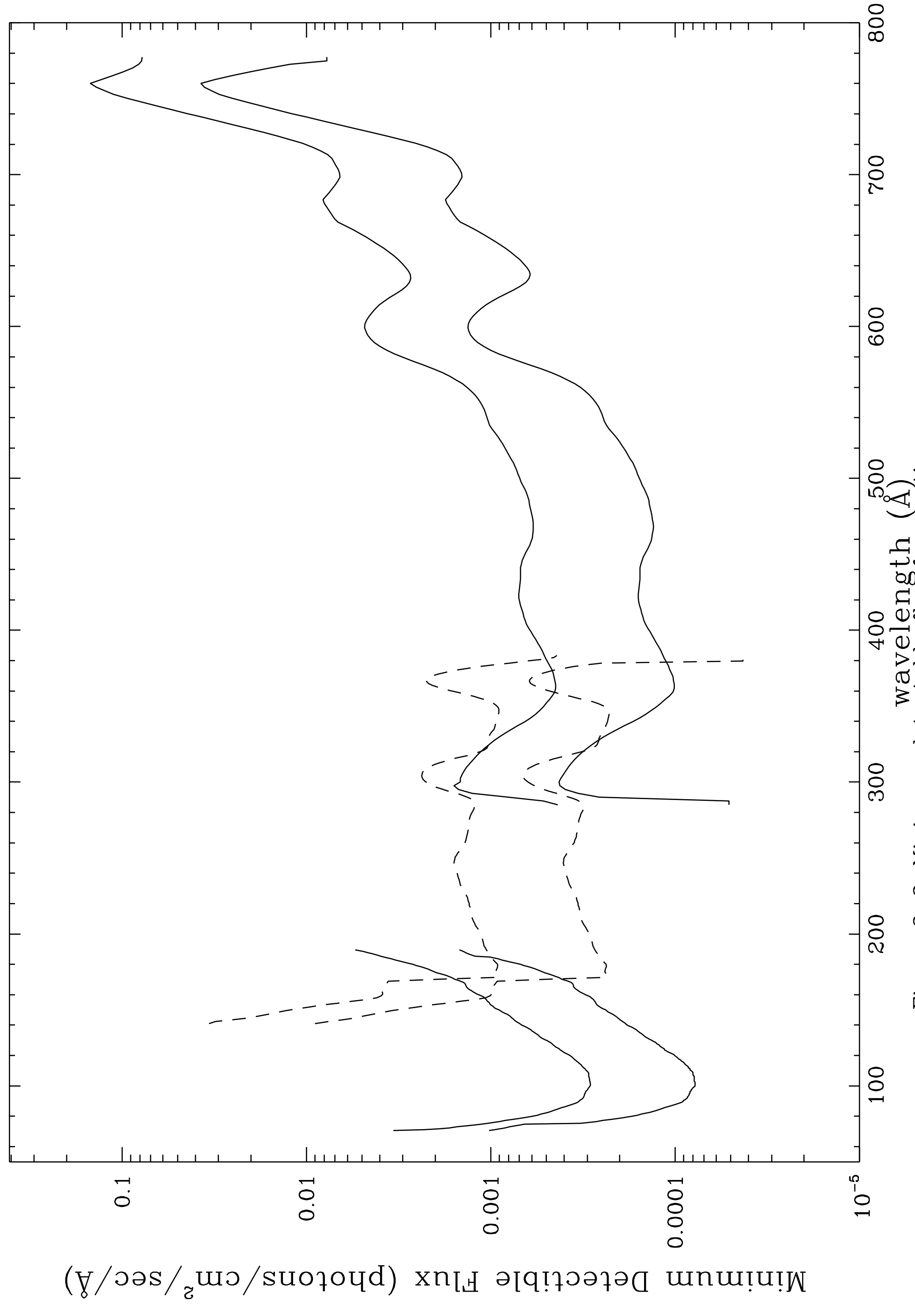

Figure 3−3: Minimum detectable flux for continuum sources.
Upper curve: 1(Å)/bin; lower curve: 10 (Å)/bin.

3.3.3.1 Emission Line Sources

Figure 3-2 shows a graph of the MDF function for line emission in each channel, in photon flux units, appropriate for comparison to a list of integrated line fluxes. Proposers using model spectra in photons/cm^2/sec/Å should use the continuum MDF function in the next section. The plot was made using values from the second column in the tables *sw_mdf.txt, mw_mdf.txt*, and *lw_mdf.txt*, which are available from the *ftp* site as given in section 3.2[3]. The function for the medium wavelength channel is set off as a dashed line to distinguish it from the short and long wavelength ranges.

The nominal exposure of 40K seconds used to produce the MDF was chosen somewhat arbitrarily, so the shape of the function is more important than the levels literally depicted here. If a source's expected flux ($\mathcal{F}$) is marginal or below the MDF function, a 3-σ observation might be achieved with a longer integration. Since σ for Poisson counting statistics is equal to the square root of the time-integrated source signal (S), the signal-to-noise S/σ is proportional to $\sqrt{T}$. This means a 3-σ measurement can be obtained from a flux lower than the MDF by multiplying the observation time by the factor: $\left(\frac{\mathrm{MDF}}{\mathcal{F}}\right)^2$. More detailed formulae for calculating observing times and signal quality are presented in section 3.7. The practical limit on the duration of any single observation will be determined by the Peer Review Panel and scheduling requirements.

Example: Emission source observability An example spectrum for an arbitrary late-type star model is shown in figure 3-4. The model consists of fluxes at a number of wavelengths, in photons/cm^2/sec. Lines have been approximated as δ-functions, with an intrinsic width of $\lambda/\Delta\lambda \simeq 10^3$. The intervening HIcolumn was estimated as 10^{18}/cm^2, and the ratio HeI/HI is 0.1. The spectrum is plotted on the same scale as the MDF function (figure 3-2). Lines observable in 40K seconds can be identified visually by comparing the two plots or by comparing the model fluxes to values interpolated from the files *(sw/mw/lw)_mdf.txt*.

Because of the steepness of the SW MDF, the lines between 70 and 100 Å will not all be observed. The medium and long wavelength spectra could be fairly bright, but the features near the airglow transitions at 304, and 584 Å will fall on top of high backgrounds, which will introduce noise later when the background is subtracted. Comparing the model fluxes with the numerical MDF listing shows that the stronger lines near 256 and 304 Å should be visible, but the line near 584 Å will probably not be observed. Lines longer than 650 Å, while not near any airglow features, will likely fall prey to decreasing effective area and high ISM attenuation.

3.3.3.2 Continuum Sources

The MDF for continuum sources depends much more strongly on how the data are binned during post-processing. Interesting features of some faint sources may be rendered detectable by using wider spectral bins. Figure 3-3 presents the MDF of each Spectrometer

[3] See section 1.4.1 for basic orientation if you have not used *ftp* before.

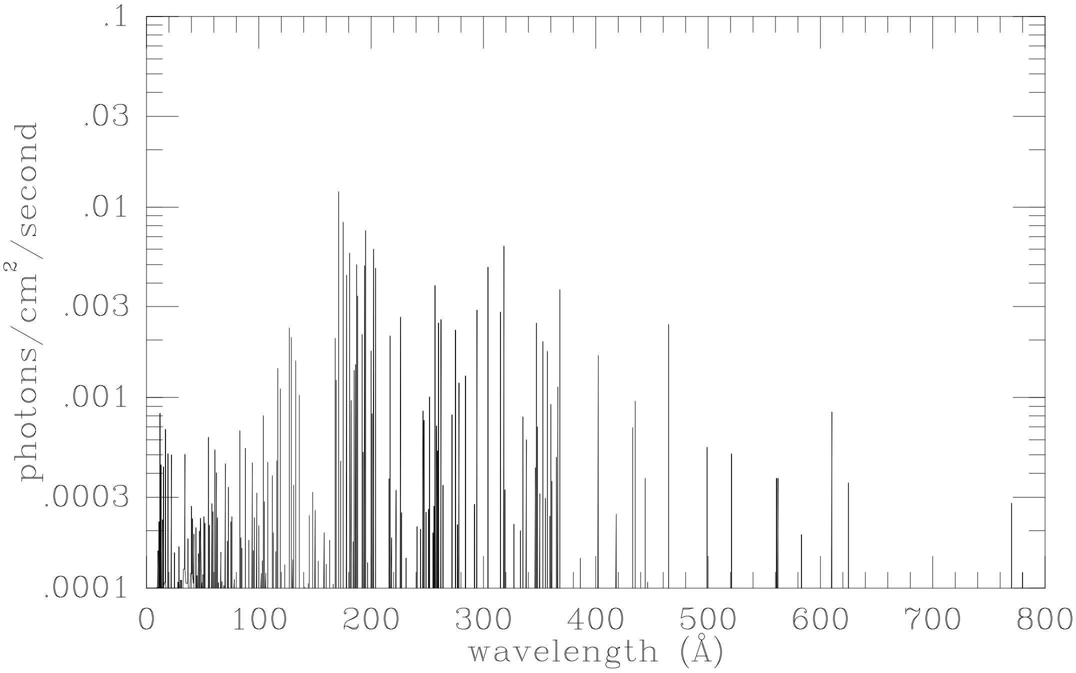

Figure 3-4: Example of a model spectrum for a late-type star, including estimated ISM absorption from HI$=10^{18}$/cm^2, HeI/HI= 0.1.

channel for two sizes of wavelength bins. Like the MDF for emission sources, this function is based on a 40K second observation, and shows the flux required for a 3-σ measurement. Each of the upper curves corresponds to 1-Å wide bins, and the lower curves to an alternative binning at 10 Å per bin. Again, the medium wavelength channel is set off as a dashed line. Column three of table *(sw/mw/lw)_mdf.txt* gives numerical values for the use of a 1-Å bin.

To scale the MDF for any bin size, divide the 1-Å MDF function by $\sqrt{N}$, where N is the width of the bin in Angstroms. This conversion method produces a relatively conservative (high) MDF for wavelengths not dominated by the background, but is a minimal flux near the airglow features. At 584 Å for example, the ratio of the 1-Å to the 10-Å MDF is about 3.5, much closer to $\sqrt{10}$ than at 400 Å, where the 10 Å binning requires only about the one fifth the flux as the 1-Å binning for a 3-σ measurement.

The bin size should be balanced against the requested integration time such that flux from the target at the telescope exceeds the resulting MDF level while providing sufficient spectral resolution for the proposed science.

Example: continuum source observability A possible model spectrum for G191-B2B is plotted in figure 3-5, in photons/cm^2/sec/Å on a linear scale. The white dwarf model program that produced the spectrum assumed an intervening neutral hydrogen column of 1.76×10^{18}/cm^2 and a ratio of helium to hydrogen of HeI/HI= 0.086. Comparison with the continuum MDF indicates that a 40K second exposure should produce a very bright spectrum with 1-Å bins. Prominent features include a HeIIabsorption feature at 304 Å and the HeIabsorption edge at 504 Å. The first will get lots of interference from diffuse emissions but the 504 edge should still have good S/σ at the 1-Å binning.

There is a more thorough discussion of the spectral resolution in section 3.5, which may be applied to continuum sources to determine the best bin size for a particular measurement.

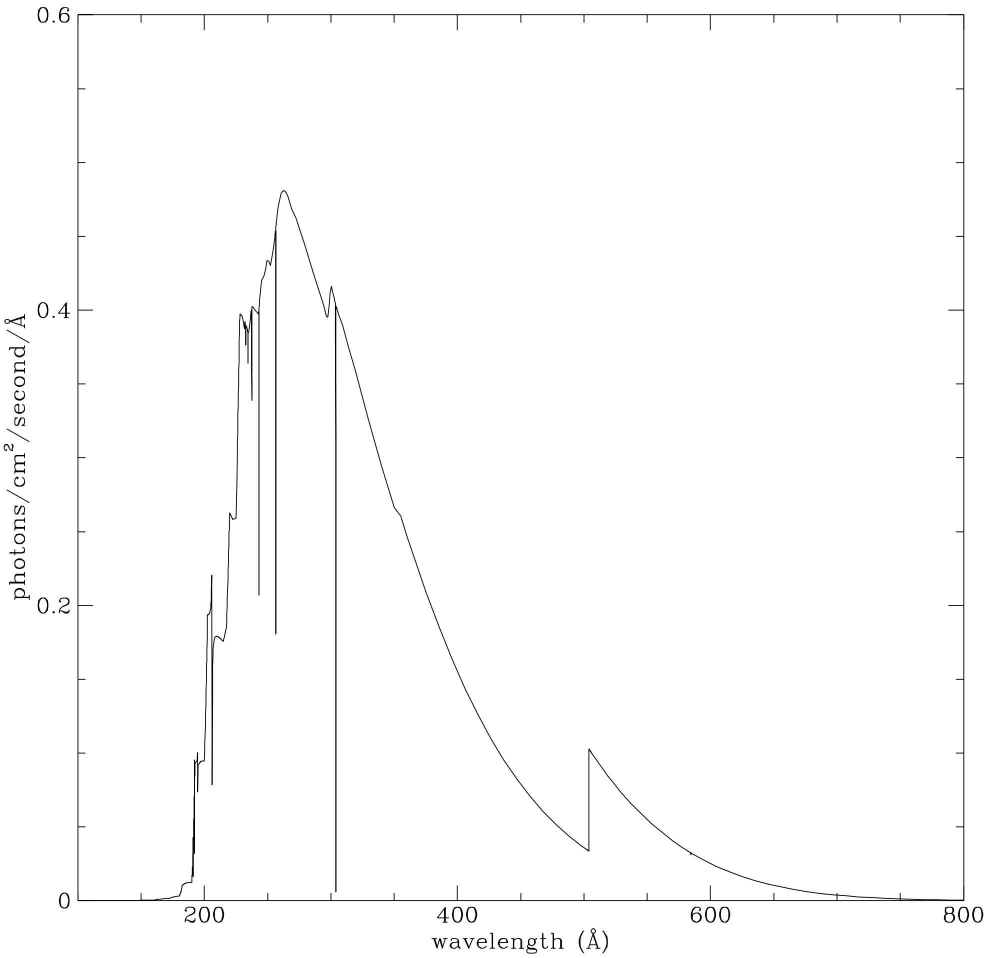

Figure 3-5: Model spectrum for G191-B2B; HI= 1.76×10^{18}, HeI/HI= 0.086. Model contributed by Dr. David Finley

3.4 Effective Area Functions

After establishing that a target object is likely to be detected by the Spectrometer, proposers should estimate the source count rates in the instruments using their model spectrum and the Spectrometer effective area. Once the source count rates and predicted background levels are known, proposers can use them to determine integration times that will meet their scientific requirements.

The effective area of each Spectrometer channel has been measured in both pre-launch and in-orbit calibrations. Functions for first-order ($n = -1$) effective areas derived from in-orbit calibration data are plotted in figure 3-6. Numerical values are available from the CEA/EUVE *ftp* site in the files *sw_ea1.txt*, *mw_ea1.txt*, and *lw_ea1.txt*. The Spectrometer channel effective area functions pictured in this Handbook and currently available in the *ftp* site are the most current values. Only these effective areas should be used for all proposal calculations under the current UCB/EUVE Call for Observing Proposals.

Expected Spectrometer count rates in each detector from a target object may be obtained by using effective area functions in one of two formulas in sections 3.4.1 or 3.4.2, depending on whether the target is to be considered a line source or a continuum source.

The simplifying assumption that all the light in each bin was from a single wavelength in first order will be sufficient for most cases, but proposals for continuum objects whose intensities peak at short wavelengths may need to address the effect of contamination from higher orders. See section 3.4.3, and the files for higher-order effective areas, *sw_ea2.txt, mw_ea2.txt,* and *lw_ea234.txt* in the directory *nra97/data* of the CEA/EUVE *ftp* site. Diffuse and extended sources are considered in section 3.10.

3.4.1 Count Rates From Emission Line Sources

Spectrometer count rates for narrow emission features can be calculated by multiplying the integrated source flux by the local value of the effective area:

$$S'_{em} = A_{eff}(\lambda) \times \mathcal{F}(\lambda) \qquad (3\text{-}1)$$

where S' is the source count rate in the resolution element centered at λ, in counts/sec, A_{eff} is the effective area in cm^2, and $\mathcal{F}$ is the source flux at the telescope, in photons/cm^2/sec. Raw source counts are simulated by multiplying this instrument count rate by an integration time.

The width of a spectral resolution element, $\Delta\lambda$ is assumed for the bin width in all technical reviews unless another bin width is explicitly stated. See section 3.5 for spectral resolution element sizes.

Because the Spectrometer channel bandpasses overlap, some features may be detected in both the short and medium, or the medium and long wavelength channels. Efficiencies, count rates, and the size of a resolution element will differ (see section 3.5), but the total projected counts can be combined to improve statistics as long as they come from detector areas with comparable background rates.

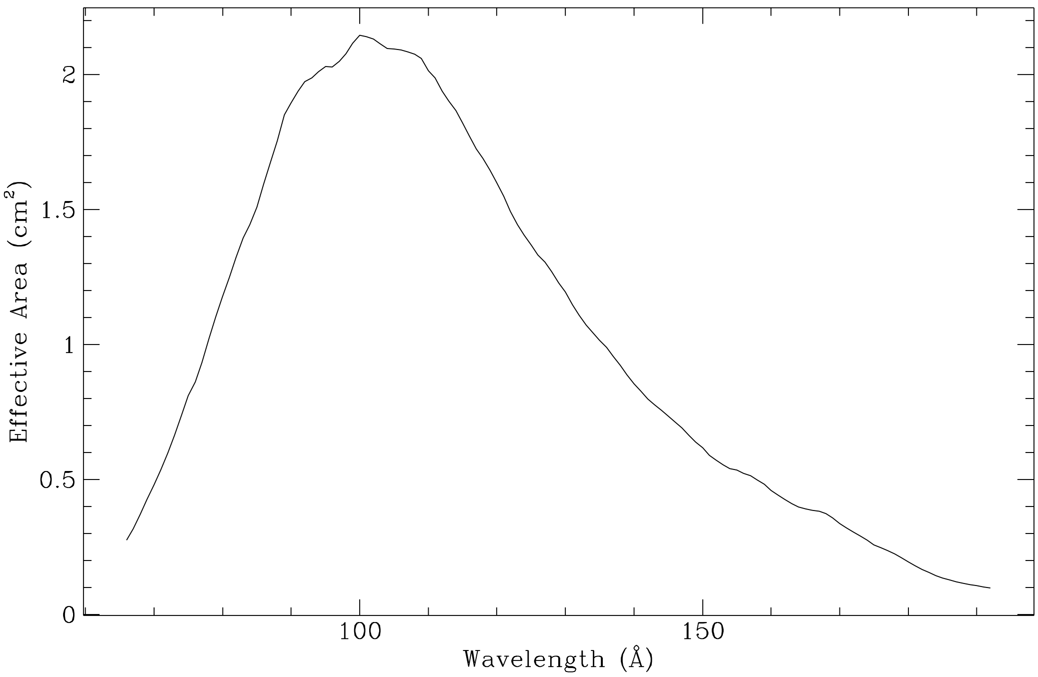

Figure 3-6: a) Spectrometer effective area, short wavelength channel.

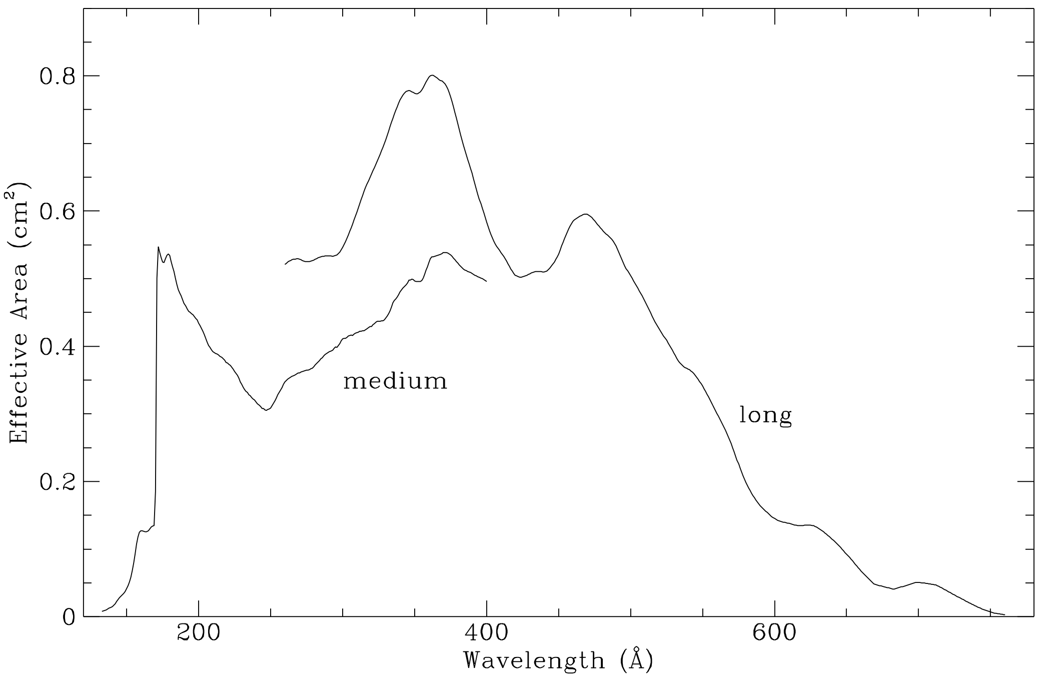

Figure 3-6: b) Spectrometer effective area, medium and long wavelength channels.

Emission/Absorption features in continuum sources

For broad lines or blends, a choice of bin size must be made, and the product of flux and effective area must be integrated over the width of the feature, as for a continuum source. Any object with both continuum of radiation and emission (or absorption) features should also be justified as a continuum source, and model spectra should be in units of photon flux/Å. For such observations, proposers must show that the features can be detected above (in) the continuum with the required S/N ratio.

Example: emission line source count rates Estimate detector count rates in each Spectrometer channel for lines of the late type star model spectrum in section 3.3.3.1. Since the lines are intrinsically narrow, distribution of the counts on the detector is entirely a function of instrument resolution. Multiplying the model source flux by values interpolated from the A_{eff} table using equation 3-1 produces Spectrometer count rates in counts/sec. The IRAF/EUV task **specmod** can also be used with a list of line fluxes as input, to produce instrument count rates for narrow emission features. Table 3-1 lists the projected count rates and widths for several emission features in the short, medium, and long wavelength channels. According to these instrument count rates, a 40 Ks observation would result in about 67 counts from the 104.1 Å line the short channel. The line at 171.06, will be detected in the short channel with 152 counts, and the medium channel with 242 counts. A line at 583.5 Å will have only about 1–2 counts in the long channel, and will be lost in the background from HeI584.33 Å. Those lines that do not have airglow interference will produce good measurements as long as they are well above the noise.

3.4.2 Count Rates From Continuum Sources

Model fluxes for continuum sources should have units of photons/cm^2/sec/Å. To produce instrument count rates from a continuum source spectrum, the A_{eff} function and spectrum must be partitioned with some bin size w, large enough to give adequate count rates. The product of the source spectrum with the A_{eff} function is then summed over some wavelength region of interest. Equation 3-1 becomes the sum:

$$S'_{cont}(\lambda) = \sum_{j=1}^{N} \mathcal{F}(\lambda_j)\, A_{eff}(\lambda_j)\, w \tag{3-2}$$

where $\mathcal{F}$ is the model source flux in photons/cm^2/sec/Å, $A_{eff}(\lambda_j)$ is the effective area function at wavelength λ_j, the center of the jth bin, in cm^2. The region of interest spans bins 1 through N, and w is the bin width in Å. This formula represents a binning which must

Table 3-1: Predicted count rates for a late type star model in the form of a line list

λ (Å)	source flux (photons/cm^2/sec)	instrument count rate (cts/sec) SW	MW	LW
83.0	6.70×10^{-4}	9.35×10^{-4}	-	-
104.1	8.04×10^{-4}	1.68×10^{-3}	-	-
127.0	2.32×10^{-3}	3.03×10^{-3}	-	-
129.0	2.07×10^{-3}	2.54×10^{-3}	-	-
171.06	1.20×10^{-2}	3.83×10^{-3}	6.05×10^{-3}	-
187.2	4.97×10^{-3}	6.00×10^{-4}	2.38×10^{-3}	-
222.0	3.25×10^{-4}	-	1.08×10^{-4}	-
246/247	1.61×10^{-3}	-	4.92×10^{-4}	-
303.8	4.83×10^{-3}	-	2.00×10^{-3}	2.72×10^{-3}
368.0	3.68×10^{-3}	-	1.97×10^{-3}	2.92×10^{-3}
583.4	1.91×10^{-4}	-	-	3.52×10^{-5}
610.0	8.39×10^{-3}	-	-	1.16×10^{-3}

be applied by the observer in reducing the spectrum. In using this formula for planning purposes, proposers must choose a spectral bin width that will demonstrate the viability of the program proposed. A raw source count spectrum is simulated by multiplying by the integration time, $\mathcal{T}$ in the sum.

Example: continuum source count rates A simulated raw count spectrum for the G191-B2B model was obtained using the IRAF/EUV Spectrometer simulation task, **specmod**, in the **euv.euvspec** package.

For this example, we made a target spectrum into an image with .1 Å resolution. **Specmod** was then run on the image with a bin width of .2 Å. The resulting spectra were oversampled with respect to the resolution element size in all channels, so they were reblocked at .5, 1.0, and 2.0 Å to show the best resolution achievable with the Spectrometer. The spectra for the medium and long wavelength channels are shown in figure 3-7 as counts integrated over 40K seconds.

In examining the spectrum, we see that the OIV absorption edge at 298 Å in the medium wavelength and HeIat 504 Å in the long band are easily identified, along with some narrow absorption features. There is a large contribution from geocoronal emission near the oxygen edge, and the absorption line at 304 Å may be lost in subtraction noise.

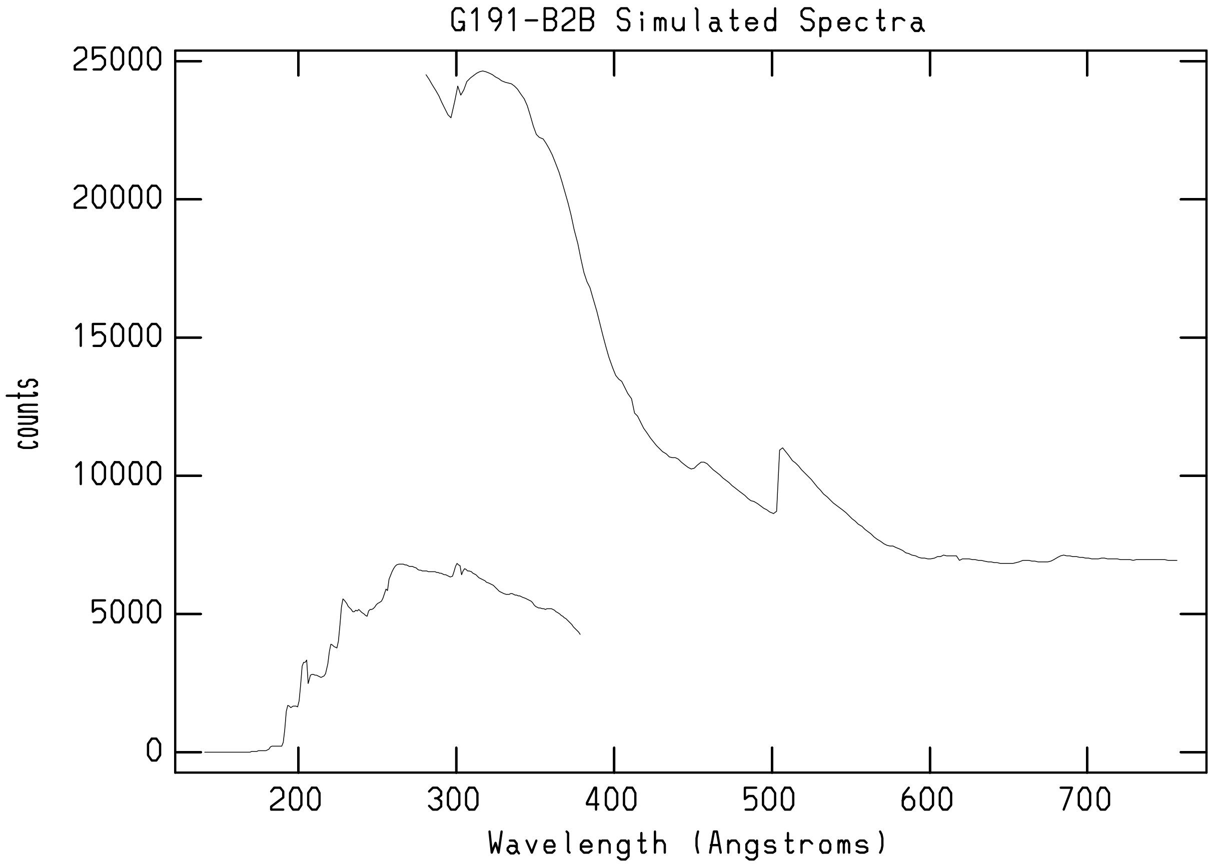

Figure 3-7: Simulated EUVE spectra for G191-B2B in medium and long wavelength channels. Source counts only.

3.4.3 Order Confusion

The EUVE Spectrometer design allows some light from higher (n ≤ -2) inside orders to be imaged on each detector. Because the instrument is slitless, and each channel spans nearly a factor of three in wavelength, higher orders may be present in any spectra of very bright objects. Overlapping orders will make evaluation of some continuum intensities particularly complex, so it is advisable for observers to give this problem some consideration when writing proposals. Higher order spectra are superimposed on the first order spectra, at the spectral position $\lambda_n = n \times \lambda_1$.

To assist proposers in modeling their source throughputs, the effective areas, in cm^2, of the first few higher orders, as determined from a combination of pre-launch measurements and calibration observations, are shown graphically in figures 3-8, 3-9, and 3-10 below. Tabular versions of the effective areas are available from the CEA/EUVE *ftp* site, from the directory *nra97/data*, as detailed in section 3.2. The files are called *sw_ea2.txt, mw_ea2.txt,* and *lw_ea234.txt*. The absolute errors are estimated at $\leq 15\%$. The graphs and/or tables can be used to estimate the intensity of the higher order throughputs, based on the proposer's model of the source flux at the telescope.

Only -2nd order efficiencies are plotted for the short and medium wavelength channels; estimates of second order effects will be considered sufficient for the purposes of Technical Justification. In the long wavelength channel, -2nd -3rd and -4th orders are shown; proposers should consider carefully which are likely to affect their science program.

Example: Higher order contribution in emission spectrum In the late type star example above, the oxygen line at 610 Å in the long wavelength channel had a low count rate and a total of 2-3 counts in 40K seconds. In addition, the second order flux from the 303.8 Å line will also be imaged nearby. According to figure 3-10 and equation 3-1, this could be as much as:

$$4.83{\times}10^{-3}\,\text{photons/cm}^2\text{/sec} \times 0.0335\,\text{cm}^2 \times 40,000\,\text{seconds} \simeq 6 - 7\,\text{counts}$$

While this quantity may be successfully estimated and subtracted, the noise introduced in the process may render the detection questionable.

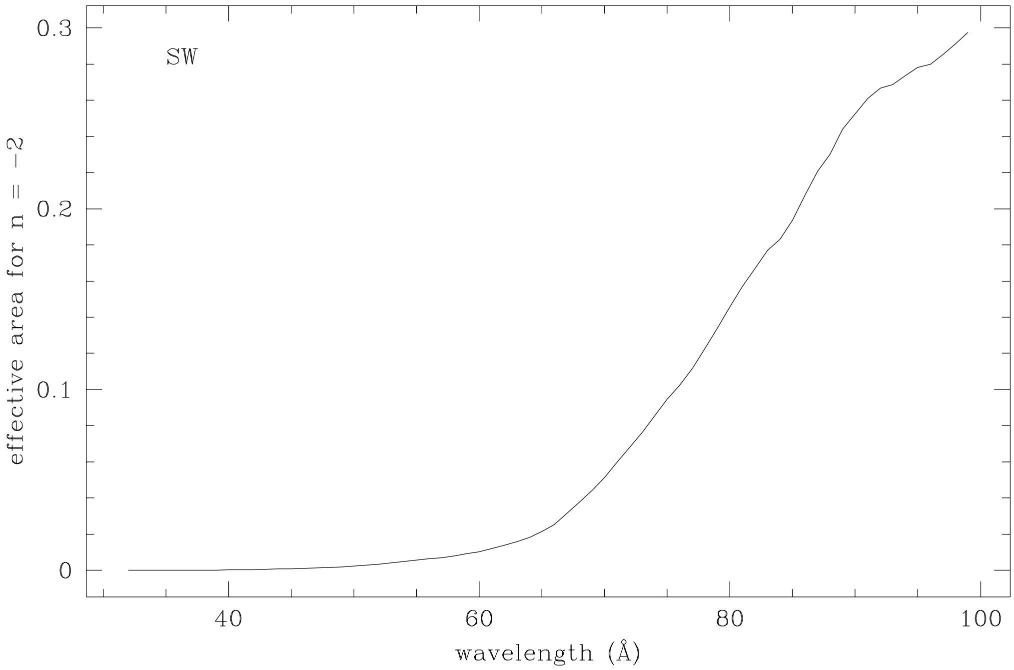

Figure 3-8: Short Wavelength second order effective area, in cm^2. Counts in -2nd order appear at $2 \times \lambda$. Errors $\leq 15\%$.

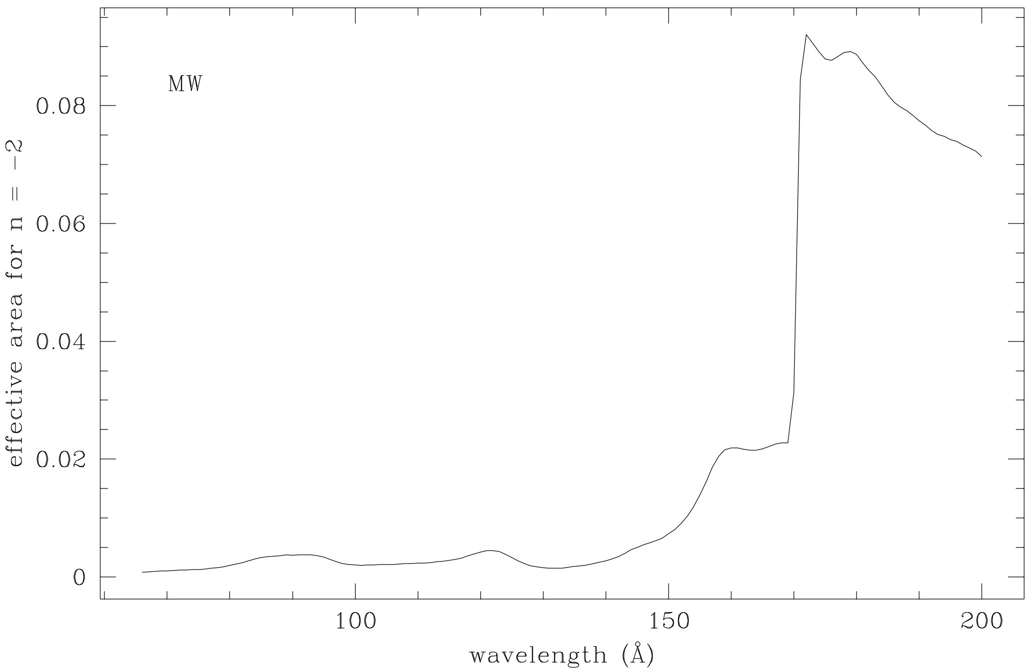

Figure 3-9: Medium Wavelength second order effective area. The spectrum will appear at values of $2 \times \lambda$. Errors $\leq 15\%$.

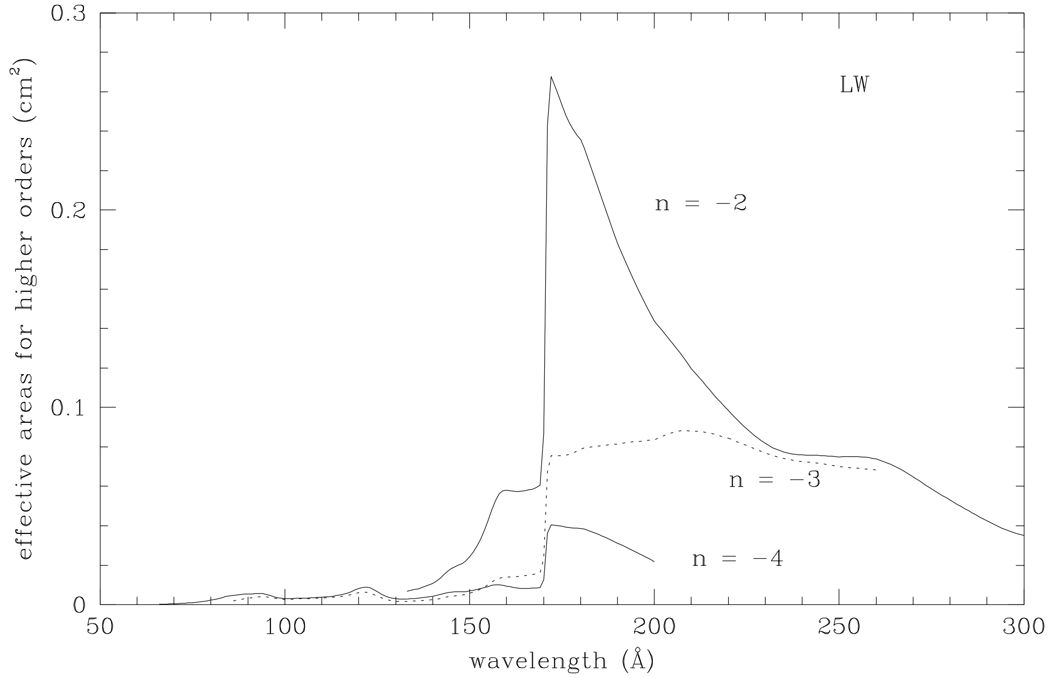

Figure 3-10: Long Wavelength inside order effective areas. Counts in nth order appear at values of $n \times \lambda$. Errors $\leq 15\%$.

3.5 Spectral Resolution

Testing the resolution of the simulated instrument spectra or features may also be desirable for some proposals. Spectral resolution has been measured at a number of wavelengths in each Spectrometer channel during calibrations both before and after launch. Figure 3-11 shows the results of these measurements, plotted as FWHM $\simeq \Delta\lambda$ in Å vs. wavelength for each channel.

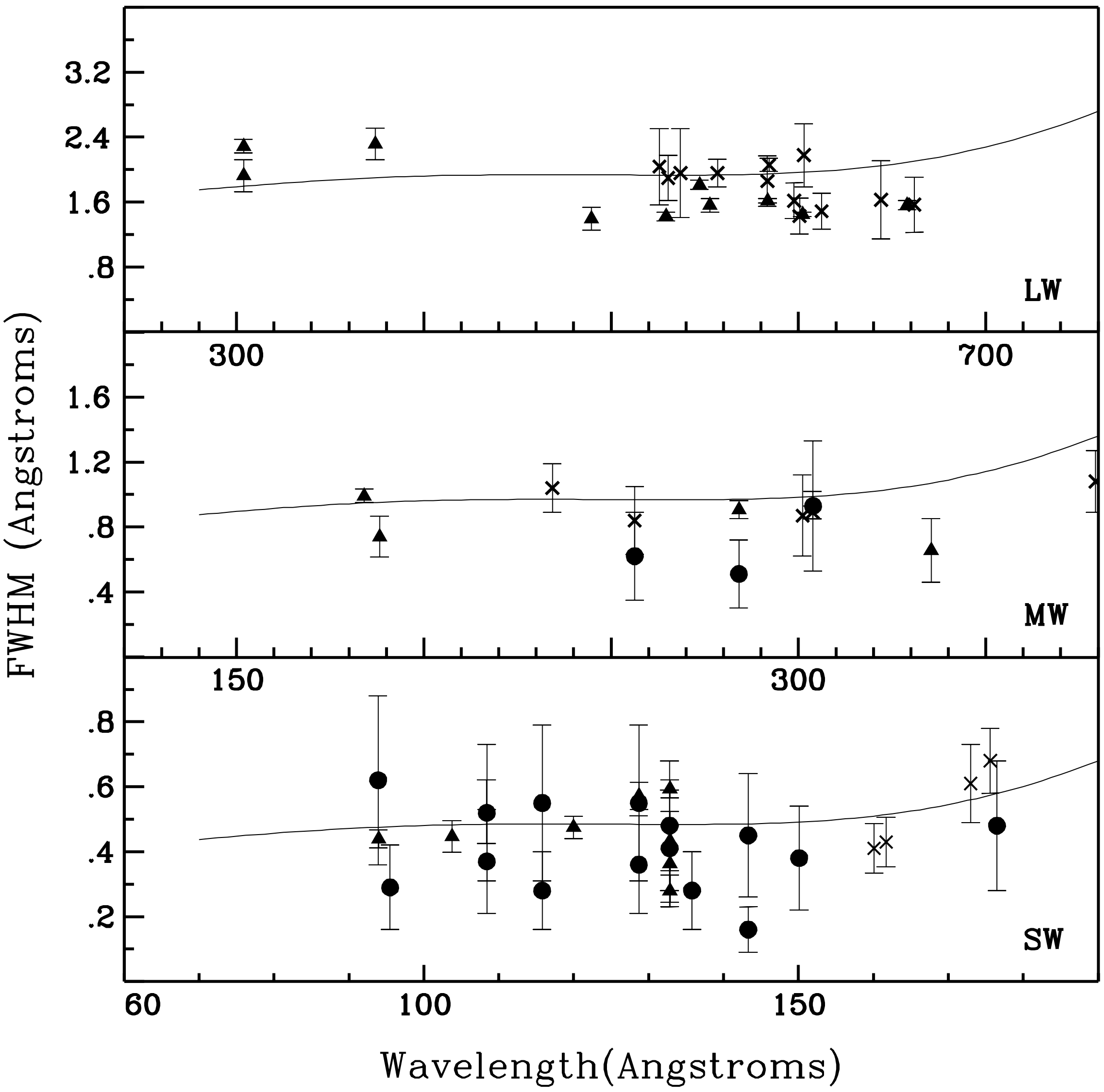

Figure 3-11: EUVE Spectral Resolution. X's: pre-launch measurements. Dots and triangles: measured post-launch. Solid line: theoretical values.

Theoretical curves based on the instrument design are overplotted. The FWHM of each unblended line approximates the size of the local resolution element ($\Delta\lambda$) in Å. Table 3-2 lists the numerical values for some of the points plotted in figure 3-11 In-orbit measurements are labeled with $*$'s. Values of the theoretical resolution function for each channel are available in the *nra97/data* directory of the *ftp* site, in the files *sw_res.txt, mw_res.txt*, and *lw_res.txt*.

Figure 3-11 shows that the size of the resolution element is fairly constant throughout most of the bandpass in each channel. The spectral resolution is expected to degrade toward the long end of each bandpass, due mainly to grating aberrations. For the purpose of Technical Justifications the size of $\Delta\lambda$ may be assumed to be approximately constant in each channel. Because of design symmetries, the width of $\Delta\lambda$ differs from channel to channel by a factor of two:

$$\begin{array}{rl} \text{LW:} & \Delta\lambda \simeq 2.0\ \text{Å} \\ \text{MW:} & \Delta\lambda \simeq 1.0\ \text{Å} \\ \text{SW:} & \Delta\lambda \simeq 0.5\ \text{Å} \end{array}$$

These nominal resolution element sizes may be used for most Technical Justification calculations. The effective resolution of any data set will be degraded if the satellite aspect is not accurately known.

Proposers who wish to observe fainter continuum sources may choose to improve the signal-to-noise in their simulated spectra by using a larger bin size during post-processing. This approach is not recommended for line sources unless the total flux is the only quantity of interest, as choosing a greater bin width will adversely affect line width and center. Observations concerned with resolving closely spaced features should be justified directly from the expected count rates, background, and the resolution element size.

Example: Line emission resolution In the late type star example, several pairs of lines are separated by 1 Å or less, but this has a different impact in each Spectrometer channel. For example, a pair of features in the MW range, at 246 and 247 Å, are shown in a simulated spectrum in figure 3-12. Since the two lines are separated by just barely the width of $\Delta\lambda = 1$ Å, their peaks are not separable, even without any background or Poisson noise. By contrast, features separated by 1 Å in the short wavelength channel such as the lines at 187 and 188 Å, are well separated; see figure 3-13.

3.5.1 Imaging Resolution

The Spectrometer's resolution in the imaging direction has also been measured, using many of the same spectral features. Some individual measurements of angular resolution appear in table 3-2, with errors. This information may be useful to any proposers who wish to observe multiple sources.

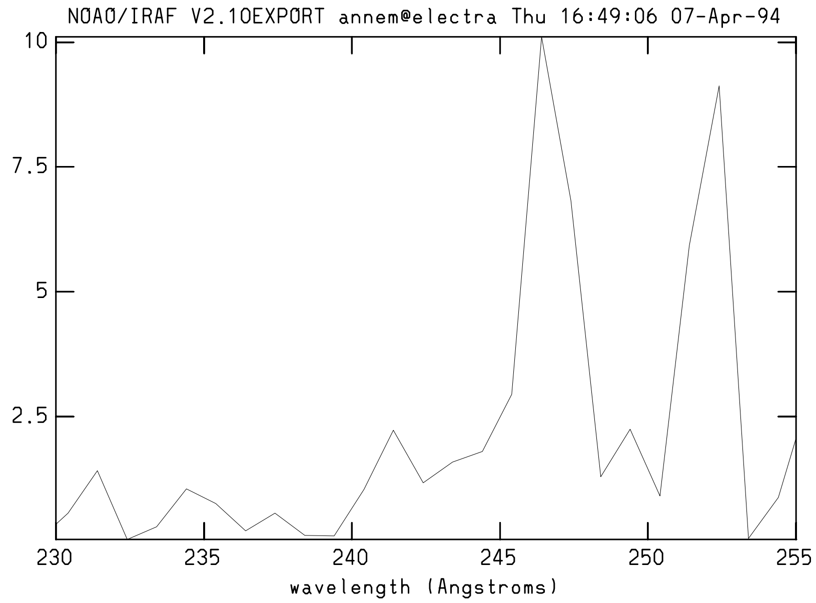

Figure 3-12: Late type star spectrum near 246/247 Å feature. Y-axis is integrated counts.

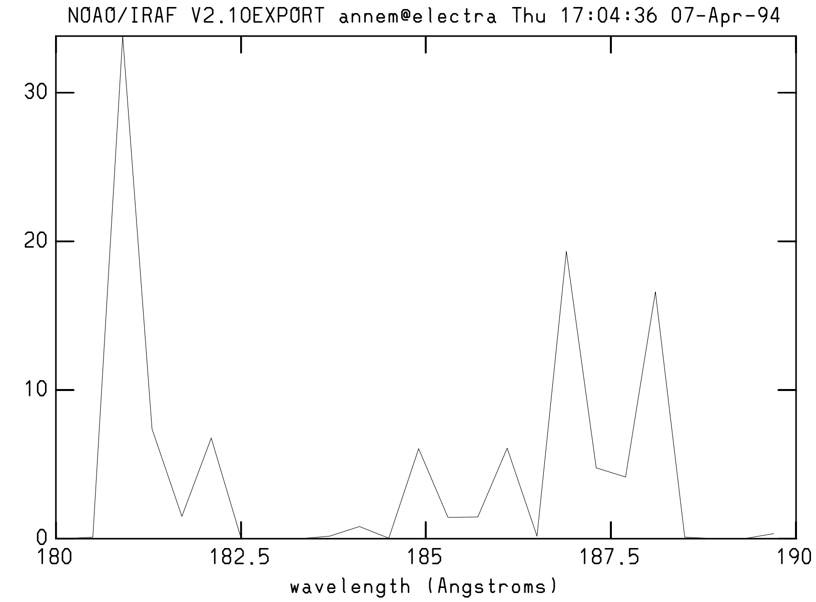

Figure 3-13: Late type star spectrum near 187/188 Å feature. Y-axis is integrated counts.

Table 3-2: Spectral Resolution Measurements. ∗ indicates in-orbit data.

channel	λ	$\Delta\lambda$ (Å)	σ (Å)	$\Delta\Theta_i$(asec)	σ_i(asec)
Short	∗93.4	0.44	0.028	16.74	2.93
	∗95.5	0.29	0.13		
	∗103.8	0.45	0.049	22.60	2.93
	∗108.4	0.52	0.21	19.67	1.67
	∗115.8	0.55	0.24		
	∗120.0	0.47	0.035	19.67	2.09
	∗128.7	0.57	0.042	12.14	3.35
	∗132.8	0.59	0.028	26.79	2.93
	∗132.8	0.36	0.12	31.40	2.93
	∗132.8	0.43	0.091	38.51	5.86
	∗132.8	0.40	0.049	23.86	6.70
	∗143.3	0.45	0.19		
	∗150.1	0.38	0.16		
	160.1	0.41	0.076		
	161.7	0.43	0.076		
	173.0	0.61	0.12		
	175.6	0.68	0.10		
	∗176.5	0.48	0.20		
Medium	∗184.1	0.991	0.042	14.65	1.67
	∗188.2	0.740	0.12	14.65	4.60
	234.3	1.04	0.15		
	256.3	0.84	0.21		
	∗284.1	0.51	0.21		
	301.1	0.87	0.25		
	303.8	0.89	0.04		
	∗303.8	0.935	0.084	19.67	1.67
	∗335.4	0.656	0.20	23.02	1.67
Long	∗303.8	2.29	0.084	20.51	1.25
	∗303.8	1.93	0.20	23.44	0.838
	∗374.12	2.32	0.20	17.58	1.67
	∗489.54	1.40	0.14	23.44	0.838
	525.8	2.04	0.47		
	∗529.3	1.42	0.056	21.35	0.419
	530.5	1.90	0.28		
	537.0	1.96	0.55		
	∗547.2	1.82	0.056	21.77	0.419
	∗552.8	1.56	0.084	20.93	0.419
	556.8	1.96	0.17		
	583.4	1.86	0.31		
	∗583.6	1.62	0.028	23.44	0.419
	584.3	2.06	0.08		
	597.7	1.62	0.22		
	600.6	1.43	0.22		
	∗602.2	1.45	0.028	22.60	0.419
	602.9	2.18	0.39		
	612.4	1.49	0.22		
	644.1	1.63	0.48		
	∗658.1	1.56	0.056	22.19	0.419
	661.9	1.57	0.34		

3.6 Estimated Background Levels

Proposers will need to make estimates of the expected background in the Spectrometer channels in order to determine the exposure times that meet their science criteria. The source signal in any spectral bin has an uncertainty proportional to the square root of the number of source counts, $\sqrt{S}$. The additional sources of background increase the signal error by a factor slightly larger than the square root of the integrated background, $\sqrt{B}$.

This section provides estimates of the average background rate in each of the Spectrometer channels, which can be used to calculate the expected background counts per spectral bin for a given exposure, and in turn for determining expected signal quality and exposure requirements. The various sources of background counts in the Spectrometer detectors and the standard method of background subtraction are described. Then two kinds of estimates are given: a single number of counts/second/Å for each channel, for use over parts of the detectors where the background is fairly flat, and a more detailed background spectrum, also in counts/second/Å, for use over sections of the spectrum and areas where the background rate is changing rapidly. The use of these rates to calculate the average total background counts over a spectrum aperture is discussed, and the results are used in section 3.7 below to determine signal quality.

3.6.1 Sources of Spectrometer background

The background components fall into three main categories:

1. Distributed background: Counts from intrinsic channel plate noise, scattered Lyman α radiation and other light scattered from the optics, and charged particle detections. These are all distributed over the entire detector. The flux level from these sources varies between daytime and nighttime data, and is somewhat dependent on the amount of solar activity [19] and the satellite's magnetic latitude [17].

2. Diffuse emissions from geocoronal helium transitions at 256, 304, and 584 Å fall within the bandpass and are imaged as broad lines in the medium and long wavelength channels, whose width is determined by the collimators' transmission functions. These features are prominent in the estimated background spectra, which are shown below in section 3.6.4.

3. There are several sources of stray light which add to the background in specific areas on the detectors. They are mostly images of geocoronal light which is focussed to some degree by the optics. Most of these leaks have been blocked by baffles. The brightest remaining feature is the bright left edge on the short wavelength detector. It is caused by Lyman α radiation, which is partially focussed by the mirror and reflected from the side of the grating assembly onto the detector. This feature is a fairly constant characteristic of the detectors, and is also included in the background spectra.

3.6.2 Background Subtraction Technique

Background subtraction on EUVE spectral images is usually done by averaging over the imaging direction on part of the detector near the spectrum and subtracting the average from the accumulated counts in each spectral bin. This is advantageous because averaging lowers the background deviation by the ratio of the height (Y, or imaging direction) of the background strip to that of the spectrum. We call this factor n. If spectrum and background regions are chosen so that n is an integer, the deviation of the average background in a bin of arbitrary width in the spectral direction is given by:

$$\sigma_{\overline{\mathrm{B}}} = \sqrt{\sum_{i=1}^{n} \mathrm{B}_i / n^2} \qquad (3\text{-}3)$$

where $\overline{B}$ represents the averaged background, and B_i denotes the background in bin number i in the *imaging* direction.

The background count rates given throughout this section represent counts/second/Å, averaged over n times the spectrum height, although the bar notation will generally be omitted. When multiplied by bin width (X, or spectral direction) in Å and time in seconds, they give the integrated background counts (B) in a spectral bin. The standard deviation in the background, due to Poisson noise in photon counting detectors is given by $\sigma_{\mathrm{B}} = \sqrt{\mathrm{B}}$. This deviation alone does NOT account for the error introduced by background subtraction; the factor n, which appears below in formulae for calculating signal quality and exposure times in section 3.7, accounts for the error introduced by combining Poisson statistics.

Factor of n for Handbook background estimates.

For the purpose of calculating signal quality, proposers may use the value $n = 10$ to typify the ratio of spectrum height (Y direction) to background height with all background rates given here. No background subtraction technique will be successful on features with low intensities unless the integration time is sufficient to make the feature visible above the the Poisson noise.

3.6.3 Distributed Background

The distributed background in each detector from sources in category 1 above has been monitored continuously since launch.

After one year, the detector pulse height threshold in the short and medium wavelength detectors was lowered to maintain sensitivity as the gain of the detectors decreased with use. The upper pulse height threshold was lowered as well, to decrease the intrinsic detector background in those channels. The thresholds in the long wavelength detector were also lowered slightly.

To obtain estimates of the average background count rates, the per-pixel count rates were averaged over a large area on each detector near the spectrum, multiplied by a spectrum height of approximately 10 pixels, and the result converted to counts/second/Å. We use a script B ($\mathcal{B}$) for the average counts/second/Å. which can be used to estimate the total background associated with a spectral bin of any width on an otherwise "quiet" area of the detector. The values are:

$$\mathcal{B} \simeq 5.4{\times}10^{-4} \text{ counts/second/Å in SW}$$

$$\mathcal{B} \simeq 2.9{\times}10^{-4} \text{ counts/second/Å in MW}$$

$$\mathcal{B} \simeq 1.7{\times}10^{-4} \text{ counts/second/Å in LW}$$

The average distributed background rate is then multiplied by the width of a spectral bin in Å to produce the background count rate per bin:

$$\mathrm{B}' = \mathcal{B} \times w. \tag{3-4}$$

Use the count rate per bin with the expected source count rate to compute integration time from your statistical requirements, using the formulas in section 3.7. To obtain the estimated total background counts per bin, multiply by the spectral bin width and the integration time:

$$\mathrm{B} = \mathcal{B} \times w \times \mathcal{T}. \tag{3-5}$$

Use the total background counts to calculate the S/σ. This method of estimating the background is sufficient for features which are *not* near any detector edge or geocoronal feature, and are affected only by the sources of distributed background mentioned in category 1 in section 3.6.1 above.

Example: Line emission background For a bin width of $w = \Delta\lambda = .5$ Å in the SW detector, and our nominal observing time:

$$\mathrm{B}_{SW} = 5.4{\times}10^{-4} \times .5 \times 40,000 = 11 \text{ counts}.$$

And similarly for the MW and LW channels, with $\Delta\lambda = 1.0$ and 2.0 Å, respectively:

$$\mathrm{B}_{MW} = 2.9{\times}10^{-4} \times 1.0 \times 40,000 = 12 \text{ counts}$$

$$\mathrm{B}_{LW} = 1.7{\times}10^{-4} \times 2.0 \times 40,000 = 14 \text{ counts}$$

These values may be used for narrow emission lines, wherever the average background counts per bin are required, and the feature is well separated from detector edges or geocoronal features.

An inspection of the calibration target spectrum in figure 3-14 gives an idea of the background in proportion to a relatively bright line source. The source is AU Mic, a late-type star with many emission lines. The distributed background has about 10–12 counts in each pixel, with a deviation of about 3–5.

Background subtraction will be more difficult for features near detector edges or the airglow lines, since the background may be greater than the source signal. The appropriate section of the background spectrum presented in the next section should be used in these cases.

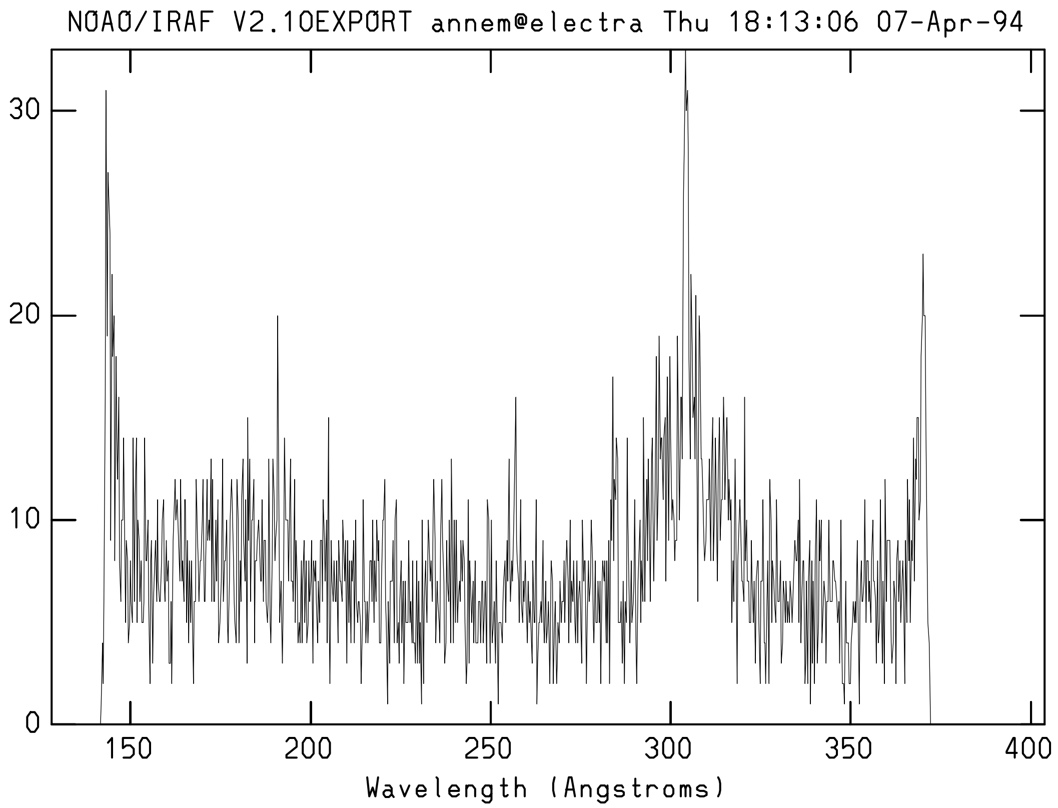

Figure 3-14: Raw spectrum of a late-type star in MW, showing typical background. Y axis scale is accumulated counts per bin.

3.6.4 EUVE Estimated Background Spectra

Spectra which simulate the average background count rate over the entire bandpass were made from composite exposures totaling about 1.5×10^6 seconds, and including many different pointing directions and airglow conditions. First, average count rates were computed over an area ten times the spectrum height (Y) on each detector, to make a one-dimensional spectrum. Since a wide range of airglow count rates was observed during the first seven months of Spectrometer calibration pointings, the airglow features were scaled to slightly above the mean of those observed, to make the background estimate conservative at these wavelengths. Recall that the FWHM of the airglow features is limited to 20 arc minutes by the collimator transmission. Each spectrum was then multiplied by the spectrum height in pixels ($10 \approx 42\overset{\frown}{''}$) and fit with a smooth polynomial function.

The resulting curves approximate the average backgrounds summed over the full spectrum height in the imaging direction, in units of counts/second/Å. They can be used to estimate the background counts for continuum source spectra, blended features, or features that fall on detector edges and airglow lines, where background levels are dominated by sources from categories 2 and 3 of section 3.6.1, and may be changing rapidly. The spectra include background from all sources, so the distributed background estimates should not be added. Figures 3-15, 3-16, and 3-17 show the EUVE estimated background spectra in the short, medium and long wavelength bandpasses. The numerical values used to make the plots are available from the CEA/EUVE *ftp* site in the directory *pub/nra97/data*. The filenames are *sw_bgspec.txt, mw_bgspec.txt*, and *lw_bgspec.txt*.

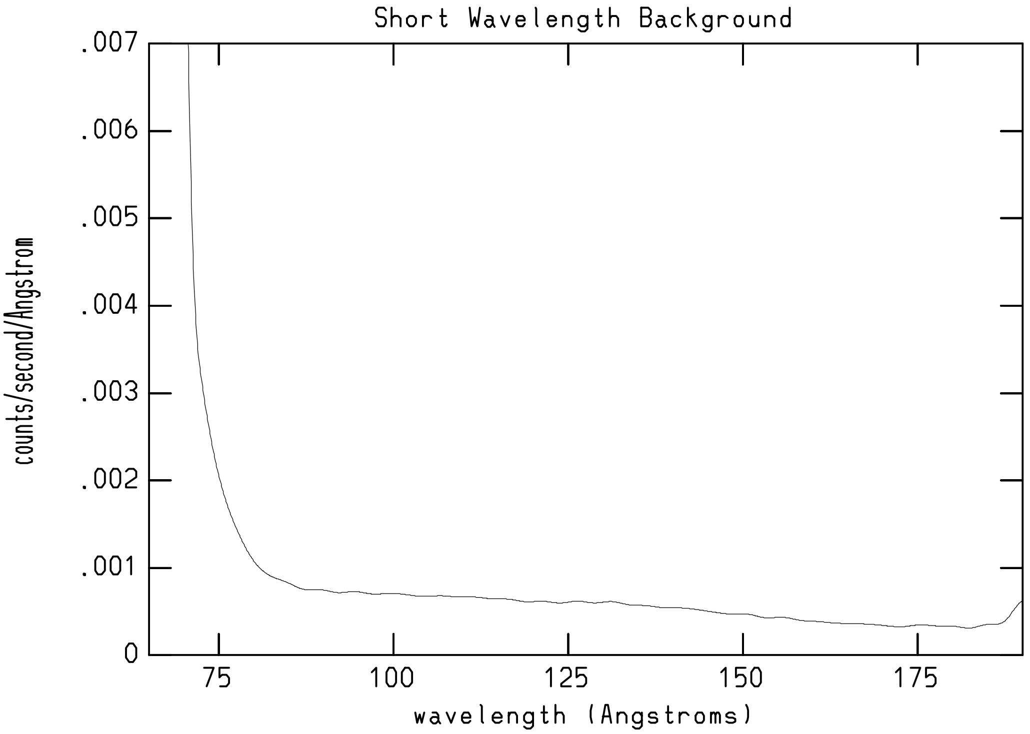

Figure 3-15: Spectrometer background count rate spectrum for SW

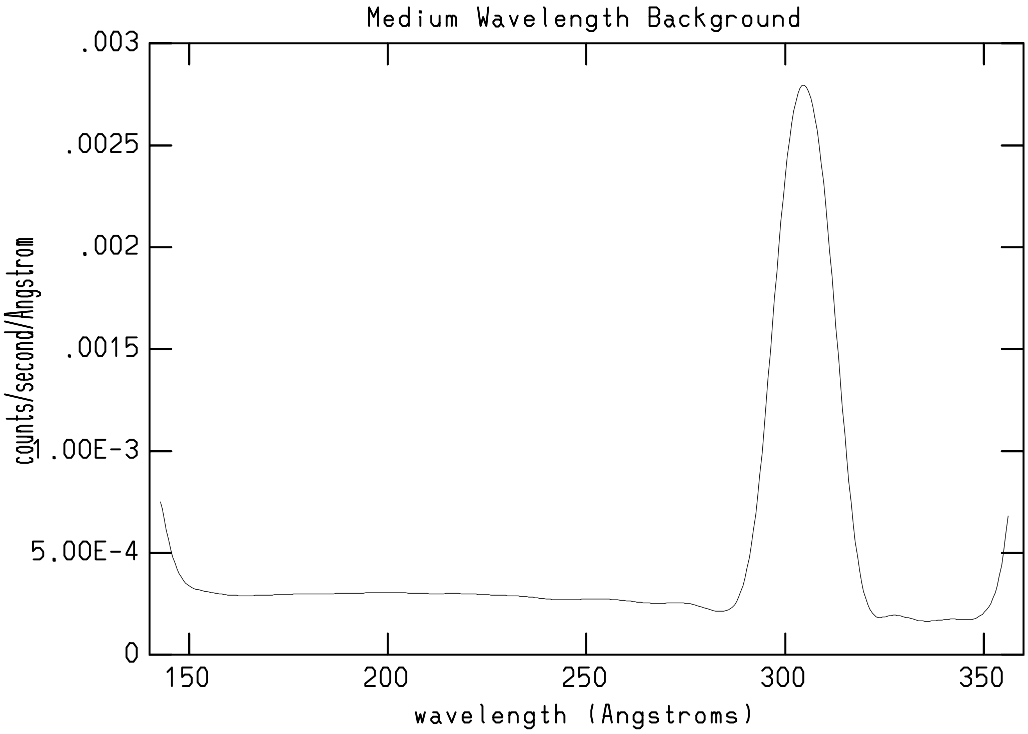

Figure 3-16: Spectrometer background count rate spectrum for MW

A few notes on particular features of the spectra:

- The short wavelength detector has a very bright leading edge, due to Lyman α radiation being scattered by surfaces on the grating holder. Similar reflections have been baffled out of the other channels.
- All the detectors show some rim brightening at a factor of about 1.5 to 3 times the distributed background level, due to distortions in the detector's potential field near the edges.
- The medium wavelength spectrum has a single broad feature from the HeIIline at 304 Å. The same line is also visible at the short end of the long wavelength spectrum, in combination with the rim brightening. Since the half-width of the the collimator response in the long wavelength channel is greater than $(304 - 280)$ Å, the 304 feature is cut off at the short end of the LW spectrum.
- The 304 Å airglow emitted by singly ionized helium can vary by orders of magnitude, depending on the angle of the Spectrometer's boresight with respect to the earth's shadow and the inner ion-trapping region of the earth's magnetic field. The height of the 304 Å features in the background spectra are slightly above-average values, based on rates in the first 7 months' calibration pointings

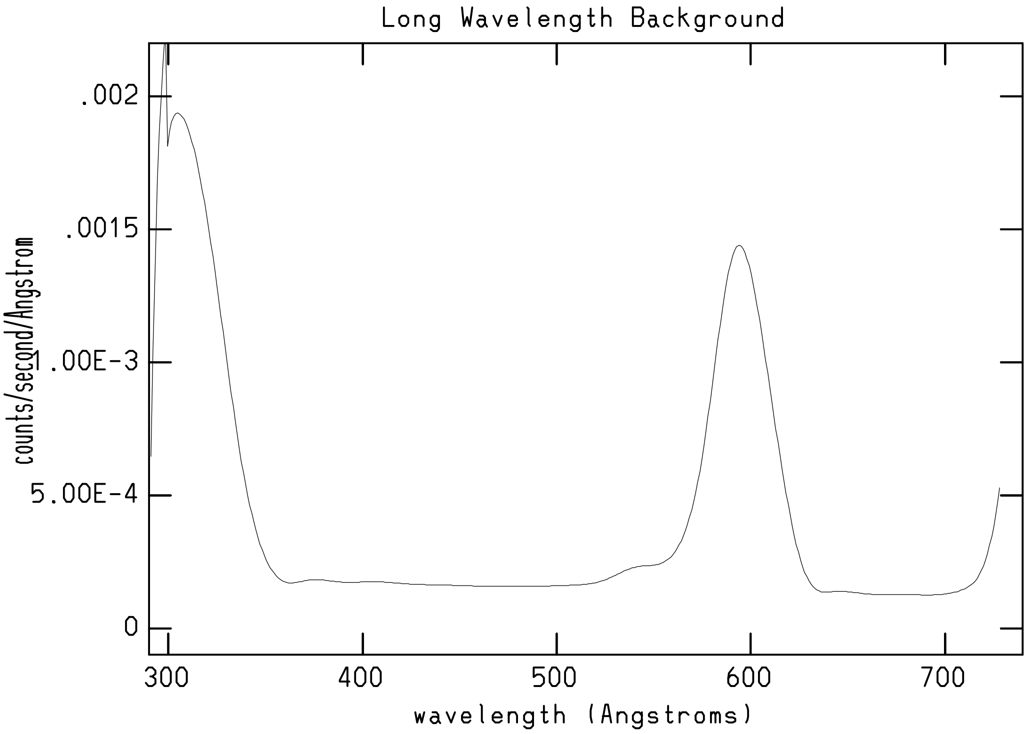

Figure 3-17: Spectrometer background count rate spectrum for LW

- The feature near 600 Å in the long wavelength plot includes both HeIat 584 Å in -1st order, as well as 304 Å in second order. It is slightly larger than $20\overset{\frown}{\prime}$ FWHM.
- The small "wiggles" in the background spectra are mostly artifacts of a polynomial fitting process, EXCEPT the small shoulder shortward of the 584/608 Å feature in the long wavelength channel. This is the 537 Å line of Helium I.

The spectra furnish estimates of B and $\sqrt{B}$ when multiplied by a spectral bin width w and an exposure time $\mathcal{T}$, but they do not contain representative levels of Poisson noise. Recall the discussion in section 3.6.2: the increase in noise due to background subtraction is proportional to $1/\sqrt{n}$, where n is the ratio of the background sampling area to the spectrum aperture. When using the integrated spectra for background estimates in S/σ calculations in the next section, a value of $n = 10$ should be used. The ratio of background to source signal near the geocoronal lines will still be of critical concern for any observation in these regions.

The background in spectral bins under a continuum is produced by simply rebinning the background spectrum at the desired resolution, but the proposer must justify the bin size used in terms of their science goals. For example, if the goal is a comparison to some model spectrum, the required signal-to-noise should be demonstrated over the entire spectral region to be fit. For lines in regions where the channel spectra overlap (140-190 Å, 280-380 Å), background count rates should be calculated separately for the bin size to be used in each each channel, and added, like the source count rates. Procedures for using background rates and counts to determine exposure times and signal quality are defined in section 3.7.

Example: Background for continuum sources To simulate the raw count background for observations of continuum sources, the background spectrum should be rebinned at the resolution required by science goals, and multiplied by the bin width and integration time. As an example, suppose a proposer wishes to create a background spectrum for a continuum source in the MW Spectrometer channel, with bins the size of a resolution element: 1 Å. The proposer can use the IRAF/EUV task **mkeuvspec** or any similar routine to rebin the background spectrum and convert it to cts/second. The standard IRAF task **imarith** can then be used to multiply by the integration time $\mathcal{T}$. The resulting background count spectrum appears in figure 3-18. for $\mathcal{T} = 60$ ksec.

This background is relatively low compared to the source spectrum produced for our G191-B2B model, but the broad geocoronal features will dominate over features of the object spectrum for some continuum objects. An example is shown in figure 3-19, which is part of an actual raw spectrum from a 31K second observation of a white dwarf star. The airglow feature at 304 Å has many more counts that the 171 Å edge visible at the left.

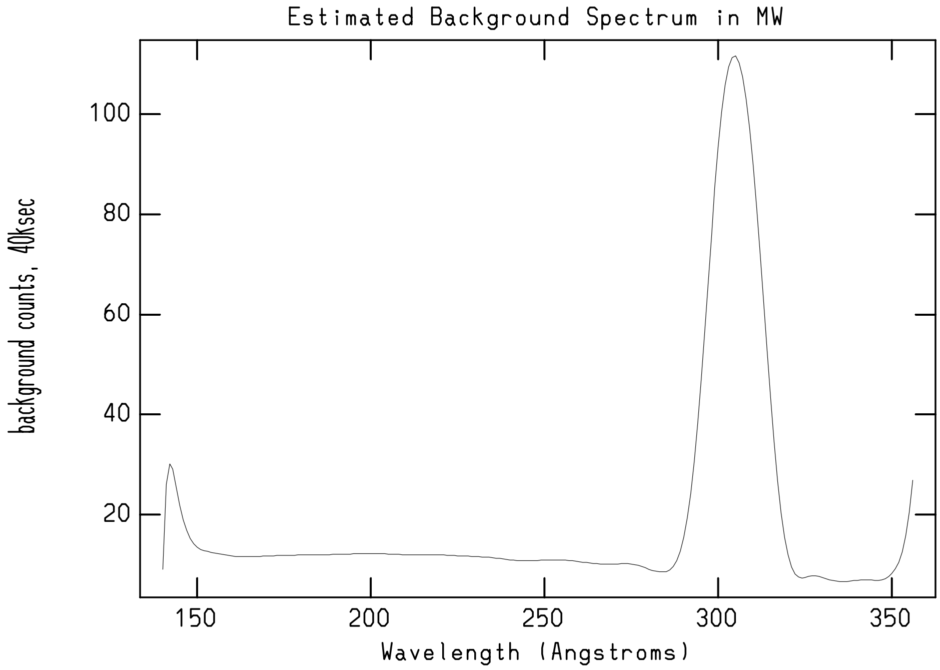

Figure 3-18: Simulated background spectrum for MW, scaled for a 40 ksec observation, in 1-Å bins.

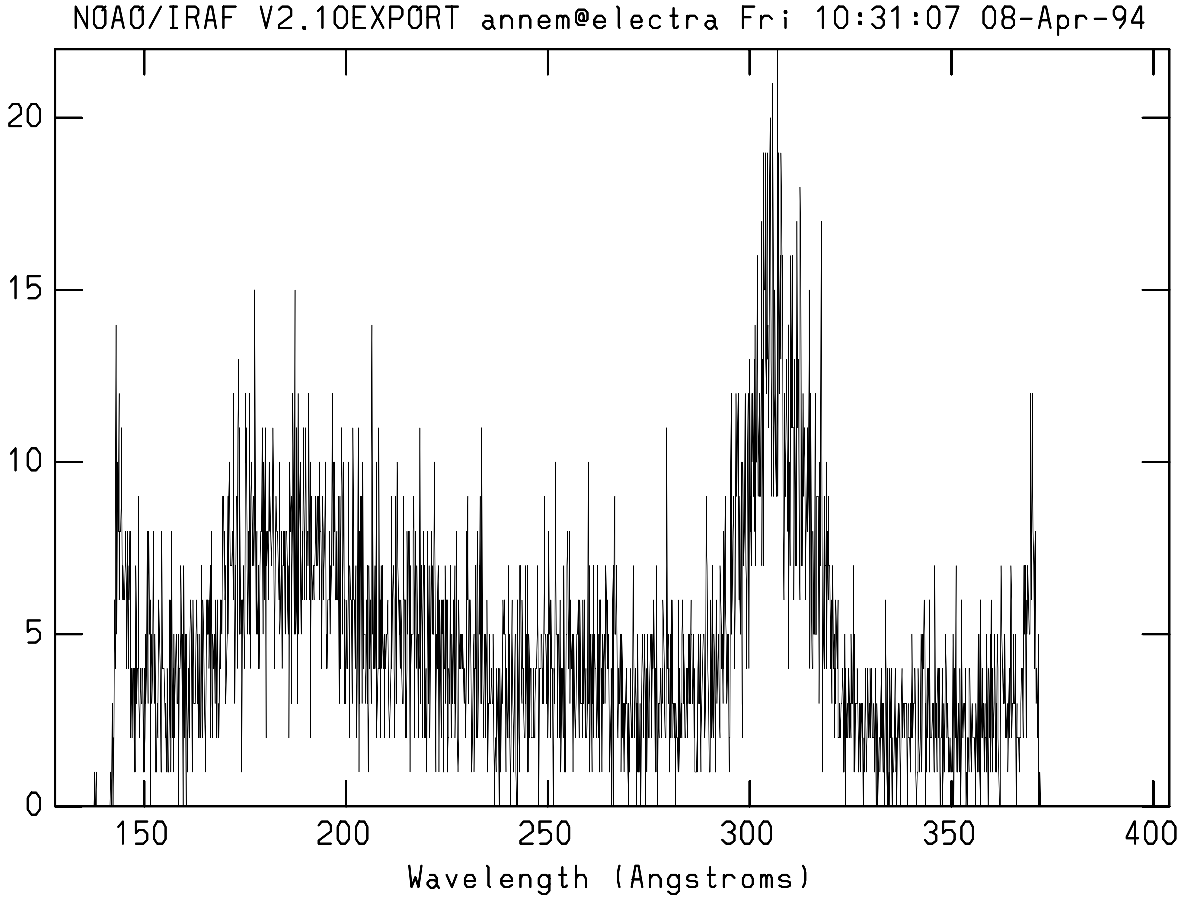

Figure 3-19: Raw spectrum of the white dwarf WD1845+019 in MW, showing typical background and noise level. No rebinning.

3.7 Detection Quality

Technical Justification of observations requires proposers to demonstrate that measurements with a signal-to-noise ratio adequate for their science program will be obtained for at least one wavelength in the spectrum of each target, using their source model and proposed integration time. This section presents formulas for calculating the signal (S), standard deviation (σ) and the signal-to-noise (S/σ), in terms of the instrument source count rate, background count rate, and integration time. We illustrate calculations for the emission and continuum sources, and invert the formula to calculate integration times from S/σ requirements.

The source signal in a bin is the difference between the total counts (T) and the background counts (B). The estimated standard deviation of the source counts (S) in a spectral bin is defined by:

$$\sigma_S(\lambda) = \sqrt{{\sigma_T}^2 + {\sigma_B}^2}$$

where σ_B denotes the standard deviation of the accumulated background, and σ_T is the standard deviation in the total counts, S + B. The uncertainties in S and B are given by $\sqrt{\mathrm{S}}$ and $\sqrt{\mathrm{B}}$. Applying this rule, and using the average in equation 3-3 as an estimate of the total background, we have:

$$\sigma_S = \sqrt{\mathrm{S} + \mathrm{B}(1 + 1/n)} \tag{3-6}$$

The signal-to-noise is estimated by the ratio of the number of signal counts to the signal deviation, S/σ_S. If the signal and background counts are written in terms of the count rates and the integration time, $\mathcal{T}$, we see that the signal-to-noise will increase as the square root of the observation time:

$$\frac{\mathrm{S}}{\sigma_S}(\lambda) = \frac{\sqrt{\mathcal{T}}\,\mathrm{S}'}{\sqrt{\mathrm{S}' + \mathrm{B}'\,(1 + 1/n)}} \tag{3-7}$$

where primes denote the rates of signal and background events in some spectral bin at wavelength λ. So to double the ratio S/σ_S one must multiply the observation time by a factor of four.

To calculate an exposure time from S/σ requirements, simply invert equation 3-7:

$$\mathcal{T} = \left(\frac{S}{\sigma_S}\right)^2 \times \frac{\mathrm{S}' + \mathrm{B}'(1 + 1/n)}{{S'}^2} \tag{3-8}$$

We can substitute one of the count rate expressions from equations 3-1 or 3-2 for the source count rate, S$'$.

Background and background count rates are obtained by multiplying the appropriate count rate per Å ($\mathcal{B}$ in equations 3-4 and 3-5) by the spectral bin width, (w) in Å and the time. Use the distributed background from section 3.6.3 for lines away from airglow or edges, and the background spectrum values for continuum or lines near airglow features. Expanding the expressions for S/σ and $\mathcal{T}$, we obtain formulas for signal quality in a single spectral bin, in terms of source flux, effective area, and time:

$$\frac{\mathrm{S}}{\sigma_S} = \frac{\mathcal{F}\mathrm{A}_{eff}\mathcal{T}}{\sqrt{\mathcal{F}\mathrm{A}_{eff}\mathcal{T} + \mathcal{B}w\mathcal{T}(1+1/n)}} \quad \text{(lines)} \tag{3-9}$$

or

$$\frac{\mathrm{S}}{\sigma_S} = \frac{\mathcal{F}\mathrm{A}_{eff}\ w\mathcal{T}}{\sqrt{\mathcal{F}\mathrm{A}_{eff}\ w\mathcal{T} + \mathcal{B}w\mathcal{T}(1+1/n)}} \quad \text{(continuum)} \tag{3-10}$$

for the S/σ ratio, and

$$\mathcal{T} = \left(\frac{\mathrm{S}}{\sigma_S}\right)^2 \times \frac{\mathcal{F}\mathrm{A}_{eff} + \mathcal{B}w(1+1/n)}{(\mathcal{F}\mathrm{A}_{eff})^2} \quad \text{(lines)} \tag{3-11}$$

or

$$\mathcal{T} = \left(\frac{\mathrm{S}}{\sigma_S}\right)^2 \times \frac{\mathcal{F}\mathrm{A}_{eff}\ w + \mathcal{B}w(1+1/n)}{(\mathcal{F}\mathrm{A}_{eff}\ w)^2} \quad \text{(continuum)} \tag{3-12}$$

for the integration time.

Example: Late star emission S/σ Evaluate the measurement quality for lines in the late type star example. Suppose we want to know what signal-to-noise would be achieved for the spectral line at 171.06 Å in a 40K second observation. Assuming the line is narrower than the resolution element $\Delta\lambda$, and multiplying equation 3-1 by $\mathcal{T}$, the number of counts in the short wavelength line after 40K seconds would be ~153. The background at 171 Å in SW was calculated in section 3.6 to be ~11 counts. With n = 10 for the ratio of background to spectrum height, we obtain a signal deviation of:

$$\sigma_{SW}(171.06) \ = \sqrt{153 + 11 \times (1.1)} = 13 \text{ counts},$$

so that the signal-to-noise ratio is about:

$$\frac{S}{\sigma_{SW}}(171.06) \ \simeq \frac{153}{13} \ \simeq 11.8$$

The same line would also be imaged in the MW channel, with about 242 signal counts and 12 counts in background, yielding a signal-to-noise of:

$$\frac{S}{\sigma_{MW}}(171.06) \simeq \frac{242}{\sqrt{242 + 12 \times (1.1)}} \simeq 16$$

The line has better signal-to-noise in the MW channel. For a line this far above the background, the S/σ is dominated by the source counts and hence the integration time.

Reverse this process to calculate an integration time. Suppose we require the S/σ ratio of the feature at 222 Å to be 5, and apply equation 3-8. Again, the bin size is assumed to be $\Delta\lambda$, which in the MW is 1 Å:

$$\mathcal{T} = \; 25 \times \left[\frac{1.08{\times}10^{-4} + 2.9{\times}10^{-4}\,(1.1)}{1.166{\times}10^{-8}} \right] \; = \; 9.15{\times}10^{5}\,\text{seconds.}$$

It requires quite a long observation.

Example: Continuum Detection Quality We have the signal count rate in the MW channel from our G191-B2B simulation in figure 3-7. To estimate signal-to-noise for some wavelength λ in a continuum, we will examine the signal near the O IV edge at 298 ÅṠince we have a nice bright source, we will work at the limit of MW spectral resolution, and use 1-Å bins, the resolution shown in the figure. First, we apply equation 3-2 and the integration time to obtain the source counts in bins spanning the minimum and maximum of the edge feature. Since our original simulated spectrum has .2 Å bins, j in equation 3-2 is 5:

$$\mathrm{S}_{min} = \sum_{j=1}^{5} \mathcal{F}(\lambda_j)\,\mathrm{A}_{eff}(\lambda_j)0.2 \times \mathcal{T} = 6377\,\text{counts}$$

$$\mathrm{S}_{max} = \sum_{j=1}^{5} \mathcal{F}(\lambda_j)\,\mathrm{A}_{eff}(\lambda_j)0.2 \times \mathcal{T} = 6722\,\text{counts}$$

The background is mostly from the wings of the 304 Å airglow feature. We use the count rates from the MW background spectrum, integrated over a 1-Å bin on either side of the edge, and multiply by $\mathcal{T}$ = 40K seconds to get the integrated background in each bin. Letting n = 10, and applying equation 3-6 for the signal deviation to each side gives:

$$\sigma_{S_{max}} = \sqrt{6722 + 84(1.1)} = 82.5$$

$$\sigma_{S_{min}} = \sqrt{6377 + 71(1.1)} = 80.3$$

So the signal-to-noise is about 80 both above and below. When we subtract the source counts to get the height of the edge, in counts, the error for the edge detection is:

$$\sigma_{diff} = \sqrt{{\sigma_{S_a}}^2 + {\sigma_{S_b}}^2} = 115$$

This is a substantial percentage of the difference of 395 counts, despite the fact that both individual measurements had high S/σ.

3.8 Time-Critical Observations

Timing information for all photon detections and software tools for analysis of transient and periodic events will be available to Guest Observers. Besides limitations on photon event timing accuracy, the main constraints that will complicate the analysis of time-critical data arise from the interplay between source brightness, the ability to correct for instrument deadtimes, the source variability, and the intervals available for data acquisition.

3.8.1 Photon Timing Accuracy

Timing accuracy is fundamentally limited by the number of time-bits available in the spacecraft software format. The Explorer Platform clock is synchronized to ground UT within 1 msec, and event times are assigned by the payload electronics with an accuracy of 8 msec. If it is necessary to convert EUVE's photon arrival times to heliocentric times with accuracies better than 60 msec, knowledge of the spacecraft ephemeris is also required. The position information necessary for making these corrections is stored in the telemetry and is made accessible to the GO through the IRAF/EUV software tools.

Deadtime is primarily due to the limited capacity of the electronics and the capacity of the telemetry stream. The maximum count rate the telemetry can support is 437.5 cts/s. This is the *total* number of photon "slots" available to *all seven* detectors, which usually operate continuously. The geocoronal EUV background counts occupy a major fraction of these slots. The instrument software algorithm that assigns telemetry slots insures that some counts from each detector are recorded, but it is possible that some source photons will not be recorded if either a source or the background in that detector becomes very bright. The EGO Center may request the shutdown of one or more scanning telescope detectors during observations of very bright sources, such as the moon, or in the event of sudden increases in the background.

Another factor limiting the time resolution is the accuracy with which deadtime correction can be performed. Deadtime is monitored in the instrument software with a time resolution of 2 seconds, and can be corrected for at this interval. EGO Center reduction tools will be available to help observers reconstruct intrinsic light curves, but the practicality of correcting the count rates on small time scales will remain limited even after the best possible processing.

3.8.2 Counting Statistics and Observation Timing

The time resolution for even the brightest EUV sources will be limited by counting statistics and the partition of the observation time used in reductions. The EGO Center provides IRAF software tools to extract spectra at full resolution and to rebin them as desired. Proposers should make exposure and signal-to-noise calculations for each segment of the observation period that is to be analyzed separately.

Example: Variable Source Measurements Suppose an observer wished to monitor a variation in the flux at 303.8 Å in our model emission source. If this requires a 3–σ measurement for each observation, then using the instrument count rate from table 3-1 and the estimated background rate from the spectrum in section 3.6, and assuming a bin width of $\Delta\lambda = 1.0$ Å for MW, one can calculate the minimum acceptable integration time from equation 3-8:

$$\mathcal{T} = \frac{9\left[2.00\times 10^{-3} + 2.78\times 10^{-3}(1.1)\right]}{4.00\times 10^{-6}} \approx 11500 \text{ seconds}$$

So in spite of the high background, 4 such observations could be made in 50K seconds.

The longest strictly continuous integration time available is one orbit nighttime, which varies from 1800 to 2200 seconds. Proposers should request as much time as necessary for each observation, but should be aware that the observation will be interrupted once per orbit, for about 57 out of every 90 minutes. For strictly periodic sources, integration times up to half the period may be desired, and sources with a period closer to the orbital period of the satellite may require longer observations for adequate sampling. Uninterrupted observing time should be specifically requested, since long observations may otherwise be interrupted to service programs requiring shorter and more frequent observations.

Observations of events with very long, non-uniform periods, such as sudden brightening in CV stars, should be proposed as a targets of opportunity (TOO's); see section 3.9 below.

3.9 Targets of Opportunity (TOO)

Requests for targets of opportunity will fall into one of two classes:

1. conditional requests, where the opportunity is expected, but is not a regular or predictable event.
2. Observations of serendipitous events that may be bright in the EUV.

Any conditional proposal of the form "if condition A occurs, then observe target B" should be proposed for as a normal target, but should also be identified on the proposal information and target list forms as a conditional TOO. Investigators must provide clear, measurable criteria for deciding observability, and give their best estimate of when these conditions are expected to occur. The observer will be responsible for conducting any ground-based monitoring necessary to predict a sudden event in time for an observation request to be honored. Once a conditional TOO proposal is accepted by the EGO Peer Review Panel, the proposal's Principal Investigator must notify the EUVE Principal Investigator at Berkeley, at the EUVE Guest Observer Center, egoinfo@cea.berkeley.edu, as soon as the TOO is observable, and must present clear evidence that the criteria have been met.

In the case of an unanticipated TOO, a request must be submitted to the Project Office, addressed directly to the Project Scientist at GSFC. The request must identify the principal

Guest Observer and include the target location and a Scientific Justification. Prospective GO's should consult the current UCB/EUVE Call for Proposals for correct and complete instructions for submitting TOO proposals.

In either case, the Guest Observer must also notify the EUVE Principal Investigator at Berkeley as soon as the request is submitted, so that preparations can be made by the ESOC staff, pending approval. A response time in the EUVE exteneded mission will be on a best bet effort, but a response time of as little as 24 hours after approval may be possible.

3.10 Diffuse and Extended Sources

The Spectrometer may be used to observe sources whose light is spread diffusely across the aperture or extend across more than 1 arc minute in the field of view. Such sources include the moon, planetary atmospheres, emission nebulae, supernova remnants, and the ISM. Any source larger than 20 arc minutes should be considered a diffuse source. Sources smaller than 20 arc minutes may be considered extended sources. Objects that are significantly smaller than 1 arc minute, such as planets and comets can be observed as point sources.

Since the Spectrometer is a slitless instrument, the count rate per bin and line width for observations of diffuse or extended sources will be determined by the transmission of the wire-grid collimators and the size of the source. Most observations of diffuse ($> 20'$) sources will only be practical in the medium and long wavelength channels, where the collimators limit the width of spectral features, but spectral resolution will be somewhat degraded as a result. Even a "narrow" emission feature from a diffuse source will be 20 arc minutes wide, FWHM. Observations of extended sources smaller than 20 arc minutes may produce narrower features. Spectral observations of diffuse or extended sources will therefore require more observing time [27] than those of point emission sources.

Since the wire-grid collimators limit the field of view in the spectral direction only, angular resolution will be poor to non-existent for truly diffuse sources, such as the ISM. Extended sources produce spectra whose angular extent in the imaging direction is determined by their size along the direction tangent to the aperture radius, as projected onto the field of view. This is a different direction for each Spectrometer channel, and it means that angular extent can be minimized or maximized in only one channel for any given roll angle.

Figure 3-20 shows the relative positions of aperture plate openings, detectors, and the dispersion (X) and imaging (Y) directions on each detector in the DS/S. Roll angle is specified as the angle from a radius halfway between the LW and MW detectors and parallel to the deep survey filter bars, pointing toward the MW detector.

If a proposer wishes to align one of the Spectrometer channels with a particular source axis, the request should be made in the section of the Target Summary Form of the Target Summary Form set aside for special pointing requirements, by stating the direction and angle between north and the dispersion (spectral) direction for the channel to be aligned. For example, someone proposing to make observations of Jupiter might give the desired orientation of the long wavelength dispersion direction to the plane of the Io Torus as XX degrees west of north. Any requested Spectrometer roll angle may have to be adjusted to

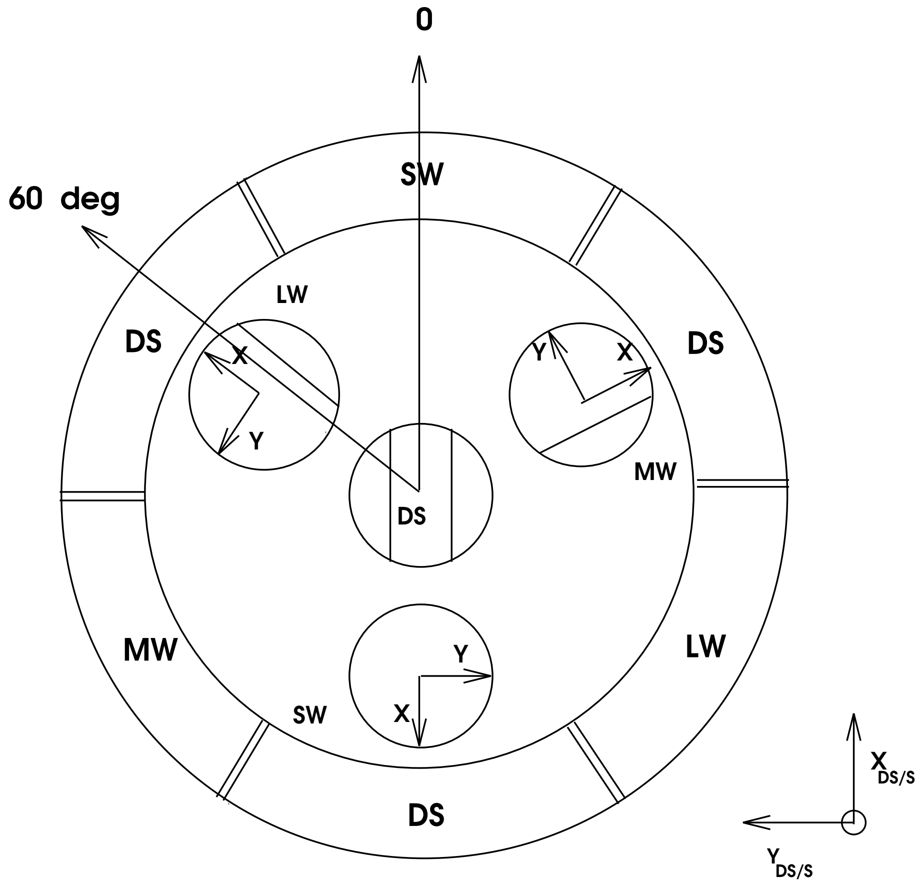

Figure 3-20: Orientation of Spectrometer detectors to DS/S aperture. Observer is looking *toward* the focal plane, from in front of the telescope.

conform to physical and time constraints imposed by the scheduling process (see section 4.2).

3.10.1 Models and Count Rates for Diffuse Source Simulations

Models used to simulate diffuse or extended objects should generally be two-dimensional, and give flux in units of photons/cm^2/sec/Å/sr, with the bin size clearly indicated on proposals. Since any extended source will produce wide spectral features, the formula used to estimate source count rates is derived from equation 3-2 for continuum sources. The expression for the instrument count rate in equation 3-2 becomes a double sum:

$$\mathrm{S}'_{diff} = \sum_{i=1}^{M} \sum_{j=1}^{N} \mathcal{F}_{ji}(\lambda) \mathrm{A}_{eff}(\lambda_i) \Delta\lambda_j \Delta\theta i \tag{3-13}$$

where $\mathcal{F}_{ji}(\lambda)$ is the (two-dimensional) flux distribution of the source in wavelength/image angle space, with the image axis oriented along the selected source axis. The spectral bin size is $\Delta\lambda_j = 20\overset{\frown}{'}$ for diffuse sources. This is equivalent to about 16 and 32 Å at FWHM in the medium and long wavelength channels, respectively. Smaller values of $\Delta\lambda_j$ will apply for sources smaller than 20 arc minutes in the spectral direction for each detector. The FWHM angular resolution element, $\Delta\theta i$ on the detector is approximately 20-25$\overset{\frown}{''}$, and the entire spectrum height is about 42$\overset{\frown}{''}$, or 10 pixels.

If the total flux from an extended ($<$ 20 amin) source can be estimated from previous observations, it may be assumed for the Technical Justification that the target has a uniform surface brightness. Existing flux measurements from diffuse sources must be adjusted to compensate for the size of the instrument field of view before use in planning EUVE observations.

Proposers may use the one-dimensional first order effective areas in this expression. For extended sources, proposers should divide the angular extent of the source in the direction to be oriented along the imaging axis (Y) by the size of $\Delta\theta i$ to determine the value of M. For diffuse sources, proposer must decide how much of the Spectrometer detector height they wish to include in their "aperture", or how it should be divided to provide maximum coverage of the field of view in each part of the wavelength range.

Some extended sources may produce multiple spectra from brighter subregions, depending on separation and the source's orientation to the aperture, as noted above. See section 3.11 on evaluating multiple sources in the field of view.

3.10.2 Background for Diffuse Source Spectra

The background spectra in section 3.6 are in units of photon flux/Å and are only appropriate for point sources, as they represent a sum over the average spectrum height of $\Delta\theta i$. To estimate the background rate for an extended source at a single wavelength, multiply the background spectrum by the resolution element, $\Delta\lambda_j$ and the height of the object spectrum, h, in units of $\Delta\theta i$:

$$\mathrm{B}_{diff}(\lambda) = \sum_{j=1}^{N} \mathcal{B} \times h \times \Delta\lambda_j \tag{3-14}$$

where $\Delta\lambda_j$ is equivalent to $20\overset{\frown}{'}$ or the source size in the dispersion direction, whichever is less, and h is the spectrum height divided by $\Delta\theta i = 25 - 42\overset{\frown}{''}$. Then calculate the signal-to-noise or integration time as in section 3.7.

Because larger objects may leave little or no detector area available for sampling the background, observations of diffuse sources will in general result in poorly resolved, confused spectra unless accurate models of the spatial distribution of the source flux or background are available (see section 4.5.3).

3.11 Imaging Multiple Sources

Some binary sources and extended sources with internal structure may be observable with the EUVE Spectrometer. In these cases, Guest Observers will be interested in knowing whether the two objects can be resolved as separate spectra in the imaging direction. The full width at half maximum of the angular resolution is roughly $\widehat{25''}$ as of this writing. The angular separation of two sources must be at least this great for their light to be imaged as separate spectra. Technical Justification must be done separately for each part or object for which a spectrum is required.

To evaluate the possibility that spectra from different areas of a multiple or extended source may be resolved at specific wavelengths, see the information on angular resolution in table 3-2, columns four and five.

3.12 Quick Reference to Parameters and Equations

Numerical Constants

resolution element	$\Delta\lambda_{SW} \simeq 0.5$	Å
	$\Delta\lambda_{MW} \simeq 1.0$	Å
	$\Delta\lambda_{LW} \simeq 2.0$	Å
spectrum height	$\simeq 42$ arc seconds	
distributed background	B $\simeq 5.4\times10^{-4}$	cts/sec/Å in SW
	B $\simeq 2.9\times10^{-4}$	cts/sec/Å in MW
	B $\simeq 1.7\times10^{-4}$	cts/sec/Å in LW

Symbol Definitions

$A_{eff}(\lambda)$	spectrometer channel effective area in cm^2. Function of λ
$\mathcal{F}(\lambda)$	model source flux at spectrometer aperture after ISM absorption
S′	source count rate in a spectral bin, in counts/sec.
S	Total source counts in a spectral bin after integration over time $\mathcal{T}$.
$\mathcal{B}$	Background count rate in cts/second/Å. Function of λ near airglow features and detector edges.
B′	background count rate in a spectral bin
B or $\overline{\mathrm{B}}$	accumulated background counts in a bin, averaged over n times the spectrum height
$\mathcal{T}$	integration time in seconds
T	total integrated signal from sources and background
$\Delta\lambda$	spectral resolution element in Å
$\Delta\theta i$	imaging resolution element, in arc seconds
n	ratio of background region height to spectrum height in the imaging direction
w	spectral bin width in Å
i	bin number in the imaging direction
j	bin number in the spectral direction

Formulas

S'_{em}	source count rate from emission line with width $< \Delta\lambda$	$S'_{em} = A_{eff}(\lambda) \times \mathcal{F}(\lambda)$
S'_{cont}	source count rate from continuum source using bin of width w Å	$S'_{cont}(\lambda) = \sum_{j=1}^{N} \mathcal{F}(\lambda_j)\, A_{eff}(\lambda_j) w_j$
B'	background count rate in a spectral bin	$B' = \mathcal{B}(\lambda) \times w$
B or $\overline{B}$	time integrated background counts in a bin, averaged over $n\times$ spectrum height	$B = \mathcal{B}(\lambda) \times w \times \mathcal{T}$
σ_S	standard deviation of integrated source signal	$\sigma_S = \sqrt{S + B(1 + 1/n)}$
$\frac{S}{\sigma_S}$ (lines)	Signal-to-noise ratio for lines with width $< \Delta\lambda$	$\frac{S}{\sigma_S}(\lambda) = \frac{\mathcal{F} A_{eff}\, \mathcal{T}}{\sqrt{\mathcal{F} A_{eff} \mathcal{T} + B(1+1/n)}}$
$\frac{S}{\sigma_S}$ (continuum)	Signal-to-noise ratio for continuum in bin of width w	$\frac{S}{\sigma_S} = \frac{\mathcal{F} A_{eff}\, w \mathcal{T}}{\sqrt{\mathcal{F} A_{eff} w \mathcal{T} + B(1+1/n)}}$
$\mathcal{T}$ (lines)	Integration time for emission lines of width $< \Delta\lambda$	$\mathcal{T} = \left(\frac{S}{\sigma_S}\right)^2 \times \frac{\mathcal{F} A_{eff} + B'(1+1/n)}{(\mathcal{F} A_{eff})^2}$
$\mathcal{T}$ (continuum)	Integration time for feature for continuum in bin of width w	$\mathcal{T} = \left(\frac{S}{\sigma_S}\right)^2 \times \frac{\mathcal{F} A_{eff}\, w + B'(1+1/n)}{(\mathcal{F} A_{eff}\, w)^2}$
S_{diff}	integrated source counts from diffuse or extended source in bin $\Delta\lambda_j \leq 20^{\frown\prime}$ wide and $\Delta\theta i$ high	$S_{diff} = \sum_{i=1}^{M} \sum_{j=1}^{N} \mathcal{F}_{ji}(\lambda) A_{eff} \mathcal{T} \Delta\lambda_j \Delta\theta i$
B_{diff}	integrated background counts for extended source with bin of width $\Delta\lambda_j$ and height h	$B_{diff}(\lambda) = \sum_{j=1}^{N} \mathcal{B} \times h \times \Delta\lambda_j$

Chapter 4

OBSERVING WITH THE EUVE SPECTROMETER

This chapter describes the interactions of Guest Observers with the EGO Center before, during, and after their observations are made. The EGO Center at CEA in Berkeley is responsible for conducting the technical review to assure the practicality of proposed observations, acquiring and reducing EUVE Spectrometer data, and for providing software tools and facilities for the completion of spectral reductions by Guest Observers. Specific sections include information on the technical review which is conducted by the EGO Center scientists, observation scheduling, data acquisition, nominal reductions, and delivery, and the facilities and services available to Guest Observers through the EGO Center.

4.1 Proposal Technical Review

Proposal review is performed under supervision of the EUVE Science Advisory Board (ESAB), and consists of a Technical Review, followed by the Scientific Peer Review. After proposals are received by the ESAB, the proposed observation plans are reviewed by EGO Center scientists, who review their feasibility and identify difficulties that might arise. Technical reviewers use the assumed flux at the telescope, the estimated source count rates and backgrounds, and the science goals, such as required signal to noise, or other expected results. The scientific material used to justify the estimates of source flux, hydrogen column density, and observed flux at the telescope are evaluated in the Scientific Peer Review only. During Technical Review, any reasons why the observations as proposed may not fulfill the scientific criteria are summarized, and adjustments may be suggested. The Reviews and any recommendations are passed to the EUVE Peer Review Panel for consideration in their evaluations of proposal scientific merit. Other details of proposal selection are described in Appendix A of the current UCB/EUVE Call for Proposals..

4.2 Observation Scheduling

The Berkeley operations team begins observation scheduling as soon as the details of the approved proposals become available. Scheduling is conducted in cooperation with the Flight Operations Team (FOT) at CEA. All observations are scheduled at least 4 weeks in advance, and science plans are approved by the FOT before implementation. Observation scheduling for the current Call for Proposals will begin sometime after February 1998, and these observations will commence in March, 1998.

4.2.1 Coordination and Communication with the GO

Most communications concerning target parameters, scheduling, and data acquisition take place between Guest Observers and the EGO Center. Proposers submit electronic target lists with their proposal, by which they confirm their target coordinates and other information such as special timing and pointing requirements. The EGO Center will help GOs to define pointing and timing requirements that support their stated scientific goals, but any substantial changes in observing programs must be approved on a case-by-case basis by the ESAB.

To assist GOs who will be making simultaneous observations with other instruments, tentative schedule information is made available well in advance through the CEA/EGO Home-Page on the World Wide Web. Once observations are scheduled in an approved science plan, the EGO Center notifies each PI of the planned date and time of their observations, via electronic mail.

Observations of calibration targets may be scheduled independently by the EUVE science team as often as once per month. Proposers who wish to make new observations of calibration targets used in previous Cycles, or who wish to request that a particular target be observed for instrument calibration purposes, should acquaint themselves with the policies on data rights for calibration objects in the current UCB/EUVE Call for Proposals, Appendix A.

Unforeseen schedule changes are occasionally necessary for various reasons. Every effort is made to insure that GO science is not compromised.

4.2.2 Physical Pointing Constraints

There are several types of physical constraints that may affect the scheduling of any pointed spectroscopic observation. GOs are not expected to anticipate them, but should be aware that they may limit the times when a target can be observed, and the length of any single pointing. Constraints on EUVE may be of special concern to those whose programs require observations to be coordinated with other satellites or observatories.

The most important physical constraints are listed below. These and several less stringent conditions are all tested by the *Target Visibility* routine referred to in section 3.3.

- Spectrometers and Scanners must point no more than 90° from the anti-sun direction[1].
- Roll angles are usually restricted to a range of $\leq 33°$ in order to prevent overheating of the Modular Power Subsystem (MPS) and MACS portions of the PED. This requirement is balanced against the need to adequately illuminate the solar panels.
- At least one guide star, from among the on-board list of 1060 stars, must be in the star trackers' field of view, subject to the other constraints. Availability of guide stars may require changes in the spacecraft roll angle during any observation. Guide stars must be free from interference from nearby objects to be usable.
- The lunar disk must not be near the field of view of either the instruments[2] or the star trackers.

[1] The anti-sun constraint may be violated under special circumstances, upon approvable by the observatory director.
[2] Unless, of course, it is the target!

The total number of observations with special pointing or timing requirements will of necessity be limited. Conflicts are avoided whenever possible during scheduling, but it is of the utmost importance for GOs to keep the EGO Center apprised of their progress in scheduling such observations, and to answer queries from the EGO Center as promptly as possible.

4.2.3 "Dithered" Observations

Since flat fields are not available for the Spectrometer, the effect of detector fixed pattern noise (see the box in section 2.2.4) is alleviated for bright continuum sources by pointing the Spectrometer at a series of randomly chosen locations near the target, rather than at a single location for the entire observation. This effectively washes out spatial QE modulations caused by the patterns of deformed micro-channels. The pointing changes are made during orbit daytimes, when the detectors are off. Any defocussing of the spectra is minimized by the EGO Program reduction software, which corrects event positions using the satellite aspect reports to produce the equivalent of an on-boresight observation.

Because the increased number of pointings has some impact on scheduling and operations, the final decision on which observations are dithered rests with the EUVE Project Scientist. Targets that warrant this treatment are identified by the EGO Center scientists using standard criteria, and the EUVE operations team at Berkeley creates a succession of different pointings in the schedule. However, given that this treatment can make a substantial difference in the quality of certain observations, it behooves proposers to identify any bright targets which they feel may be candidates for dithered observations in their Technical Justification.

4.3 Data Acquisition

All spectroscopic data is obtained during orbit nighttime, in periods of approximately 25 to 33 minutes. The observation begins when ESOC instrument controllers transmit the necessary pointing and instrument commands for a scheduled target to the satellite from the ESOC at Berkeley. One 24-hour period of pointed observation results in $\simeq$ 25,000 seconds of nighttime data acquisition. Guest Observers need not be present in the ESOC during data acquisition. The ESOC staff are advised, if necessary, by an EGO Center scientist who is assigned to supervise the observation and act on the GO's behalf.

4.3.1 Events That May Affect Data Acquisition

There are of course various types of unexpected events that may affect any observation. These phenomena do not require changing the Spectrometer pointing or schedules, but their effect on observing time is accounted for in the planning process whenever possible, and compensatory time is added to the observation.

- Earth occultation, may result in a temporary loss of source signal, but this time does not count against the approved exposure time as noted above.

- Transits of the South Atlantic Anomaly (SAA), cause automatic detector shutdowns.
- Interference from the moon and/or the planets in or near the field of view of any of the instruments is usually ruled out in the planning stages. If this were to happen accidentally, the telemetry stream could be saturated with flux from these intervening sources.
- Lapses in data acquisition may affect the observation of time-critical events. Review section 3.8 for more information on time-critical observations.
- Should any of the Spectrometer channels fail during an observation, the advising EGO Center scientist may recommend use of alternate targets, and/or alternate pointing positions, where second order ($n = -2$) spectra will be available off-axis (see section 2.2.3).
- Observations may also be interrrupted by TOOs or emergency instrument shutdowns.

Observers are notified if their observations must be interrupted for long periods, and interrupted observations are rescheduled for completion whenever possible. Observers are notified again when their observations are complete so that they may plan to start their analysis as soon as the nominally reduced data can be delivered.

4.3.2 Deep Survey Observations and Data

Data acquired during spectroscopy observations from the co-axial Deep Survey imaging instrument are now routinely made available to GOs. These data are provided in data formats similar to those used for spectroscopic data.

Since the Deep Survey instrument is co-aligned with the Spectrometer, The Deep Survey data taken during spectroscopy observations is rendered suspect by the central deadspot described in section 2.3. For this reason, all spectroscopy pointings are now routinely offset to avoid placing the Deep Survey image in the deadspot. Radial pointing offsets of $1.5 - 2$ arc minutes are the current norm, as derived from the most recent maps of the deadspot [22]. The shifts are corrected in event processing and do not defocus the spectra or change the bandpass appreciably.

4.3.3 Data Transmission to the EGO Center

EUVE data are transferred to NASA ground stations via the Tracking Data Relay Satellite System (TDRSS). Figure 4-1 is a block diagram of the communications system between GSFC and the CEA, which relies primarily on a 1.5 Mb T1 NASCOM data line. During each TDRSS satellite contact, recorded data are downloaded, and science data and engineering monitors are transmitted in real time. EUVE telemetry is received by the ESOC at CEA and immediately archived as raw telemetry. Data from each "real time pass" (RTP) are immediately analyzed, displayed and inspected by the ESOC staff to assess instrument and satellite health. GOs are notified immediately in the event of any anomaly that requires an adjustment of the observing plan.

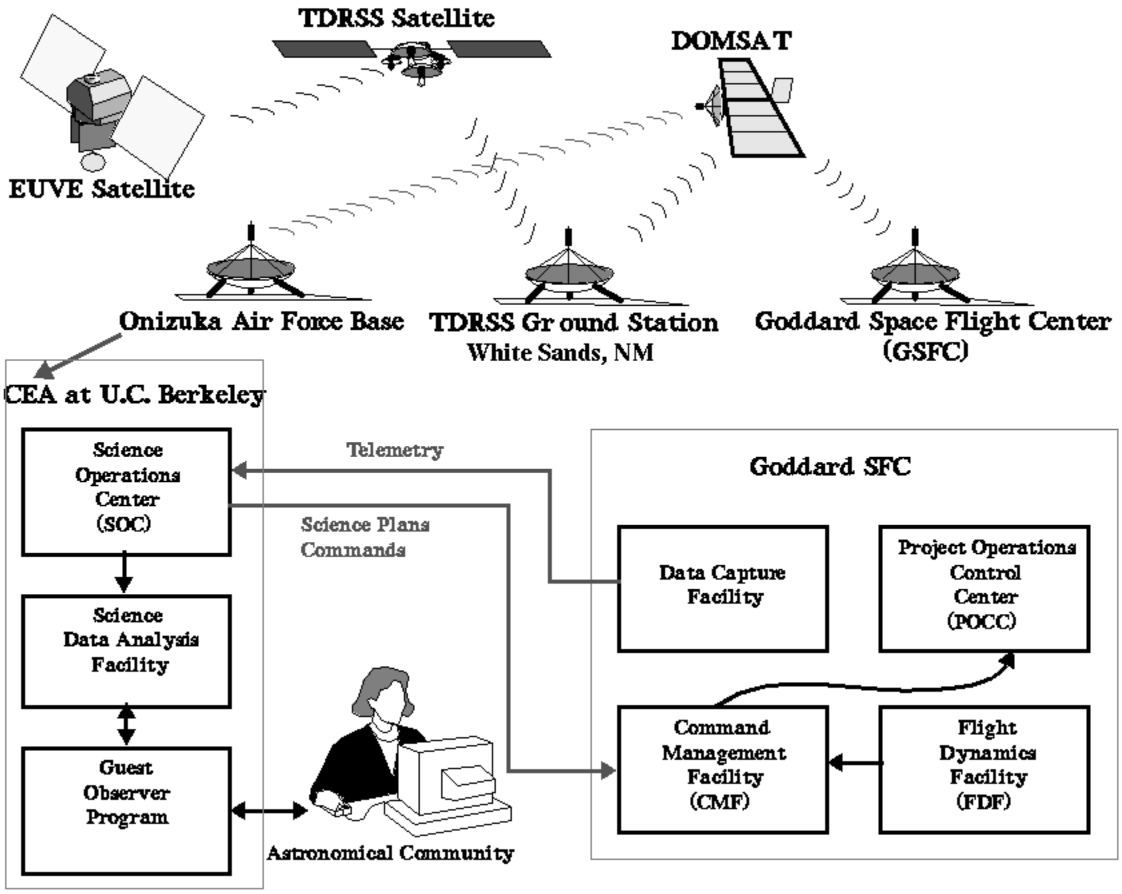

Figure 4-1: EUVE NASA–CEA communications network

4.4 EGO Center Data Processing and Delivery

Data is normally received from GSFC immediately after transmission via TDRSS. Telemetry is stored in raw format upon arrival in the EUVE telemetry archive before data reduction is performed. The steps of data reduction at Berkeley, from the satellite telemetry to nominally reduced spectra, are outlined briefly in this section, followed by a description of the data products delivered to GOs.

Each Guest Observer's data are selected from the data stream and batch-processed using the EUV layered software packages in IRAF (the Image Reduction and Analysis Facility).

The EGO Center software facilities are set up to do nominal data reduction in three separate phases:

1. Telemetry restructuring into Space Telescope (ST) format tables
2. Pipeline processing into Quick Position-Oriented Event (QPOE) files

3. Nominal extraction of raw count spectra into IRAF images using standard apertures

First, the telemetry is decommutated, photon events are separated from instrument health and satellite housekeeping data, and all the data are reformatted by specialized IRAF tasks into time-ordered ST tables.

Second, an automated "pipeline" program performs standard steps to remap events from spectrometer detector coordinates to wavelength (λ, corresponding to detector X) and imaging angle (Θ_i, corresponding to detector Y). The pipeline corrects event coordinates from spacecraft aspect reports and corrects for some instrumental effects, such as large-scale detector distortions. Wavelength and imaging angle scales are applied from a set of instrument reference data tables, derived from Spectrometer calibration observations (see section 2.2.5). Determination of λ and Θ_i for each event is done under the assumption that the target is a point source (no structure), and that all events result from first order dispersions. DS imaging events are remapped from detector coordinates to RA and Declination sky-coordinates.

The list of photon events for each detector is then resorted in position order and stored as an IRAF-compatible QPOE file for processing with IRAF/EUV tasks. The output QPOE file contains the arrival time, detector coordinates, aspect-corrected detector coordinates, and wavelength/imaging angle coordinates (for spectrometer data), for each event. The data in QPOE format may be selected and filtered to create various images. Two of the standard products delivered to the GO are (2048×2048) images made from the raw detector coordinates and the corrected coordinates, the latter of which includes the transformations to the wavelength and angle scales (spectrometer data) or sky-coordinate scale (imaging data), in the image header.

Figure 4-2 shows the flow of pipeline processing, and stages at which information from the spacecraft, instrument engineering monitors, and calibration data are input.

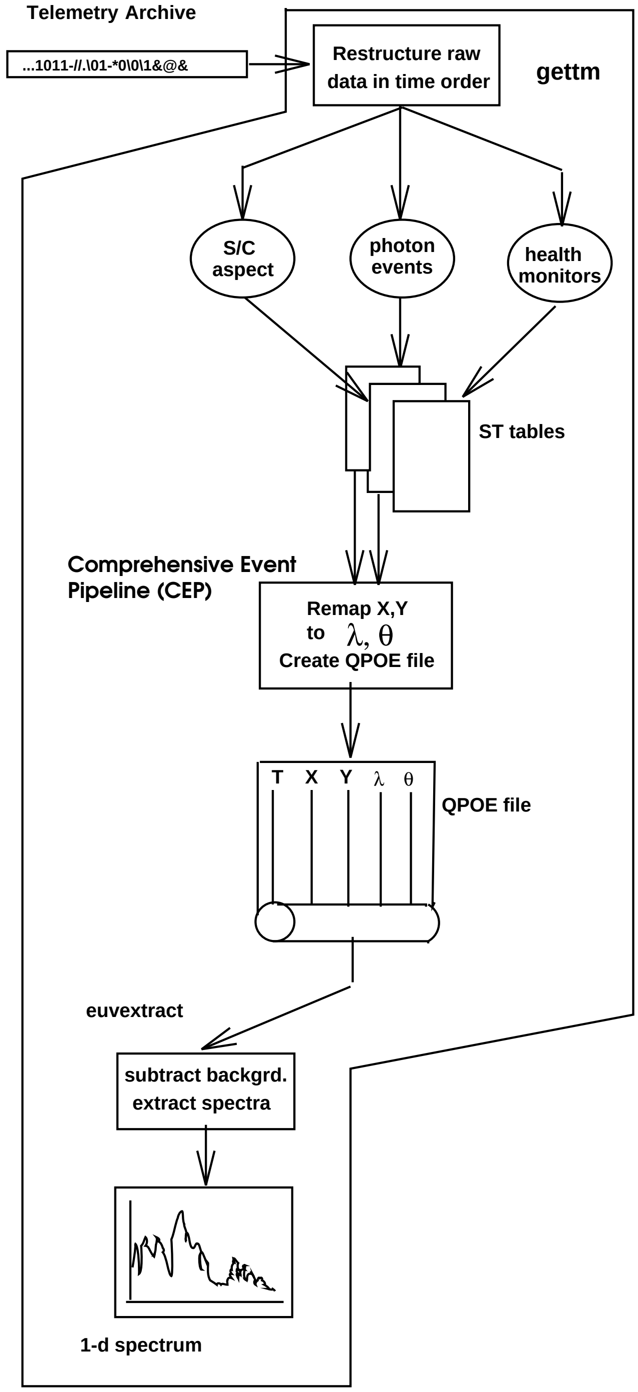

Figure 4-2: Spectrometer pipeline processing

After the spectrometer science data are sorted into separate QPOE files for short, medium, and long wavelength channels, preliminary spectra are extracted from the images using standard apertures and the background subtraction technique outlined in section 3.6. These spectra are not optimized, due to the use of a simple pre-programmed extraction algorithm. Each background-subtracted spectrum is stored as a 2048-pixel spectral image. The data reduction software and nominal data processing performed by the EGO Center is described in more detail in [1].

Data products are distributed on CD-ROM, so that analysis may be done at the Observer's home institution. All data products are delivered to the GO as FITS[3] files. Guest Observers receive a standard set of data products including:

- Raw telemetry tables
- QPOE format event files
- Two-dimensional raw detector images
- Two-dimensional imaging and spectral images
- Three Nominally extracted 1-d spectra

4.5 Guest Observer Data Analysis

The IRAF/EUV layered software package, which is tailored to perform most operations in the reduction of EUVE data, is available to GOs via CEA's *ftp*site, at ftp.cea.berkeley.edu. Observers may contact the EGO Center, via electronic mail at egoinfo@cea.berkeley.edu, to receive assistance in using the software and interpreting features in their data.

4.5.1 IRAF Reduction Tools

All EUVE spectral reduction tools provided by the EGO Center for use on EUVE QPOE and IRAF images are interactive IRAF tasks with on-line documentation. Any IRAF installation, with the addition of the **tables** package can be used to refine the analysis of the QPOE files, images and spectra.

The IRAF/EUV software enables GOs to preform specialized data filtering and selection using the instrument data in telemetry, to rerun the event pipeline with improved instrument reference data, and to produce light curves from the QPOE files.

The EGO Center Software User's Guide provides detailed descriptions of the software, and instructions for operations particularly useful in analyzing EUV data. Software, documentation, and assistance will be available for the basic processing tasks listed below. The basic operations are represented in figure 4-4, in relation to data flow.

- Creating wavelength-calibrated QPOE files from ST tables and instrument reference data
- Browsing and rebinning QPOE files
- Selecting data from "good times" based on instrument engineering monitors

[3]FITS: Flexible Image Transport System

- Calculating geophysical observation parameters from spacecraft housekeeping data
- Filtering and manipulating QPOE file event lists
- Time binning and making light curves
- Flux calibration and removal of higher orders
- Spectrum extraction the GO

The use of the tabular engineering data with IRAF/EUV data selection tasks allows GOs to create and analyze subsets of the original QPOE event listing, selecting data according to their criteria for instrument performance and/or observing conditions. Observers can select data from their observing run on the basis of count rates, pointing direction, time bracketing, or a number of other factors.

The EGO pipeline can also be run on the telemetry by GOs to produce new QPOE files when improved instrument reference data become available.

4.5.2 GO Facilities at CEA

Guest Observers may come to the EGO Center after their observations have been processed, in order to become acquainted with the software and their data. During the EUVE Extended mission, such visits may be contingent upon available resources, and GOs should check with the GO Center by sending electronic mail to egoinfo@cea.berkeley.edu. Computing facilities available to Guest Observers at the EGO Center include disk space for temporary data storage (1 Gig), color graphic workstations running IRAF under UNIX, and access to data reduction software. Guest Observer computer accounts are also available for remote usage. Requests for EGO Center visits or temporary computer accounts should be made via electronic mail to egoinfo@cea.berkeley.edu. Figure 4-3 shows the EGO Center computing network, the EUVE data storage facilities.

Scientific and technical support is available to Guest Observers through the EGO Center during their visit, and throughout the data reduction process. The EGO Center's research associates support routine data processing and assist Observers in using the IRAF/EUV software packages. EGO Center scientists assist GOs in special cases. Products of reductions from EGO Center visits may be transferred to the Observer's home institution via CD-ROM, magnetic tape, or *ftp*.

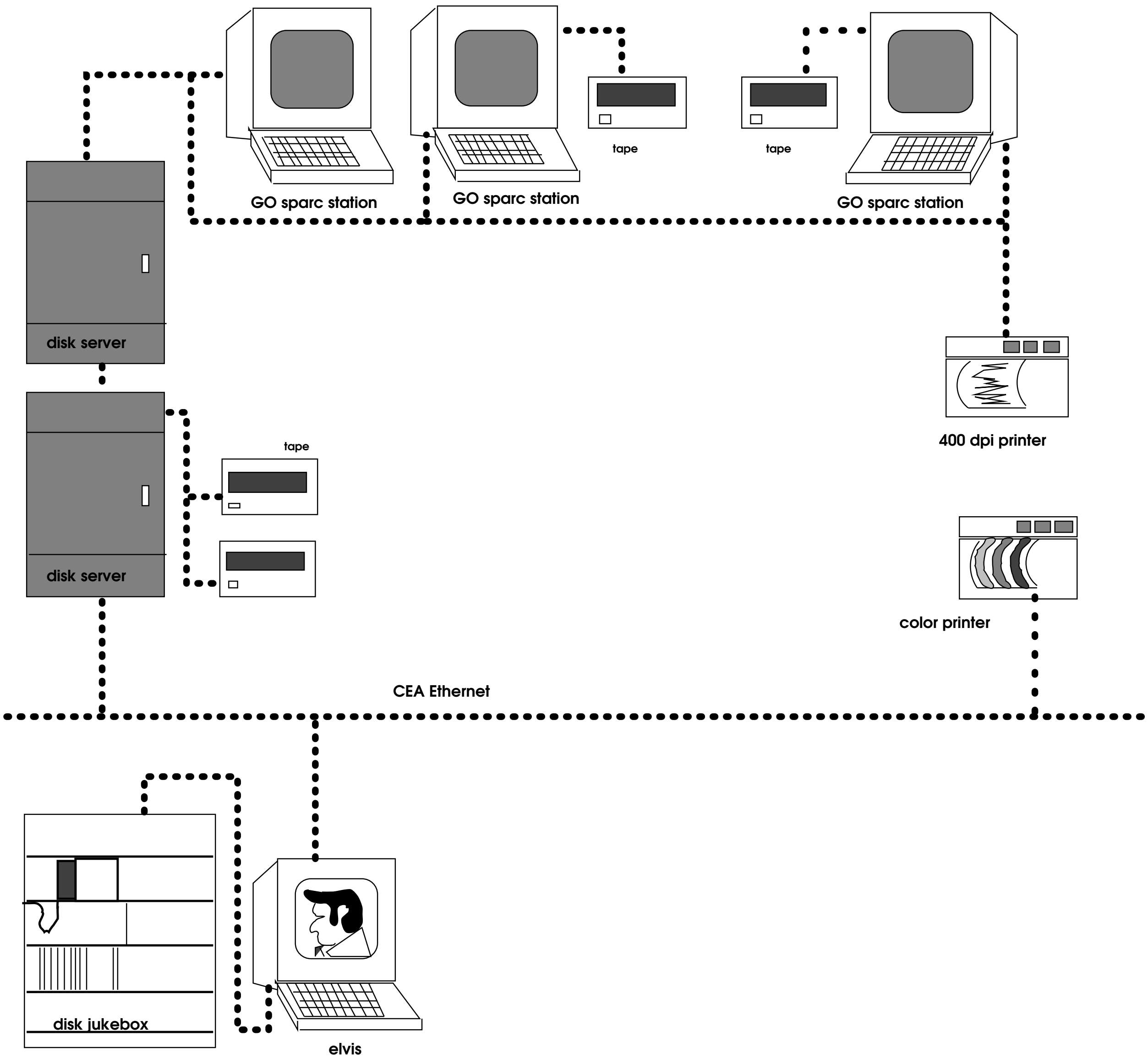

Figure 4-3: EUVE Guest Observer computing facilities

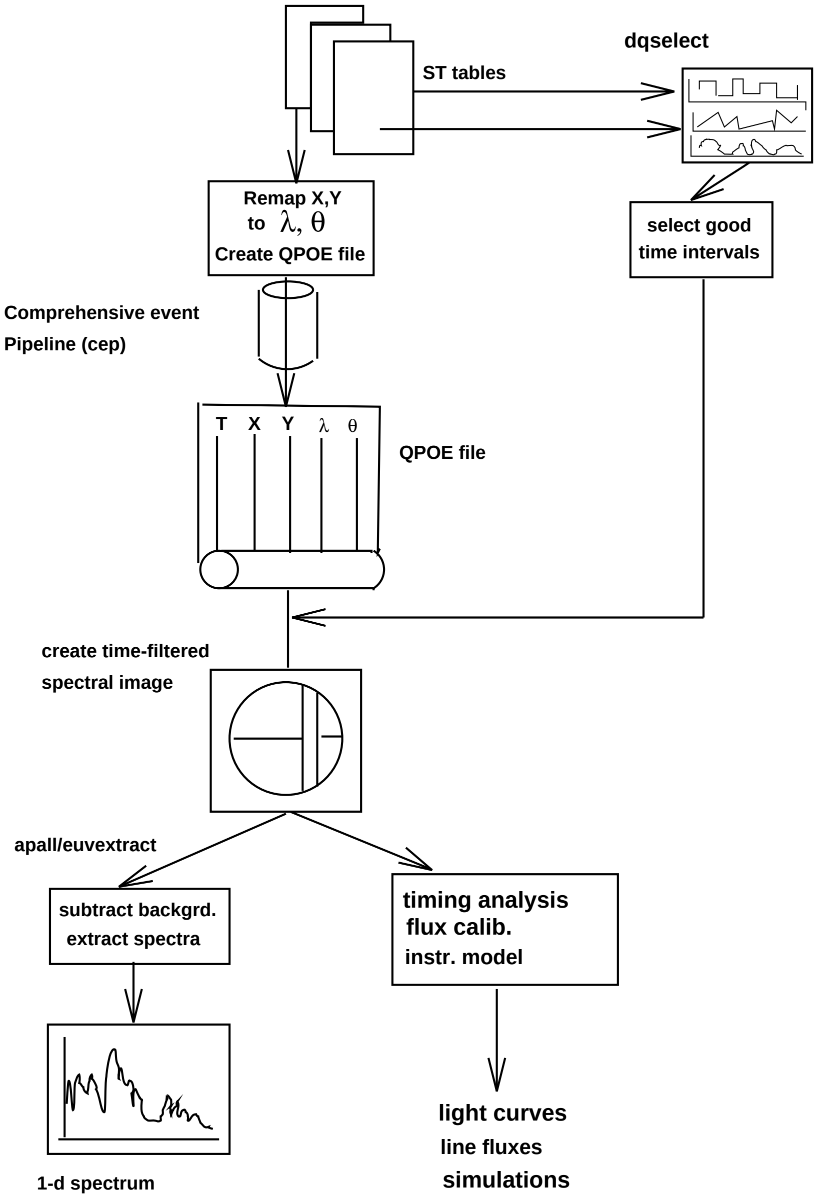

Figure 4-4: Interactive Guest Observer processing

4.5.3 Non-standard Data Reduction

The standard Spectrometer analysis system is designed to handle most observations proposed by EUVE Guest Observers. EUVE Guest Observers desiring complex data analysis may need to work closely with the EGO Center staff and scientists to ensure reliable results. Observations requiring time-resolved spectroscopy can be analyzed by partitioning the data in time, and repeating the analysis for each time interval. Additional tools to support timing analysis are provided, in the form of time-binning and deadtime correction tasks. In general, support for non-standard data analysis is handled on a case-by-case basis, and selected operations are sometimes earmarked for more complete treatment and the creation of specialized software tasks.

4.5.4 Archiving

All GO data products are archived on tape or CD-ROM at the EGO Center. When the GO proprietary period on any set of data expires, the data become available through the EUVE public data archive at the CEA. This archive is most easily accessible through CEA's *WWW* site at www.cea.berkeley.edu.

SKY SURVEY INSTRUMENTS

A.1 Short Wavelength Scanners

Two of the three survey telescopes, called Scanners A and B, are identical, and operate in two bandpass sections between 100 and 500 Å. They have identical Wolter-Schwarzschild Type I mirrors with gold electroplated surfaces. They have a field of view of about 5°, and a focal ratio of 1.41. A cross sectional diagram of the Short Wavelength Scanner design (Type I) is shown in figure A-1. The scanners' characteristics are summarized in table A-1, and described in more detail in [9], [8], [21], and [29].

Table A-1: EUVE Short Wavelength Scanners

Short Wavelength Mirrors

Focal Length	56.22 cm
f/ratio	1.41
Geometric Area	138.0 cm
Field of View	5° diameter
Average Graze Angles	5°, 5° (primary, secondary)
Surface coating	Au, ~ 1000 Å
FWHM (optical)	1 – –2.4 $\widehat{''}$

Short Wavelength Filters

Quadrants	Material	Bandpass
0,1 (A)/2,3 (B)	Lexan/boron 2400 Å/1000 Å	44–240 Å
2,3 (A)/0,1 (B)	Al/Ti/carbon 2000 Å/250 Å/600 Å	140–360 Å

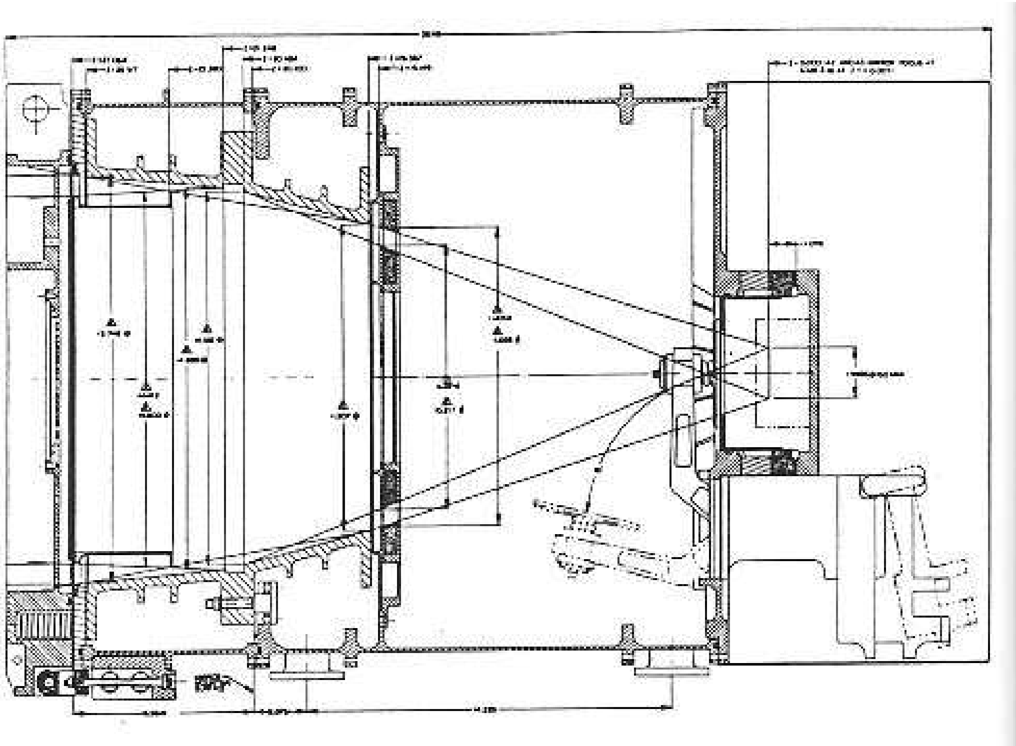

Figure A-1: Cross-sectional diagram of short wavelength scanner.

Because the beam "footprint" at grazing incidence is quite large, the amount of light scattered by a few tens of angstroms' surface roughness in these mirrors can be considerable. Much of the light is scattered within a small angle of the specular direction, but enough lands outside the central image that the difference between the image FWHM and the half energy width (HEW) must be taken into account when processing images. A plot of the scattering histogram for one of the mirrors in shown in figure A-2, where the solid line shows the expected distribution of light from a perfect surface.

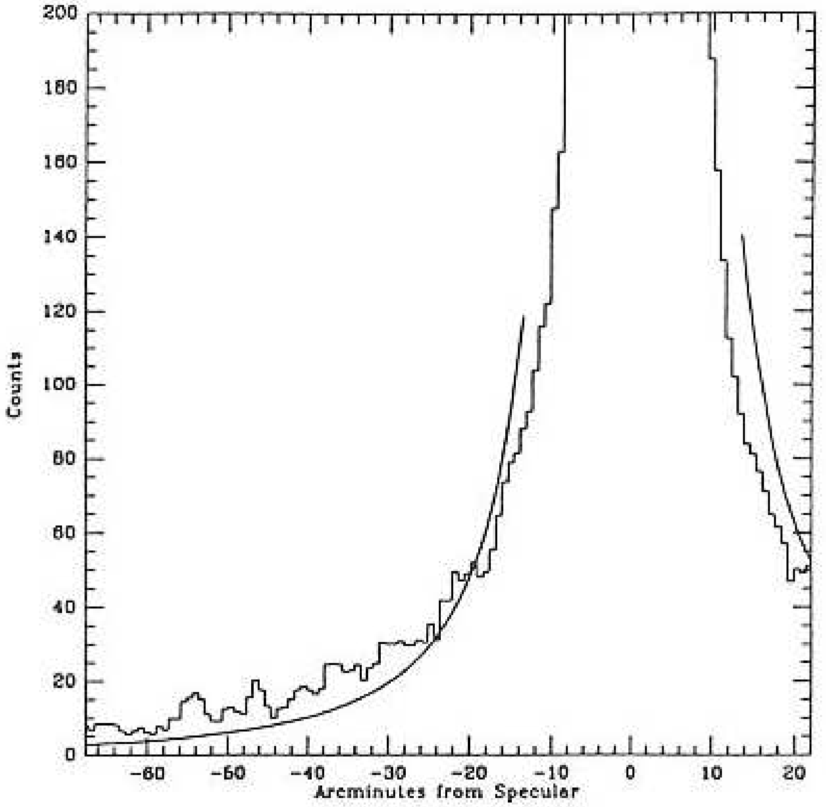

Figure A-2: Scanner mirror scattering histogram.
Solid line is theoretical imaging profile.

The converging beam from each mirror strikes a two-inch diameter MCP detector with a filter divided radially into four quadrants. Two quadrants of the filter are Lexan/boron, with a bandpass similar to those pictured in section 2.3 on the Deep Survey instrument. The boron prevents oxidation and suppresses transmission of Lyman alpha. The other two quadrants are aluminum with a layer of carbon providing a long-wavelength cutoff. Figure A-3 shows the filter configurations and orientations for all three scanners. The detectors have magnesium fluoride (MgF_2) photocathodes deposited on the front channel plates to enhance detection at the shorter wavelengths. See section A.3 for a discussion of scanner effective areas.

Each scanner,including the long wavelength instrument described below, has a magnetic "broom" designed to divert charged particles that enter through the telescope aperture. The broom consists of a solenoid magnet concentric with the optical axis, placed between the primary and secondary mirror sections. It is designed to reject electrons with energies up to 15 keV and heavy thermal ions with energies up to .3 eV.

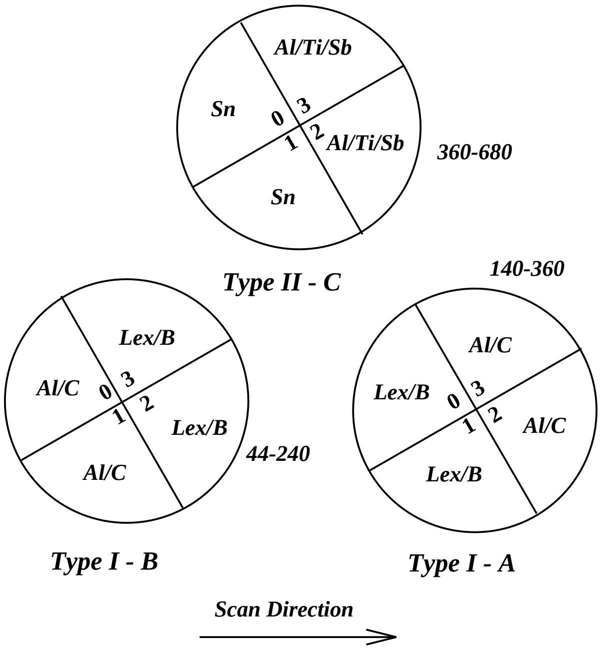

Figure A-3: Scanner filter configuration

A.2 Long Wavelength Scanner

The third survey instrument, often called Scanner C, operates at longer wavelengths between 400 and 900 Å. The mirror design, filter materials and detector photocathode all differ from those of the short wavelength scanners. Figure A-4 shows the long wavelength instrument in cross-sectional view.

Scanner C has a Wolter-Schwarzschild Type II mirror with a diameter of 40 cm and a focal length of 70 cm. The surface is coated with $\sim 13\mu m$ of electroless nickel. Its aperture size is comparable to the short wavelength scanners. It has a 4° field of view, and a geometric area greater than the combined short wavelength scanners. The filters have the same quadrant geometry. Two filter quadrants are made of tin, protected by a thin (100 Å) layer of SiO. The other two quadrants are multilayer "sandwiches" of antimony between layers of titanium, with a layer of aluminum next to the detector. They have been nicknamed "dagwood" filters. The detector has no deposited photocathode. Table A-2 gives characteristics of the long wavelength scanner.

Table A-2: EUVE Long Wavelength Scanner

Long Wavelength Mirror

Focal Length	70.0 cm
f/ratio	1.75
Geometric Area	407.0 cm
Field of View	4° diameter
Average Graze Angles	29°, 21° (primary, secondary)
Surface	$\sim 13\mu$ Nickel
FWHM (optical)	2.3 $''$

Long Wavelength Filters

Filter Quadrants	Material	Bandpass (Å)
0,1	Sn/SiO 3484 Å/100 Å	520–750
2,3	Ti/Sb/Al 374 Å/686 Å/1256 Å	400–600

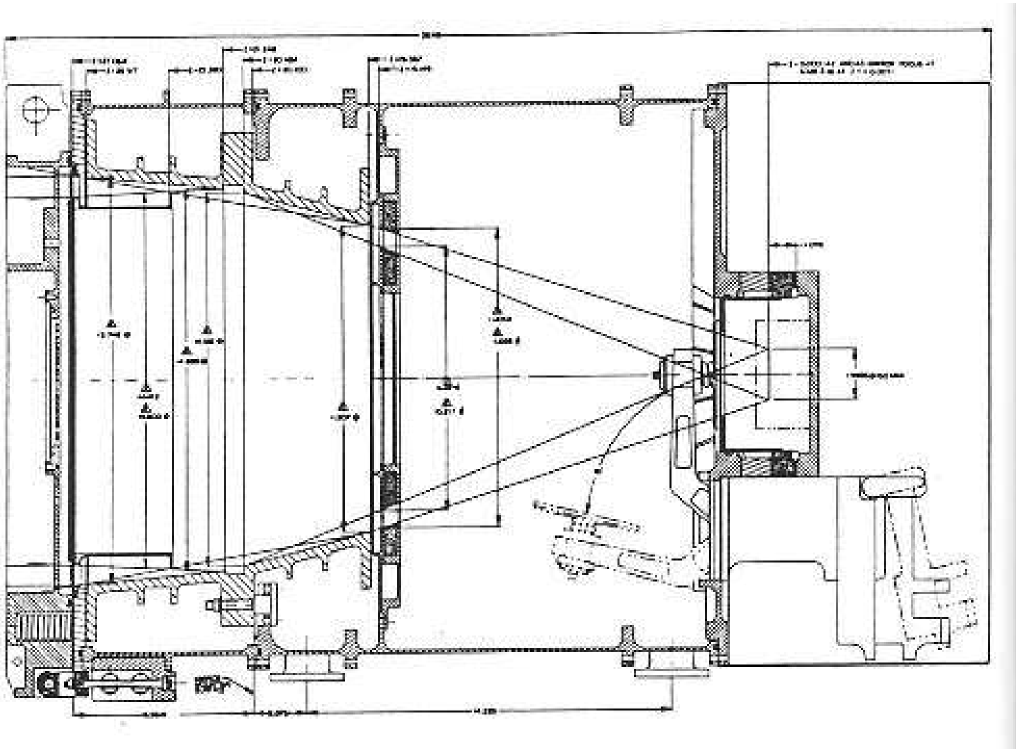

Figure A-4: Cross section of Long Wavelength Scanner (Scanner C)

A.3 Scanner Effective Areas

The effective areas of each of the scanning instruments has been measured in pre-launch calibration and from pointed calibration observations of bright sources. Model fits to the effective areas of the combined short wavelength scanners are shown in figure A-5. Effective area measurements for the long wavelength scanner are shown in figure A-6. Areas for each of the like quadrants in Scanners A and B have been averaged to produce a net effective area each short wavelength bandpass: Lexan/boron, and aluminum/titanium/carbon. Models for the tin/SiO and aluminum/antimony/titanium ("dagwood") filters in the long wavelength scanner are not yet established.

Effective areas are important, but the quality of pointed scanner observations will also depend on detector backgrounds and positioning of the source within the field of view. Optimal pointing will be chosen by the Berkeley operations team to get the best possible focus for each source in each desired bandpass, while avoiding interference from the filter frames near the center of the field of view. Further commentary on the scanner effective areas, background count rates and performance may be found in [16], [20], and [30].

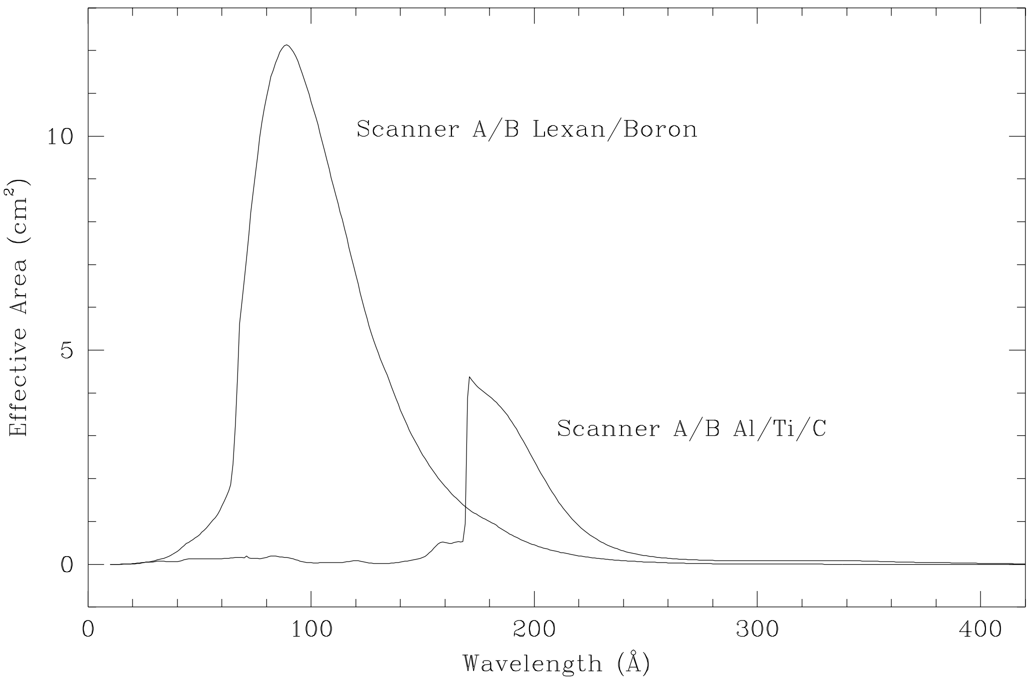

Figure A-5: Effective areas for the short wavelength scanners (Scanners A and B). The short wavelength curve is a model fit to measurements in all quadrants with Lexam/boron filters. The longer wavelength curve is derived from measurements of all the aluminum/titanium/carbon quadrants.

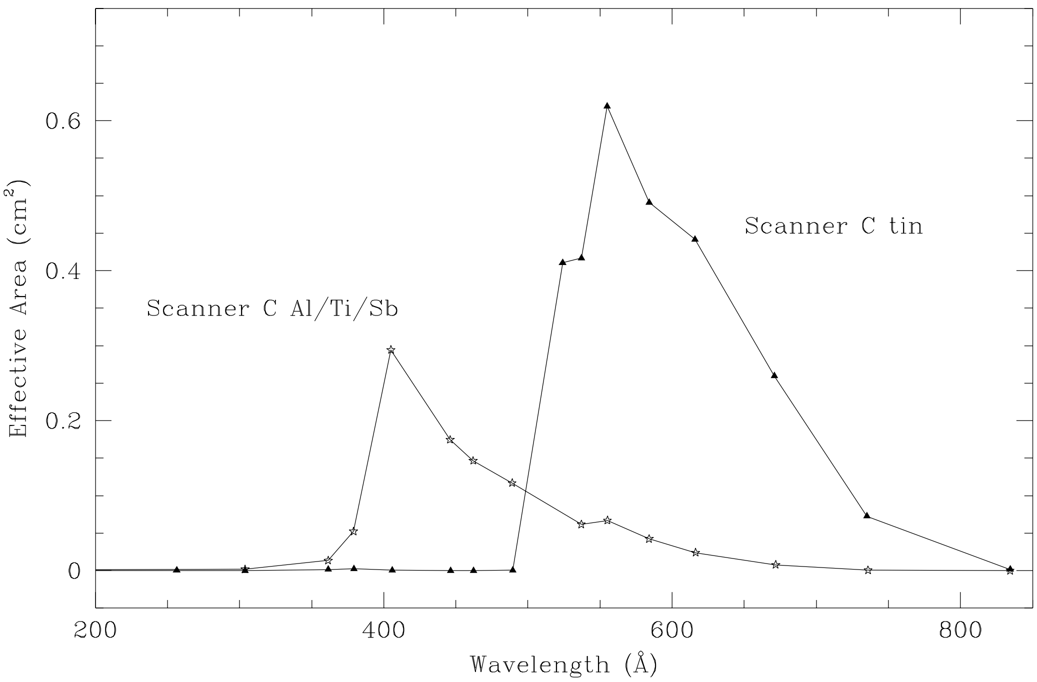

Figure A-6: Effective areas for the long wavelength scanner (Scanner C). The short wavelength curve is a model fit to measurements in quadrants with "Dagwood" filters, of aluminum/titanium/senobium. The longer wavelength curve is derived from measurements of the tin/SiO quadrants.

Appendix B

LIST OF EUVE PROJECT ACRONYMS

ADC	Analog-to-Digital Converter
ADS	(NASA) Astrophysics Data System
C&DH	Command and Data Handler (MMS)
CDP	Command and Data Processor
CEA	Center for Extreme Ultraviolet Astrophysics
DFFS	Digital Fine Sun Sensor
DS/S	Deep Survey/Spectrometer
EA	Effective Area (A_{eff})
EGO	EUVE Guest Observer
EP	Explorer Platform
EUVE	Extreme Ultraviolet Explorer
ESOC	EUVE Science Operations Center
FHST	Fixed Head Star Tracker
FOT	Flight Operations Team (NASA)
FTP	File Transfer Protocol
FWHM	Full Width at Half Maximum
GSFC	(NASA) Goddard Space Flight Center
HEW	Half Energy Width
IRAF	Image Reduction and Analysis Facility
IRU	Inertial Reference Unit
ISM	Interstellar Medium
ISW	Instrument Software
MACS	Modular Attitude Control System
MCP	Microchannel Plate
MDF	Minimum Detectable Flux
MMS	Multi-Mission Spacecraft
MPS	Modular Power Subsystem
NASCOM	NASA Astronomical Satellite Communications
NIST	National Institute of Standards and Technology
PED	Platform Equipment Deck
POCC	Payload Operations and Command Center
QPOE	Quick Position Oriented Event
RIF	Relay Interface
ROSAT	Röntgensatellit
SAA	South Atlantic (Magnetic) Anomaly
SAG	Space Astrophysics Group
TDRSS	Tracking Data Relay Satellite System
TIF	Telescope Interface
TM	Telemetry
TOO	Target(s) of Opportunity
URL	Uniform Resource Locator

COLUMN DENSITIES IN THE INTERSTELLAR MEDIUM: A BIBLIOGRAPHY[1]

1. Anderson, R. C. and Weiler, E. J. 1978, *Ap. J.*, **224**, 143.
2. Anderson, R. C., Henry, R. C., Moos, H. W., and Linsky, J. L. 1978, *Ap. J.*, **226**, 883.
3. Baliunas, S. L., and Dupree, A. K. 1979, *Ap. J.*, **227**, 870.
4. Barstow, M. A., Fleming, T. A., Diamond, C. J., Finley, D. S., Sansom, A. E., Rosen, S. R., Koester, D., Marsh, M. C., Holberg, J. B., and Kidder, K. 1993a, *M. N. Roy. Ast. Soc* , in press.
5. Barstow, M. A., Wesemael, F., Holberg, J. B., Werner, K., Buckley, D. A. H., Stobie, R. S., Fontaine, G., Rosen, S. R., Demers, S., Lamontagne, R., Irwin, M. J., Bergeron, P., Kepler, S. O., and Vennes, S. 1993b, *Advances in Space Research: Recent Results in X-ray and EUV Astronomy,* ed. J. Trümper (New York: Pergamon Press), in press.
6. Bates, B., Catney, M. G., Keenan, F. P. 1986, *Adv. Space Res.*, **6**, 47.
7. Bertaux, J. L., Lallement, R., Kurt, V. G., and Mironova, E. N. 1985, *Astron. & Astrophys.*, **150**, 1.
8. Bohlin, R. C. 1975, *Ap. J.*, **200**, 402.
9. Bohlin, R. C., Savage, B. D., and Drake, J. F. 1978, *Ap. J.*, **224**, 132.
10. Bohlin, R. C., Hill, J. K., Jenkins, E. B., Savage, B. D., Snow, T. P., Spitzer, L. and York, D. G. 1983, *Ap. J. Supp.*, **51**, 277.
11. Boksenberg, A., Kirkham, B., Pettini, M., Bates, B., Carson, P. P. D., Dufton, P. L., and McKeith, C. D. 1975, *Ap. J. (Letters)*, **202**, L91.
12. Bowyer, S., and Malina, R. F. 1991, *Extreme Ultraviolet Astronomy,* ed. R. F. Malina & S. Bowyer (New York: Pergamon), 397.
13. Brown, A., Drake, S. A., Van Steenberg, M. E., and Linsky, J. L. 1991, *Ap. J.*, **373**, 614.
14. Bruhweiler, F. C., and Kondo, Y. 1982, *Ap. J.*, **259**, 232.
15. Bruhweiler, F. C., Oegerle, W., Weiler, E., Stencel, R., and Kondo, Y. 1984, *IAU Colloquium No. 81, Local Interstellar Medium*, ed. Y. Kondo, F. C. Bruweiler, and B. D. Savage (NASA CP-2345), p. 64.
16. Bruhweiler, F. C., and Vidal-Madjar, A. 1987, *Scientific Accomplishments of the IUE*, ed. Y. Kondo (Dordrecht: Reidel), 467.
17. Cash, W., Bowyer, S., and Lampton, M. 1979, *Astron. Astrophys.*, **80**, 67.
18. Centurion, M., Vladilo, G., Molaro, P., and Beckman, J. E. 1986, *Adv. Sp. Res.*, **6**, 43.
19. Cowie, L. L., and Songalia, A. 1986, *Ann. Rev. Astron. Astrophys.*, **24**, 499.
20. Cox, D. P., and Reynolds, R. J. 1987, *Ann. Rev. Astron. Astrophys.*, **25**, 303.
21. Crawford 1988, *MNRAS*, **233**, 923.

[1] Collected by Patrick Jelinsky, Antonella Fruscione, Isabel Hawkins, and Alexandra Wiercigroch, of the Center for EUV Astrophysics; inquiries and contributions to antonell@cea.berkeley.edu.

22. Crawford, I. A. 1991, *Ann. Rev. Astron. Astrophys.*, **247**, 183.
23. Cruddace, R., Paresce, F., Bowyer, S., and Lampton, M. 1974, *Ap. J.*, **187**, 497.
24. Crutcher, R. M., and Lein, D. J. 1984, *IAU Colloquium No. 81, Local Interstellar Medium*, ed. Y. Kondo, F. C. Bruhweiler, and B. D. Savage (NASA CP-2345), p. 117.
25. Danly, L., Lockman, F. J., Meade, M. R., and Savage, B. D. 1992, *Ap. J. Suppl.*, **81**, 125.
26. de Boer, K. S., Lenhart, H., Van der Hucht, K. A., Kamperman, T. M., Kondo, Y., and Bruhweiler, F. C. 1986, *Astr. Ap.*, **157**, 199.
27. de Boer, K. S., Jura, M. A., and Shull, J. M. 1987, in Exploring the Universe with the IUE Satellite, ed. Y. Kondo (Dordrecht: Reidel), 485.
28. Dickey, J. M., Salpeter, E. E., and Terzian, Y. 1977, *Ap. J. (Letters),* **211**, L77.
29. Dupree, A. K., and Raymond, J. C. 1982, *Ap. J. (Letters)*, **263**, L63.
30. Eder, D. C., and York, D. G. 1986, *Ap. J.*, **308**, 232.
31. Edgar, R. J. and Savage, B. D. 1989, *Ap. J.*, **340**, 762.
32. Egret, D., Wenger, M., and Dubois, P. 1991, *Databases and On-lineData in Astronomy*, ed. M. A. Albrecht & D. Egret (Dordrecht: Kluwer), 79.
33. Fahr, H. J. 1974, *Space Science Rev.*, **15**, 483.
34. Ferlet, R., Vidal-Madjar, A., and Laurent, C. 1980, *Ap. J.*, **242**, 576.
35. Ferlet, R., Vidal-Madjar, A., and Gry, C. 1985, *Ap. J.*, **298**, 838.
36. Ferlet, R., Lallement, R., and Vidal-Madjar, A. 1986, *Astr. Ap.*, **163**, 204.
37. Finley, D. S., Jelinsky, P., Dupuis, J., and Koester, D. 1993, Ap. J., in press.
38. Finley, D. S., Koester, D., and Basri G. 1994, in preparation.
39. Frisch, P. C. 1979, *Ap. J.*, **227**, 474.
40. Frisch, P. C. 1980, *Ap. J.*, **241**, 697.
41. Frisch, P. C., and York, D. G. 1983, *Ap. J.*, **271**, L59.
42. Frisch, P. C., York, D. G., and Fowler, J. R. 1987, *Ap. J.*, **320**, 842.
43. Frisch, P. C., Welty, D. E., York, D. G., and Fowler, J. R. 1990, *Ap. J.*, **357**, 514.
44. Frisch, P. C., Sembach, K., and York, D. G. K. 1990, *Ap. J.*, **364**, 540.
45. Frisch, P. C., 1991, *Extreme Ultraviolet Astronomy*, ed. R. F. Malina & S. Bowyer (New York: Pergamon), 322.
46. Génova, R., Beckman, J. E., Molaro, P. and Vladilo, G. 1986, *Adv. Space Res.*, **6**, 53.
47. Génova, R., Molaro, P., Vladilo, G., and Beckman, J. E. 1990, *Ap. J.*, **355**, 150.
48. Green, J., Jelinsky, P., and Bowyer S. 1990, *Ap. J.*, **359**, 499.
49. Gry, C., York, D. G., and Vidal-Madjar, A. 1985, *Ap. J.*, **296**, 593.
50. Heise, J., Paerels, F. B. S., Bleeker, J. A. M., and Brinkman, A. C. 1988, *Ap. J.*, **334**, 958.
51. Hobbs, L. M. 1978, *Ap. J. Suppl.*, **38**, 129.
52. Hobbs, L. M., Blitz, L., and Magnani, L. 1986, *Ap. J.*, **306**, L109.
53. Hobbs, L. M., Blitz, L., Penprase, B. E., Magnani, L., and Welty, D. E. 1988, *Ap. J.*, **327**, 356.
54. Holberg, J. B., Sandel, B. R., Forrester, W. T., Broadfoot, A. L., Shipman, H. L., and Barry, D. C. 1980, *Ap. J. (Letters)*, **242**, L119.
55. Holberg, J. B. 1984, *IAU Colloquium No. 81, Local Interstellar Medium*, ed. Y. Kondo, F. C. Bruhweiler, and B. D. Savage (NASA CP-2345), p. 91.
56. Jelinsky, P., Fruscione A., Hawkins, I., and Wiercigroch, A. 1994, in preparation.
57. Jenkins, E. B., and Savage, B. D. 1974, *Ap. J.*, **187**, 243.
58. Juda, M., Bloch, J. J., Edwards, B. C., McCammon, D., Sanders, W. T., Snowden, S. L., and Zhang, J. 1991, *Ap. J.*, **367**, 182.

59. Kahn, S. M., Wesemael, F., Liebert, J., Raymond, J. C., Steiner, J. E., and Shipman, H. L. 1984, *Ap. J.*, **278**, 255.
60. Kimble, R. A., Davidsen, A. F., Blair, W. P., Bowers, C. W., Van Dyke Dixon, W., Durrance, S. T., Feldman, P. D., Ferguson, H. C., Henry, R. C., Kriss, G. A., Kruk, J. W., Long, K. S., Moos, H. W., and Vancura, O. 1993, *Ap. J.*, **404**, 663.
61. Koester, D. 1989, *Ap. J.*, **342**, 999.
62. Kondo, Y., Talent, D. L., Barker, E. S., Dufour, R. J., and Modisette, J. L. 1978, *Ap. J. (Letters)*, **220**, L97.
63. Landsman, W. B., Henry, R. C., Moos, H. W., Linsky, J. L. 1984, *IAU colloquium No. 81, Local Interstellar Medium*, ed. Y. Kondo, F. C. Bruhweiler, and B. D. Savage (NASA CP-2345), p. 60.
64. Landsman, W. B., Murthy, J., Henry, R. C., Moos, H. W., Linsky, J. L., and Russell, J. L. 1986, *Ap. J.*, **303**, 791.
65. Linsky, J. L., Brown, A., Gayley, K., Diplas, A., Savage, B. D., Ayres, T. R., Landsman, W., Shore, S. N., and Heap, S. R. 1993a, *Ap. J.*, **402**, 694.
66. Linsky, J. L., et al. 1993b, in preparation.
67. Malina, R. F., Bowyer, S., and Basri, G. 1982, *Ap. J.*, **262**, 717.
68. Marshall, F. J., and Clark, G. W. 1984, *Ap. J.*, **287**, 633.
69. Martin, E. R. 1981, "*Components in the Interstellar Medium*", Ph. D. Dissertation, Princeton University.
70. Mauche, C. W., Raymond, J. C., and Córdova, F. A. 1988, *Ap. J.*, **335**, 829.
71. McCammon, D., Burrows, D. N., Sanders, W. T., and Kraushaar, W. L. 1983, *Ap. J.*, **269**, 107.
72. McClintock, W., Linsky, J. L., Henry, R. C., Moos, H. W., and Gerola, H. 1975, *Ap. J.*, **202**, 165.
73. McClintock, W., Henry, R. C., Linsky, J. L., and Moos, H. W. 1978, *Ap. J.*, **225**, 465.
74. Molaro, P., Vladilo, G., and Beckman, J. E. 1986, *Astron. Astrophys.*, **161**, 339.
75. Murthy, J., Henry, R. C., Moos, H. W., Landsman, W. B. , Linsky, J. L., Vidal-Madjar, A., and Gry, C. 1987, *Ap. J.*, **315**, 675.
76. Murthy, J., Wofford, J. B., Henry, R. C., Moos, H. W., Vidal-Madjar, A., Linsky, J. L., and Gry, C. 1989, *Ap. J.*, **336**, 949.
77. Murthy, J., Henry, R. C., Moos, H. W., Vidal-Madjar, A., Linsky, J. L., and Gry, C. 1990, *Ap. J.*, **356**, 223.
78. Oegerle, W. R., Kondo, Y., Stencel, R. E., and Weiler, E. J. 1982, *Ap. J.*, **252**, 302.
79. Paerels, F. B. S., Bleeker, J. A. M., Brinkman, A. C., Gronenschild, E. H. B. M., and Heise, J. 1986, *Ap. J.*, **308**, 190.
80. Paerels, F. B. S., Heise, J., Kahn, S. M., and Rogers, R. D. 1987, *Ap. J.*, **322**, 315.
81. Paerels, F. B. S., Bleeker, J. A. M., Brinkman, A. C., and Heise, J. 1988, *Ap. J.*, **329**, 849.
82. Paerels, F. B. S., and Heise, J. 1989, *Ap. J.*, **339**, 1000.
83. Paresce, F. 1984, *AJ*, **89**, 1022.
84. Polidan, R. S., Mauche, C. W., and Wade, R. A. 1990, *Ap. J.*, **356**, 211.
85. Pounds, K. A., et al. 1993, *M. N. Roy. Astron. Soc.*, **260**, 77.
86. Pye, J. P., Watson, M. G., Pounds, K. A., and Wells, A. 1991, *Extreme Ultraviolet Astronomy*, ed. R. F. Malina & S. Bowyer (New York: Pergamon), 409.
87. Rao, A. R., and Singh, K. P. 1990, *Ap. J.*, **352**, 303.
88. Ripken, H. W., and Fahr, H. J. 1983, *Astron. Astrophys.*, **122**, 181.
89. Rogerson, J. B., York, D. G., Drake, J. F., Jenkins, E. B., Morton, D. C., and Spitzer, L. 1973, *Ap. J. (Letters)*, **181**, L110.

90. Rumph, T., Bowyer, S., and Vennes, S. 1994, *A. J.*, in press.
91. Savage, B. D., and Jenkins, E. B. 1972, *Ap. J.*, **172**, 491.
92. Savage, B. D., and Bohlin, R. C. 1979, *Ap. J.*, **229**, 136.
93. Savage, B. D. and de Boer, K. S. 1981, *Ap. J.*, **243**, 460.
94. Savage, B. D., and Massa, D. 1987, *Ap. J.*, **314**, 380.
95. Shull, J. M. 1979, *Ap. J.*, **233**, 182.
96. Shull, J. M. and Van Steenberg, M. E. 1985, *Ap. J.*, **294**, 599.
97. Skuppin et al. 1987, *Astron. Astrophys.*, **177**, 228.
98. Snow, T. P. 1976, *Ap. J.*, **204**, 759.
99. Snow, T. P. 1977, *Ap. J.*, **216**, 724.
100. Spitzer, L. 1978, "*Physical Processes in the Interstellar Medium*" (New York: Wiley).
101. Stark et al. 1992, *Ap. J. Suppl.*, **79**, 77-104.
102. Stokes, G. M. 1978, *Ap. J. Suppl.*, **36**, 115.
103. Vallerga, J. V., Vedder, P. W., and Welsh, B. Y. 1993, *Ap. J.*, in press.
104. van Altena, W. F., Lee, J. T., and Hoffleit, E. D. 1991, "*The General Catalogue of Trigonometric Stellar Parallaxes*" (New Haven: Yale University Observatory).
105. Vennes, S. 1992, *Ap. J.*, **390**, 590.
106. Vennes, S., Dupuis, J., Rumph, T., Drake, J. J., Bowyer, S., Chayer, J., and Fontaine, F. 1993a, *Ap. J.*, **410**, L119.
107. Vennes, S., Dupuis, J., Bowyer, S., Fontaine, F., Wiercigroch, A., Jelinsky, P., Malina, R. F., and Wesemael, F. 1993b, in preparation.
108. Vladilo et al. 1985, *Astron. Astrophys.*, **144**, 81.
109. Wallerstein, G., Silk, J., and Jenkins, E. B. 1980, *Ap. J.*, **240**, 834.
110. Welsh, B., Vedder, P., Vallerga, J. 1990, *Ap. J.*, **358**, 473.
111. Welsh, B., Vallerga, J., Vedder, P. 1991, *Ap. J.*, **381**, 462.
112. Welty, D. E., Hobbs, L. M., Blitz, L., and Penprase, B. E. 1989, *Ap. J.*, **346**, 232.
113. Wu, F. M., Gangopadhyay, P., Ogawa, H. S., and Judge, D. L. 1988, *Ap. J.*, **331**, 1004.
114. York, D. G., and Rogerson, J. B. 1976, *Ap. J.*, **203**, 378.
115. York, D. G. 1976, *Ap. J.*, **204**, 750.
116. York, D. G. 1983, *Ap. J.*, **264**, 172.
117. York, unpublished *Copernicus* results

EUVE GUEST OBSERVER HANDBOOK ADDENDUM FOR 1997

The information in this addendum adds to or supersedes information in the 1995 edition of the *The EUVE Guest Observer Handbook* for the period starting with the release of NASA Research Announcement # 96-OSS-05. In the case of any conflict, information and wording of the current UCB/EUVE Call for Observing Proposals take precedence over that in the *Handbook* and its addenda.

The first section describes important changes in the mode of operation of the EUVE satellite. More specific points about how the change may impact proposals for EUVE science are covered in the sections relating to chapters 3 and 4. Other changes noted in this document, and not having to do with WSZ mode operations, should be self-explanatory. Please send any questions to:

egoinfo.cea.berkeley.edu

A1.1 EUVE Operating in WSZ Mode

In past observing cycles, detector event positions have been transmitted in X,Y format. The detector coordinates of each event were calculated from the coincident wedge (W), strip (S) and zigzag (Z) pulse heights produced by the MCP detector[1] before being put into the telemetry stream. However, the satellite can also transmit the raw W, S, and Z pulse heights for conversion to X,Y in later processing. Effective March 1, 1995, the default observing mode of EUVE was switched to WSZ mode to take advantage of a potential for increasing signal-to-noise in EUVE spectra.

"WSZ" transmission mode preserves additional information on the pulse height of each event, while providing equivalent event position data. The pulse heights can be used to distinguish photon events from those caused by energetic charged particles, and thus provides a mechanism for filtering out this part of the detector background. Proposers can find results of a study on the effects of pulse height filtering on a white dwarf observation in the EUVE Electronic News, vol 5, no 2b, 3/1/95 (*WSZnews*), at the URL:

http://www.cea.berkeley.edu/~science/html/sci_archive_pubs_pubs.html

[1] The operation of the EUVE microchannel plate (MCP) detectors and their electronics is described briefly in § 2.2.4 of the *The EUVE Guest Observer Handbook*.

Effect on telemetry transmission

The satellite can transmit fewer events per frame in WSZ mode. This is not usually a problem for the DS/S instruments, whose count rates are normally low, but it would occasionally affect the Scanners' throughputs. To counteract this effect, the tin filter quadrants on Scanner C , which often have the highest count rates, have been "blanked." This effectively raises the number of event slots available to the other filter quadrants in each frame of telemetry.

Scanner C tin anode blanking means that proposers who wish to use these quadrants for pointed observations must indicate their use as a special requirement of the observation on their Target Summary Form. Otherwise, the change to WSZ mode should have no significant impact on source throughputs for any target except the moon. Observations of the moon require switching the satellite back to X,Y mode.

What WSZ Mode Means for Deep Survey/Spectrometer Proposals

The change to WSZ mode may have an impact on proposal and observation planning. It is possible that the backgrounds of some spectral features, continua, and point source detections can be significantly decreased by filtering events based on pulse height. Pulse height filtering effectively eliminates the background from particle events. The total backgrounds of test spectra were reduced by 8 – 50%, depending on detector thresholds, and the width of the pulse height filters used. These gains were made at the expense of losing 2 – 14% of the source counts, which were also removed because the pulse height distributions overlap. See *WSZnews* for the statistics for each Spectrometer channel. See example A1.1 for a practical example on applying the changes.

A1.2 Changes in Observations Planning

The changes to Chapter 3 of the *Handbook* are presented in the order of their section numbers. The most notable change in EUVE operations is, that EUVE is no longer collecting daytime data, except for periodic engineering tests. Day-time date was eliminated to help streamline spacecraft operations and planning.

A1.2.1 Electronic Resources for Proposers

Please note the following changes in § 3.2:

- ◇ The address of the CEA/EUVE anonymous *ftp* site is now:

  `ftp.cea.berkeley.edu  or  128.32.154.12`

- ◇ Call for Proposals materials in the ftp site will be in the directory:

  `/pub/nra97/`

- ◇ The following URL's should be used to access WWW resources:

- CEA HomePage on the World Wide Web:

  `http://www.cea.berkeley.edu`

- EUVE Science Page:

  `http://www.cea.berkeley.edu/~science`

  The utilities for calculating ISM absorption and target visibility are still accessed from this page.

- All Call for Proposals materials will be made available from a WWW page in the CEA Web site:

  `http://www.cea.berkeley.edu/nra97`

- Access to EUVE Web pages through *telnet* port running the *lynx* Web client:

  `no longer supported by CEA`

◇ Instrument data files listed in are now in:

`/pub/nra97/data/`

◇ Using the IRAF/EUV software package:

- Current version of the IRAF/EUV software package is **1.7**, and the software may be obtained from the *ftp* site directory:

  `/pub/software/euv1.7/`

- Current version of the EUVE reference data is **1.15**, and may be obtained from the *ftp* site directory:

  `/pub/reference/egodata1.14/`

References to the EUV software package and EUVE reference data elsewhere in the Handbook should be updated as well. Always use the most recently released versions of EUV software and the reference data for preparing proposals.

A1.2.2 Potential for Lower Distributed Background

Because of the switch to WSZ mode, the distributed background estimates in § 3.6.3 may be effectively changed. GO's may be able to use the potential decrease in background to decrease the integration times required for some sources. This might have the advantage of allowing some proposals to have more targets approved. Other proposals may benefit directly from increased signal to noise as an effective increase in sensitivity which improves the scientific justification. The percentage of change in any one observation may be different from the estimates given here, as the particle environment of EUVE's orbit varies with solar activity and other factors. Proposers should still request exposure times that are reasonably certain to produce the desired results.

While the EGO Center now provides all GO's with the raw data files and IRAF software tools for doing pulse height filtering, proposers must bear in mind that this processing IS

NOT done as part of the EGO Center's nominal data reduction. GO's who do not have IRAF installed at their home institution may wish to write their own pulse-height filtering software, or visit the EGO Center to perform this reduction step.

To assist proposers in planning observations based on the lower backgrounds, we provide some variations on the example calculations of exposure times given in the GO handbook. Example A1.1 is based on a specific choice of pulse height filters: 10,000 – 30,000 for SW, 10,000 – 25,000 for MW, and 12,500 – 42,000 for LW. Each pulse height is a number in engineering units from 1 to 65k, the result of a simple algebraic conversion of the W, S, and Z pulse heights transmitted. These filters are estimated to have the following effects on the Spectrometer channel background and source count rates:

$$\begin{array}{llll} \mathcal{B}_{sw} \rightarrow 74\% \times 5.4\times10^{-4} & = & 4.0\times10^{-4} & \text{counts/second/Å} \\ \text{S}_{sw} \rightarrow 92\% \times \text{S} & & & \text{counts} \\ & & & \\ \mathcal{B}_{mw} \rightarrow 64\% \times 2.9\times10^{-4} & = & 2.1\times10^{-4} & \text{counts/second/Å} \\ \text{S}_{mw} \rightarrow 97\% \times \text{S} & & & \text{counts} \\ & & & \\ \mathcal{B}_{lw} \rightarrow 74\% \times 1.7\times10^{-4} & = & 1.2\times10^{-4} & \text{counts/second/Å} \\ \text{S}_{lw} \rightarrow 98\% \times \text{S} & & & \text{counts} \end{array}$$

Where the number of source counts, S, is calculated from equation 3-1 for emission lines or 3-2 for continuum sources. These reductions apply to the distributed background only. Airglow counts are expected to be reduced by the same fraction as the source counts.

Example A1.1 : Late star emission S/σ

This example begins in § 3.6.3 of the *Handbook*, with the determination of the estimated background for an emission line at 171.06 Å. If the background in the SW detector is reduced by 26%, the approximate decrease produced by using the 10k-30k pulse height filter, the short wavelength estimate for the background under the line becomes:

$$\text{B}_{SW} = 4.0\times10^{-4} \times .5 \times 40,000 = 8 \text{ counts},$$

where we assume a 40 ksec observation, as in Chapter 3. The source flux would also be reduced by 8% in the filtering process. This produces 141 instead of 153 counts, and a standard deviation for the line of:

$$\sigma_{SW}(171.06) = \sqrt{141 + 8 \times (1.1)} = 12 \text{ counts},$$

where 1.1 is $1/n + 1$ for $n = 10$. The signal-to-noise ratio is:

$$\frac{S}{\sigma_{SW}}(171.06) \simeq \frac{141}{12} \simeq 11.75,$$

i.e. the decrease in source counts is as significant as the decrease in background for this integration time, and the S/N is nearly the same as the previous value (11.8).

The example for the same line in the MW channel has a 36% decrease in the background and a 3% decrease in source counts. If we also assume that the integration time is longer, say 60 ksec, this produces:

$$\frac{S}{\sigma_{MW}}(171.06) \simeq \frac{352}{\sqrt{352 + 13 \times (1.1)}} \simeq 18.4$$

For this exposure time the elimination of the particle background would probably increase the S/N from about 16 to 18.

Continuing the same example, one uses equation 3-11 to calculate the desired exposure time for the 222 Å feature from the new MW source and background rates, Assuming the bin size to be $\Delta\lambda$, which in the MW is 1 Å, and a required S/N of 5:

$$\mathcal{T} = 25 \times \left[\frac{1.08\times10^{-4} + 2.1\times10^{-4}\,(1.1)}{1.166\times10^{-8}}\right] = 7.27\times10^{5}\ \text{seconds.}$$

This is roughly a 20% decrease in the integration time necessary to obtain the desired S/N, over the previous figure of 9.15×10^{5} seconds.

A1.2.3 Increased Event Timing Accuracy

The timing accuracy of the W,S,Z pulse heights is somewhat greater than that of the calculated X,Y positions given in § 3.8.1. Events telemetered in WSZ mode are time-tagged with an approximate accuracy of ±1 ms, as opposed to ±8 ms in XY mode.

A1.2.4 Longer Response Time for TOO's

Due to the streamlining of payload and platform operations, the expected response time for targets of opportunity (TOOs), as defined in § 3.9 of the *Handbook*, will be on a "best-bet" effort. The actual response time should be less than 24 hours, but this will not be guaranteed. See the announcement in the EUVE electronic news (URL above) vol 5, no 4, 4/18/95 for more details.

A1.3 Changes to Data Products, Software, and Processing

There have been several changes to GO data products and EGO Center data processing of which proposers should be aware. Some are connected to the change to WSZ mode described above.

A1.3.1 Deep Survey Data Provided

It is no longer necessary for GO's to specifically request the Deep Survey image data for their observation, as stated in § 4.3.2. The relevant data products are now delivered as FITS files on the data tape. Events from the Deep Survey (detector 7) are now included in the event telemetry table, and a Deep Survey QPOE file and remapped image are created in the course of EGO Center nominal data processing. The data products are documented in the *EGO Center Data Products Guide*, available from the CEA/EUVE *ftp* site in the directory `/pub/documents/docs1.6/`.

A1.3.2 EGO Center Data Processing and Delivery

Some parts of the EGO Center nominal data processing performed for GO's have changed significantly, due to changes in both the IRAF/EUV software packages and the changes in satellite operations described above. The current version of the IRAF/EUV software is **1.7**.

1. Events are now stored in the FITS table used to store the raw telemetry as either W,S,Z pulse heights (the default), or X,Y location, depending on the operating mode. Previously, the events were always stored in the telemetry table as the X,Y locations. This is the only substantial change in EUVE Spectrometer data products.
2. The standard processing script used to run the event pipeline on GO observations now performs the conversion of W,S,Z to event positions X,Y. QPOE files created by the pipeline have the same attributes as before, and spectral images are created as before.

A1.3.3 IRAF Reduction Tools

The software now supplied to GO's contains two new kinds of alternate pipeline scripts:

1. Scripts for creating IRAF QPOE files with event pulse heights from WSZ format data. GO's can now produce pulse height QPOE files and make pulse height filtered spectral images by applying an attribute filter in a QPOE I/O interface expression[2].
2. Scripts for generating position-remapped Deep Survey QPOE files. The use of these scripts is documented in the *EGO Center Software User's Guide*, version **1.5**. Deep survey event positions are mapped to (RA,Dec).

[2] Use of the QPOE I/O interface is also described in the *EGO Center Software User's Guide*.

BIBLIOGRAPHY

[1] The EUVE Guest Observer Center Software User's Guide, version1.4, M. Abbott, A. Miller, and L. Gauvin, The EUVE Guest Observer Center, Jan 11, 1994.

[2] The First EUVE Source Catalog, S. Bowyer, R. Lieu, M. Lampton, J. Lewis, X. Wu, J.J. Drake, and R.F. Malina, *Astro. J. Suppl.*, 1994 (in press).

[3] EUV Astronomy on the *Apollo–Soyuz* Mission: The First Detection of Stellar EUV Sources and Other Astrophysical Results, Stuart Bowyer, in *Extreme Ultraviolet Astronomy*, ed. R. F. Malina and S. Bowyer (New York: Pergamon Press), pp. 3–7, 1991.

[4] The Fabrication, Evaluation and Performance of Machined Metal Grazing Incidence Telescopes, S. Bowyer and J. Green, *Appl. Opt.*, **27**(8), 1414, 1988.

[5] Initial Performance Results form the Extreme Ultraviolet Explorer Spectrometer, C. Christian, M. Abbott, J. Dupuis, D. Finley, and P. Jelinsky. *Ap. J.*, 1993 (in preparation).

[6] On the Opacity of the Interstellar Medium to Ultra-Soft X-Rays and Extreme Ultraviolet Radiation, R. Cruddace, F. Paresce, S. Bowyer, and M. Lampton, *Ap. J.*, **187**, 497, 1974.

[7] Fairchild Space Co., *Explorer Platform User's Guide,* NASA document 408-EP-403-001, rev. A, August, 1989.

[8] Design of the Extreme Ultraviolet Explorer Long-Wavelength Grazing Telescope Optics, D. S. Finley, P. Jelinsky, S. Bowyer, R. F. Malina, *Appl. Opt.*, **27**(8), 1476, 1988. Also in *Grazing Incidence Optics for Astronomical and Laboratory Applications*, ed. S. Bowyer and J. C. Green, *Proc. SPIE*, **830**, 106–110, 1988.

[9] The Mirrors for the Extreme Ultraviolet Explorer, D. S. Finley, J. Green, S. Bowyer, R. Malina, *Proc. SPIE*, **640**, 91, 1986.

[10] The Distribution of Neutral hydrogen in the Interstellar Medium. I. The Data, A. Fruscione, I. Hawkins, P. Jelinsky, and A. Wiercigroch, *Ap. J. Supp.*, in press.

[11] The Extreme Ultraviolet Explorer Spectrometer, M. Hettrick, S. Bowyer, R. F. Malina, C. Martin, and S. Mrowka, *Appl. Opt.*, **24**, 1737, 1985.

[12] Aberrations of Varied Line-Space Grazing Incidence Gratings in Converging Light Beams, M. C. Hettrick, *Appl. Opt.,* **23**, 3221, 1984.

[13] Variable Line-Space Gratings: New Designs for Use in Grazing Incidence Spectrometers, M. C. Hettrick and S. Bowyer, *Appl. Opt.*, **22**, 3921, 1983.

[14] Results from the Calibration of the Extreme Ultraviolet Explorer Instrumentation, B. Welsh, P. Jelinsky, J. V. Vallerga, P. W. Vedder, D. S. Finley, and R. F. Malina, to appear in *Proc. SPIE,* **1343**, 1990.

[15] A Theory of the Instellar Medium: Three Components Regulated by Supernova Explosions in an Inhomogeneous Substrate, C. McKee, and J. Ostriker, *Ap. J.* **218**, 148, 1977.

[16] The Extreme Ultraviolet Explorer Bright Source List, R. Malina et. al., *Astron. J.* **107**, **(2)**, 751-764, 1994. BSL tabular data appears in ApJ/AJ CD-ROM Series, Vol. 2, 1994.

[17] The EUVE Guest Observer Program, A. B. Miller, *JBIS*, **46 (9)**, p. 357, 1993.

[18] Interstellar Medium Contiuum, Autoionization, and Line Absorption in the Extreme Ultraviolet, T. Rumph, S. Bowyer, and S. Vennes. to appear in *Astron. J.*, 1994.

[19] Solar EUV irradiance from the San marco AASI: A reference spectrum Schmidtke, et. al., *Geophysical research letters,* **vol 19**, **21**, p 2175-2178, nov 3, 1992.

[20] Background Events in Microchannel Plates, O.H.W. Siegmund, J.V. Vallerga, and B. Wargelin, in *Proc. IEEE Trans. Nucl. Sci.*, **NS-35**, pp. 524-528, 1988.

[21] Extreme Ultraviolet Quantum Efficiency of Opaque Alkaki Halide Photocathodes on Microchannel Plates, O. H. W. Siegmund, E. Everman, J. V. Vallerga, and M. Lampton, *Optoelectronic Technologies for Remote Sensing from Space*, ed. J. S. Seeley and S. Bowyer, *Proc. SPIE*, **868**, 18–24, 1988.

[22] Deep Survey Boresight dead Spot, Part II, M. Sirk, Center forEUV Astrophysics, (*internal communication*).

[23] The EUVE Public Archive: Data and User Services, B.A. Stroozas, E. Polomski, B. Antia, J. Drake, K. Chen, C. Christian, E.C. Olson, *Third Annual Conf. on Astronomical Data Analysis Software and Systems* 13-15 Oct. 1993.

[24] EUV (800-1400 Å) observations of the tropical airglow, S. Chakrabarti, *Geophysical Research Letters,* **11, no. 6**, 565-568, 1984.

[25] Microchannel Plate EUV Detectors for the Extreme Ultraviolet Explorer, O. H. W. Siegmund, R. F. Malina, K. Coburn, and D. Werthimer, *IEEE Trans. Nucl. Sci.,* **NS–31** 776, 1984.

[26] Spectroscopy of the EUV (350-1400 Å) Nightglow, S. Chakrabarti, R. Kimble, S. Bowyer, *Journal of Geophysical Research,* **89, no. A7**, 5660-5664, 1984.

[27] Spectroscopy of the Interstellar Medium in Emission Using the Extreme Ultraviolet Explorer Satellite, J. V. Vallerga, P. Jelinsky, P. W. Vedder, and S. Bowyer, in *Extreme Ultraviolet Astronomy*, ed. R. F. Malina and S. Bowyer (New York: Pergamon Press), p. 304–312, 1991.

[28] Imaging Characteristics of the Extreme Ultraviolet Explorer Microchannel Plate Detectors, J. V. Vallerga, G. C. Kaplan, O. H. W. Siegmund, M. Lampton, and R. F. Malina, *IEEE Trans. Nucl. Sci.*, **36**(1), 881, 1989.

[29] The calibration of thin film filters to be used on the Extreme Ultraviolet Explorer satellite, J. V. Vallerga, O. H. W. Siegmund, E. Everman, and P. Jelinsky, *Proc. SPIE*, **689**, 138, 1986.

[30] Low Density of Neutral Hydrogen and Helium in the Local Interstellar Medium: *Extreme Ultraviolet Explorer* Photometry of the Lyman Continuum of the Hot White Dwarfs MCT 0501-2858, MCT 0455-2812, HZ 43, and GD 153, S. Vennes, J. Dupuis, S. Bowyer, G. Fontaine, A. Wiercigroch, P. Jelinsky, F. Wesemael, and R.F. Malina. *Ap. J. Lett.*, **421**, L35-L38, 1994.

[31] The Berkeley Extreme Ultraviolet Calibration Facility, B. Welsh, P. Jelinsky, and R. F. Malina, *"X-ray Instrumentation in Astronomy II"*, ed. L. Golub, *Proc. SPIE*, **982**, pp. 335–341, 1988.

[32] Extreme Ultraviolet Explorer Science Operation Center, G. S. Wong, F. A. Kronberg, H. D. Meriwether, L. S. Wong, and C. L. Grassi, *JBIS*, **46 (9)**, p. 367, 1993.